Computational Design of Viscoelastic Gels with Tunable Mechanical Energy Dissipation

by

Aarthy Kannan Adityan

Bachelor of Technology, Naval Architecture & Ocean Engineering
Indian Institute of Technology Madras, 2011

Submitted to the Department of Mechanical Engineering
in Partial Fulfillment of the Requirements for the Degree of

Master of Science in Mechanical Engineering

at the

MASSACHUSETTS INSTITUTE OF TECHNOLOGY

May 2014
[June 2014]

Signature redacted

Signature of Author.....
Department of Mechanical Engineering
May 10 2014

Signature redacted

Certified by .....
Krystyn J. Van Vliet
Associate Professor of Materials Science and Engineering and Biological Engineering
Thesis Supervisor

Signature redacted

Certified by .....
David M. Parks
Professor of Mechanical Engineering

Signature redacted

Accepted by .....
David E. Hardt
Ralph E. and Eloise F. Cross Professor of Mechanical Engineering
Chair, Committee on Graduate Students

Computational Design of Viscoelastic Gels with Tunable Mechanical Energy Dissipation

by

Aarthy Kannan Adityan

Submitted to the Department of Mechanical Engineering
on May 10, 2014 in Partial Fulfillment of the Requirements for the Degree of

Master of Science in Mechanical Engineering

Abstract

The development of engineered materials that exhibit mechanical characteristics similar to biological tissues can enable testing the effect of ballistics and designing of protective equipment. The physical instability of existing tissue simulants over long times and ambient temperatures has propelled interest in using polymer gel systems that could potentially mimic the mechanical response of tissues. More generally, the capacity to tune the mechanical energy dissipation characteristics of such gels is of interest to a range of applications. The present work uses a computational approach to predict the material properties of such gels. A finite element model and simulation of an impact indentation test was developed, with the polymer gel properties simulated via a multiscale material modeling technique. The computational model was validated by comparing the simulated response to experimental data on polymer gels. The model was then used to predict the optimized material properties of the gels for use in diverse applications including tissue simulants.

Thesis Advisor: Krystyn J. Van Vliet
Title: Associate Professor of Material Science and Engineering and Biological Engineering

ACKNOWLEDGEMENTS

I am immensely grateful to my advisor Professor Krystyn Van Vliet for her support and academic guidance throughout all stages of my research. Her incredible patience and encouragement were vital in reinforcing my determination to complete my Master's at MIT.

I am also thankful to my thesis reader Professor David Parks for his constructive comments on my thesis, which helped me gain clarity in the communication of my work.

It has been a stimulating experience to be part of the Van Vliet Group, and I am especially grateful to the group members with whom I collaborated with for my project. My exchanges with Dr. Roza Mahmoodian were always very productive and often shaped the direction of my research. Dr. Ilke Kalcioglu's useful insights on my project, from the perspective of her experimental work, helped me understand my own research goals better. I am grateful to Wen Shen for sharing her experimental experience, to Dr. Patrick Bonnaud for his guidance in running simulations on the group cluster, and to Dr. Anna Jagielska and Dr. John Maloney for their valuable feedback during our discussions.

I thank the Institute of Soldier Nanotechnologies for funding my research.

I am incredibly lucky to have met Dean Blanche Staton during my time at MIT. Her empathy and compassion came at a crucial stage in my life, and her cheer and warm reassurance lifted my spirits when I needed it the most.

I am indebted to several members of the MIT community for their timely support. I am grateful to Leslie Regan for her assistance and quick, patient responses throughout my years in the MechE department. The experienced advice provided by Susan Spilecki at the Writing and Communication Center was instrumental in overcoming my writer's block during the central stages of my thesis. The supportive counsel of Dr. Lili Gottfried

and Kate McCarthy at MIT Medical were invaluable and I am thankful to both of them for their encouraging words.

I am tremendously grateful to Dr. Araceli Orozco Hershey for her unflagging confidence in me. Her optimism and kindhearted advice always left me motivated and energized.

I have been extremely fortunate to have close friends who have enriched my life with love and laughter, and have always given me their unquestioning support. It is my pleasure to acknowledge them - my sister, Nikila, my friends, Rima and Jemy, and my partner, Jordan.

Throughout my years at MIT, I lived at Ashdown House and I am grateful to the Ashdown community for making me feel at home. I would also like to acknowledge Drou Rus and Uma Ramakrishnan, my adopted parents on this side of the globe.

Finally, it is a pleasure to acknowledge my parents, Maddhumathi and Kannan Adityan, for their unconditional love and encouragement, which gave me the strength to pursue my ambitions.

Contents

LIST OF FIGURES

LIST OF TABLES

Chapter 1: Introduction

1.1 Research Motivation

A tissue simulant is a synthetic material that mimics the mechanical response of biological tissues, for example in response to impact loading. The design of more effective bulletproof vests and better protective armor is imperative to increasing the survivability of soldiers in the field. This requires the capability to accurately test the performance of such defensive systems against various impact forces due to blasts, bullets and other projectiles. In such experiments, tissue simulant materials are necessary as stand-ins for different types of living tissue, such as heart, liver and brain tissues, so that the effect of ballistics on such tissues can be analyzed with and without protective overlays. Tissue simulant materials are also useful in understanding mechanisms of injuries such as blunt force trauma and penetrative wounds [1].

For several decades, "ballistic gelatin" has been used as a tissue simulant as an alternative to animal tissues and cadavers. Produced by dissolving gelatin powder in water, it is inexpensive and commercially available, and approximates the density and viscosity of human muscle tissue. However its mechanical properties are very dependent on temperature and method of preparation, and will change over a period of a few days due to dehydration. It also does not exhibit a wide range of stiffness that can simulate other tissues such as internal organs [2].

Recent works in developing better alternatives to ballistic gelatin have considered polymer-based gels like the commercially available Perma-Gel™ and physically associating gels such as styrenic block copolymers [3-4]. Such polymer gels have mechanical properties that are more environmentally stable [5] as well as more tunable [6-7] compared to ballistic gelatin. A polymer gel consists of a chemically or physically crosslinked polymer swollen by a solvent. The presence of the solvent makes the gel

easily deformable, while the crosslinked polymer allows the gel to recover elastically from any applied strain [8]. The tunability of the polymer gel arises from the possibility of using different polymer crosslinking ratios, solvent loadings and solvent molecular weights [9].

In the present study, the polymer gels considered are poly (dimethyl) siloxane (PDMS) [10] gel systems developed by Dr. Joseph L. Lenhart et al. at the Army Research Laboratory (ARL). They consist of a chemically crosslinked PDMS network and a non-reactive methyl-terminated PDMS solvent (Figure 1.1c). Several PDMS samples were synthesized at ARL by varying the stoichiometric ratio of crosslinking tetrafunctional tetrakis(dimethyl siloxy)silane groups (Figure 1.1b) to the vinyl-terminated PDMS precursor (Figure 1.1a), the solvent molecular weight and the solvent loading percentage [11], and the microscale mechanical behavior of such gels was analyzed experimentally at MIT by Dr. Ilke Kalcioglu of the Van Vliet Group [12].

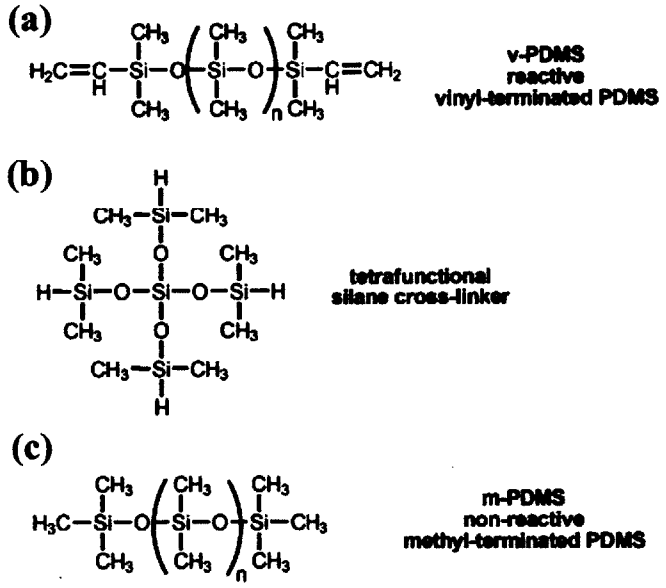

Figure 1.1: *Chemical structures of the PDMS gel network components* ***(a)*** *vinyl-terminated PDMS precursor,* ***(b)*** *tetrakis(dimethyl siloxy) silane crosslinker,* ***(c)*** *methyl-terminated non-reactive PDMS solvent (Image from [11])*

The mechanical behavior of tissues and potential tissue simulants have been studied by different experimental methods [6,13,14,15,16], both quasi-static and dynamic. For the purpose of testing and developing tissue simulant materials, it is important that both the hydrated soft tissues as well as the potential tissue simulants are studied under similar ambient and loading conditions. It is also necessary that the loading conditions and the type of mechanical behavior studied are relevant to the purpose of the tissue simulant. To that end, and for the purpose of developing tissue simulant gels for ARL purposes, high-rate pendulum-based impact indentation experiments were conducted by Dr. I. Kalcioglu (Van Vliet Group) on polymer gels and heart and liver tissues [17]. This technique, developed by Constantinides et al., enabled the characterization of impact energy dissipation and resistance to penetration of the tissues and gels under localized impact loading conditions [18-19].

By this experimental approach, Dr. I. Kalcioglu (Van Vliet Group) quantified and compared the mechanical characteristics of the candidate tissue simulant gels manufactured by ARL collaborators and provided information on which gels behave more similarly to rat tissues. This process involved providing feedback to the ARL about what parameters could be modulated to make the gels more comparable to tissues, and then repeating the experiments on newly prepared gels to validate such empirical predictions.

The present work is an effort to improve the efficiency of this process by implementing a computational model of the impact indentation experiment, so that the properties of the potential tissue simulant can be predicted and optimized. This would give material scientists a better idea of how to make such simulant gels, and reduce efforts in creating several gels and testing them experimentally. These data and approach can also provide basic correlations between composition and design of gels with tunable mechanical energy dissipation, including under mechanical loading conditions not accessible easily via experiment.

1.2 Multiscale Material Modeling

In the current study, the impact indentation experiment is modeled using finite element analysis. A macroscale finite element model, however, would consider the material as homogenous at the macroscopic level. Such an assumption would not accurately capture the behavior of a composite PDMS gel, which is affected by the heterogeneities in its microstructure including fluid-solid interactions. On the other hand, it is not conceivable to include the microstructure in the finite element model directly either, since that would involve an exceptionally fine mesh and impractical computational resources. A compromise between these two approaches is to use a multiscale model.

In the multiscale method, we consider the macroscale and the microscale. The macroscale is the scale of the finite element model, and the microscale is the scale of the material microstructure, which usually consists of distinguishable *matrix* and *inclusion* phases [20]. In the case of the PDMS gels, the crosslinked PDMS network is considered the matrix and the PDMS solvent is taken as the inclusion.

At the macroscale, the composite material is represented by a finite element mesh that is locally homogenous, and at each mesh computation point (node), the microstructure is taken into account using the concept of a Representative Volume Element (RVE), a statistically representative sample of the material (Figure 1.2). Its size is much smaller than the macroscale material dimensions but it is large enough to capture microstructural properties like volume fraction and aspect ratio of the inclusion, and material properties of the multiple phases [21].

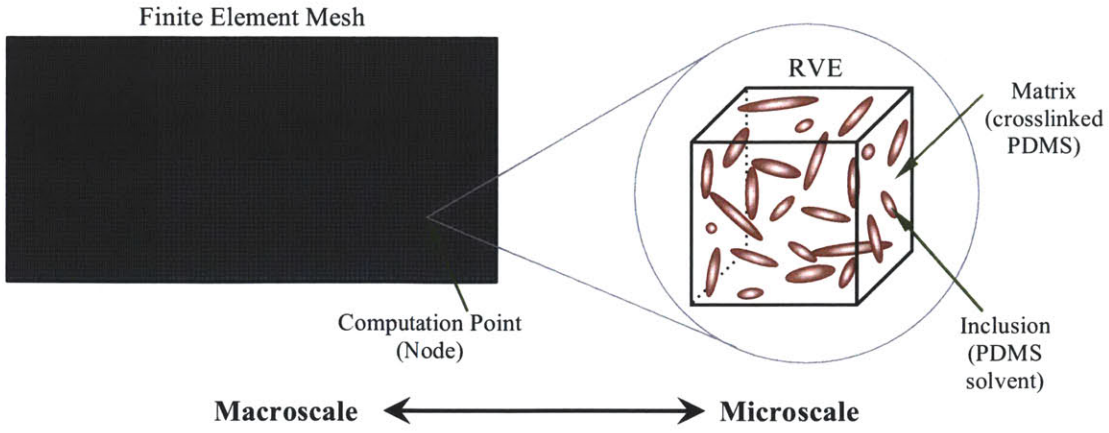

Figure 1.2: *Representation of multiscale model*

At each computation point of the mesh, the macroscale strain or stress values are used as the boundary conditions for the RVE, and the volume average of the stress or strain fields in the RVE is taken as the effective macroscopic response of the material at that point. This transition from the heterogeneous microscale-level of the RVE to the effective properties of the macroscale homogeneous material is done by scale-transition methods, such as generalized method of cells [22], asymptotic homogenization [23], direct finite element analysis of the RVE and mean-field homogenization [24]. The last of these, which is computationally efficient, is used in the present study.

The most accurate method of solving the RVE is to model the microstructure using finite element analysis (FEA) to obtain the detailed stress and strain fields within the RVE. However, meshing a complex microstructure can be troublesome and using FEA to solve the RVE at each computation point of the macroscale model would be computationally expensive, especially for non-linear elastic materials [25]. A more economical approach is mean-field homogenization (MFH), where each inclusion and the matrix are treated as separate domains, and only the average values of the stress/strain fields in these subdomains are computed rather than the detailed fields. It is generally assumed that the each domain behaves according to the macroscopic constitutive relations of the corresponding phase material [26].

Different MFH schemes exist, most based on Eshelby's solution [27] of a single ellipsoidal inclusion in an infinite elastic matrix. They differ in their derivations of the concentration tensors, which relate the stress/strain fields of the matrix and inclusions [28]. For example, in the Mori-Tanaka (M-T) scheme, which extends the Eshelby's solution, it is assumed that each inclusion behaves as if it were isolated in an infinite matrix and the matrix average stress/strain is applied as the boundary condition to the inclusion [29]. The M-T model is noteworthy for predicting the effective properties of two-phase composites, especially at low or high inclusion volume fractions [26].

Another family of MFH schemes is realized by the Double-Inclusion (D-I) model, proposed by Hori and Nemat-Nasser [30], which assumes that each inclusion is enclosed in another inclusion of matrix material and this double-inclusion is embedded in an infinite unknown material. Setting the unknown material as the matrix material, the D-I model collapses to the M-T model, whereas setting it as the inclusion material gives us the Inverse M-T model [31]. The Lielens model, also known as the Interpolative D-I model, interpolates the unknown material between the M-T and Inverse M-T models, and gives good results for intermediate inclusion volume fractions [32]. The Self-Consistent (S-C) model assumes that the unknown material is a homogeneous material equivalent to the heterogeneous composite [33]. The S-C model was developed for polycrystals and is not as well suited for two-phase composites [31]. Most of these MFH schemes have been tested against direct FEA simulations of RVEs and have been extended to multi-phase inelastic composites as well, although there is still scope for advancement in the non-linear regime [34].

Once a homogenization method is decided upon, there are two ways of implementing the multiscale model: sequential and concurrent. In the sequential approach, the microscale model is first analyzed to obtain the equivalent macroscopic behavior of the composite and then the macroscale model is solved using the properties of this equivalent material. In the concurrent approach, both the microscale and the macroscale models are executed simultaneously [35]. At each time step and mesh point of the macroscale model, the RVE is solved using the current macroscopic stress/strain as the boundary condition, and this

response of the RVE is used in the next time step of the macroscale analysis. This coupling allows for a more accurate prediction of the macroscopic response of the composite due to its microscopic heterogeneities, and is implemented in the present work.

1.3 Thesis Organization

This thesis is organized as follows:

Chapter 1 included the motivation for this research and introduced multiscale modeling, which is used to analyze the polymer gels.

Chapter 2 describes the impact indentation experiment and the finite element model developed to simulate this experiment.

Chapter 3 introduces the parameters used to characterize the energy dissipation and the resistance to penetration of the different tissue and gel samples. The simulated data from the computational model are compared to the experimental data using these parameters. The limitations of the computational model are also discussed.

Chapter 4 describes how the computational model can be used to predict the material properties of tissue simulant gels, and presents the results of such optimization in the case of heart and liver tissues.

Chapter 5 presents the conclusions of the thesis and discusses directions for future work.

Chapter 2: Multiscale Model

The experimental setup described in Section 2.1 was used by Dr. I. Kalcioglu (Van Vliet Group) to conduct her experimental analysis on tissues and candidate tissue simulant gels. The multiscale material modeling approach described in Section 2.2.3 was suggested by Dr. R. Mahmoodian (Van Vliet Group) for the purpose of this project and she also contributed to the implementation of the Digimat-Abaqus interface.

2.1 Experimental Setup

Figure 2.1 shows a schematic of the experimental apparatus used by Dr. I. Kalcioglu (Van Vliet Group) in her experiments, a commercially available pendulum-based instrumented indenter (NanoTest, Micro Materials, Wrexham, UK). The pendulum is fixed to the support frame through a pivot in the middle and it is free to rotate frictionless about this pivot. A flat punch or spherical indenter is rigidly attached to the pendulum, below the pivot, so that it can swing towards the sample, which is mounted vertically near the indenter [18-19].

The instrument was modified by adding a liquid cell to the sample mount (Figure 2.2), so that the tissue and gel samples could be tested in a fluid immersed state, which ensured that they were fully hydrated [36].

The impact force on the indenter is applied through an electromagnetic voice coil that interacts with the top of the pendulum. A parallel plate capacitor mounted on the pendulum in the same horizontal plane as the indenter is used to measure the displacement of the indenter. At the bottom of the pendulum, a pyramid of magnetically soft iron is attached, so that the pendulum can be attracted away from the sample by switching on the current in a nearby solenoid. The entire setup is housed in an acoustic

isolation enclosure at a controlled temperature (26° C) and relative humidity (50%), to reduce any vibrations or changes in ambient conditions [18-19].

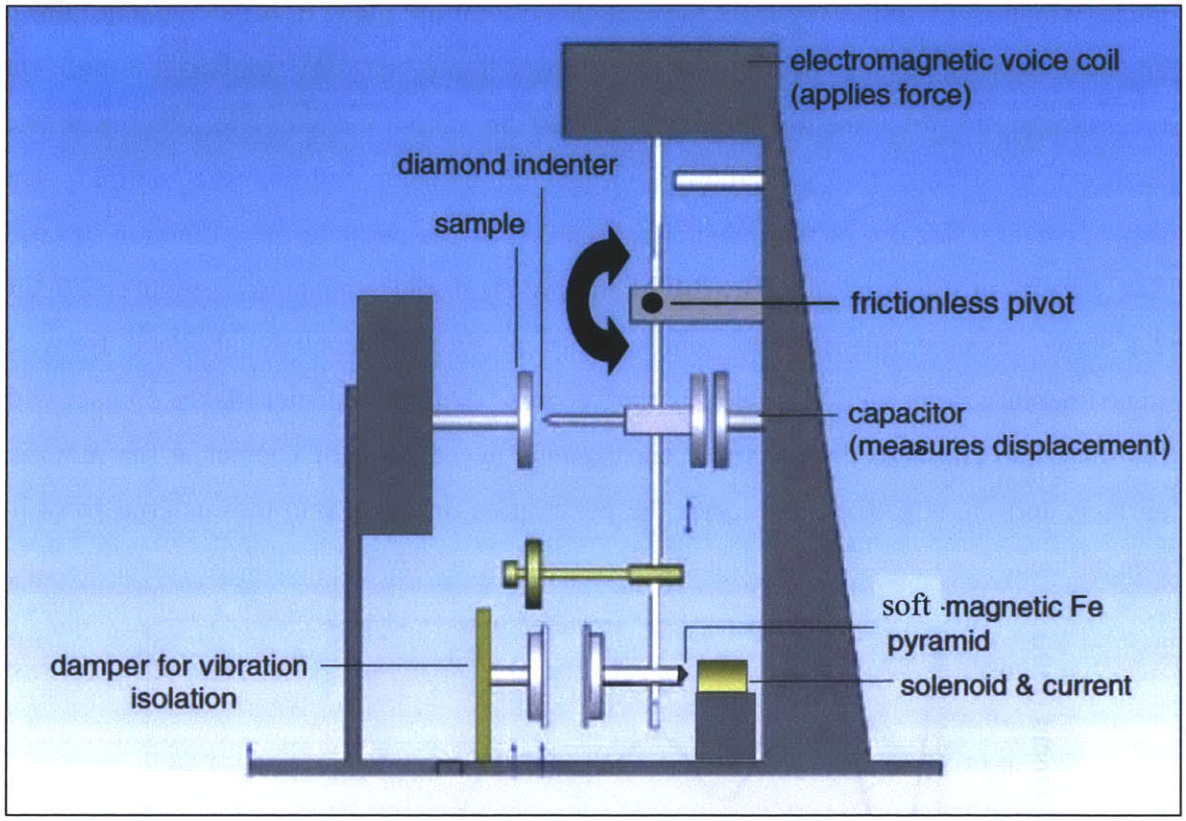

***Figure 2.1**: Experimental setup (Image from [18])*

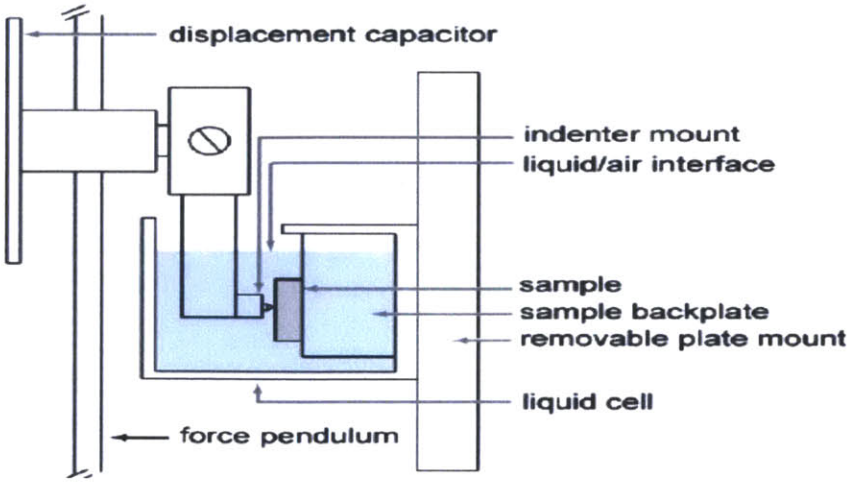

***Figure 2.2:** Setup of sample in the liquid cell (Image from [36])*

For applying an impact load to the indenter, the solenoid at the bottom is first energized so that it pulls and holds the pendulum away from the sample. The sample plate is then moved in the direction of the indenter so that the sample surface is brought to the contact plane, which is 0.5 mm away from the vertical equilibrium plane of the free pendulum. A constant current, which determines the impact force, is then applied through the electromagnetic coil at the top and is maintained throughout the test. The solenoid is then shut off to release the pendulum, so that the indenter impacts the sample. The displacement trajectory of the indenter is recorded by the capacitor as a function of time. The velocity profile is obtained by differentiating the displacement curve. Figures 2.3 and 2.4 show example displacement and velocity profiles respectively obtained from an experimental run on a PDMS gel. The time is zero when the indenter makes contact with the material. The zero displacement corresponds to the point of contact at the material surface, and the negative direction is the penetration direction into the material from its free surface.

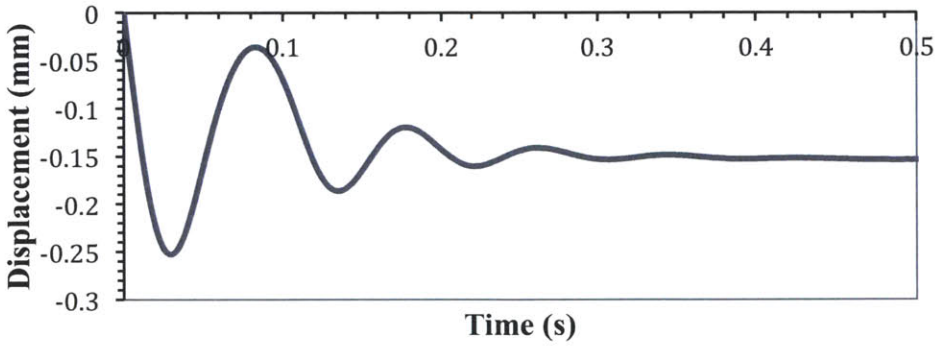

Figure 2.3: *Example displacement profile from experiment on a PDMS gel*

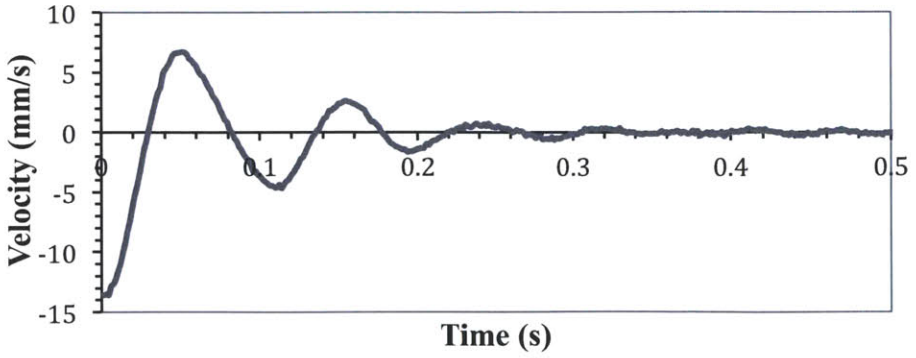

Figure 2.4: *Example velocity profile from experiment on a PDMS gel*

2.2 Finite Element Model

The commercially available finite element analysis software Abaqus was used to create a computational model of the experimental setup described in Section 2.1.

2.2.1 Mesh, Indenter and Contact Formulation

The sample sizes of gel or tissue used for testing were approximately 5-6 mm thick, 15-20 mm in length and 10-13 mm in width. A flat punch of radius 1 mm was used for testing the PDMS gels. Since the length and width are much larger compared to the contact area of the punch, the sample dimensions were approximated as a cylindrical disc of radius 10 mm and thickness 5 mm. In this way, the symmetrical nature of the indenter loading was taken advantage of, and an axisymmetric mesh of the gel sample was created. Compared to three-dimensional (3D) elements, axisymmetric elements significantly reduce the problem size and the computational resources required [37].

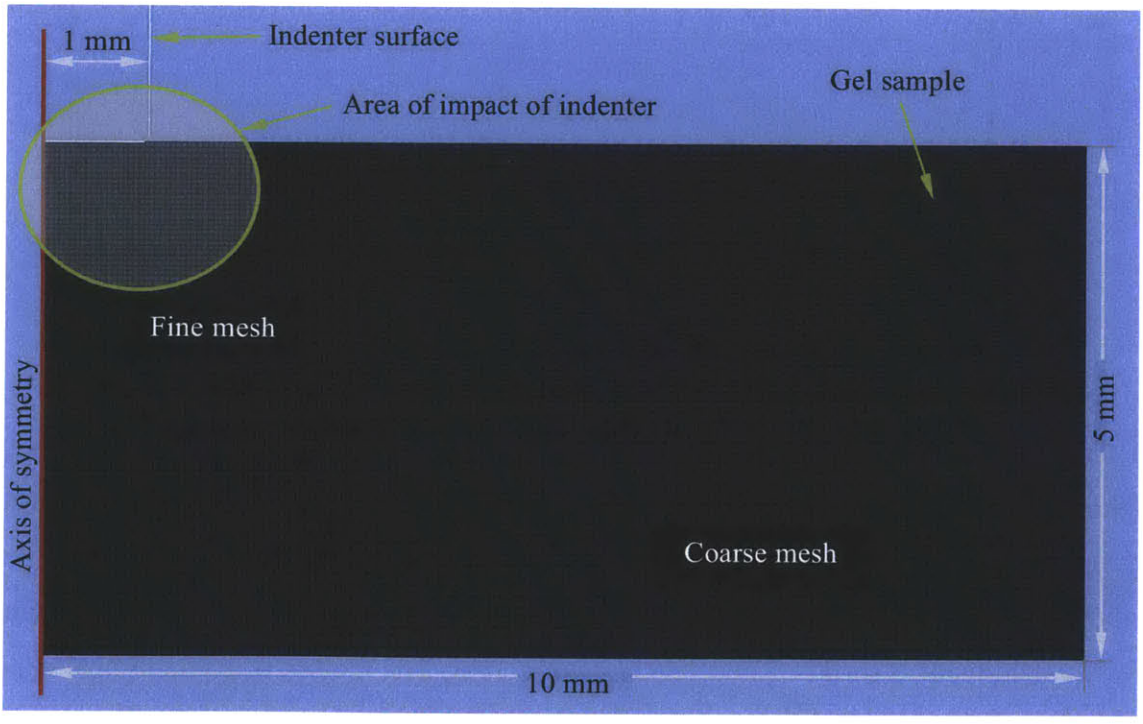

Figure 2.5: *Finite element mesh*

Figure 2.5 shows the axisymmetric mesh used to represent the polymer gel sample being tested. The element spacing was created such that the mesh is more refined near the central region where the indenter impacts the material, and coarser away from this region. The element type used was CAX4, which is a 4-node bilinear axisymmetric quadrilateral solid element [38].

A mesh convergence study (Figure 2.6) was performed so that the optimal number of elements could be used. This ensured that the mesh would accurately represent the problem while being computationally efficient. The number of elements chosen was 9750.

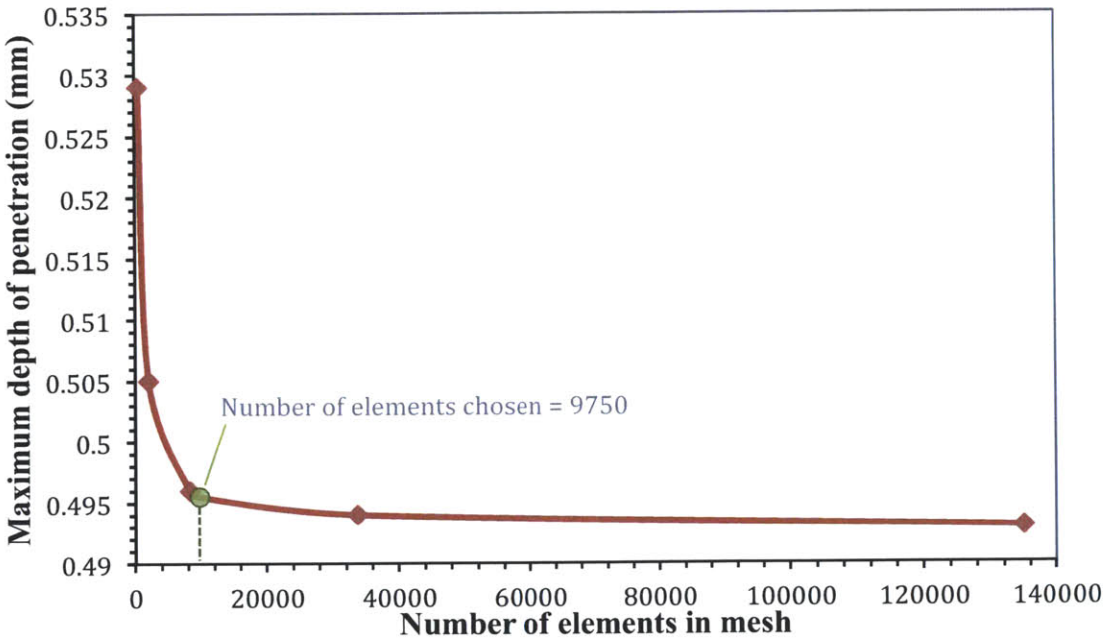

Figure 2.6: *Mesh convergence study*

The flat punch indenter was modeled as an analytical rigid surface. Since the indenter is made of a much harder material (stainless steel) than the sample and it would undergo negligible deformation within itself, modeling it as a rigid body was a natural choice. An analytical rigid surface was used since it allows the axisymmetric profile of the indenter to be defined using a series of line segments or curves. The motion of an analytical rigid surface in Abaqus is governed by the motion of its reference node, and its mass and inertial properties are associated with this single reference node. Analytical rigid surfaces

are better suited to contact modeling than rigid surfaces composed of elements because they are single-sided and greatly reduce the computational cost [39].

In the experiment, the indenter is fixed to the pendulum and its motion is governed by the forces on this pendulum. The pendulum has a spring constant, k = 10 N/m and damping coefficient, c = 0.96 Ns/m [18-19]. The pendulum mass along with the weight of the fluid extension and the flat punch, m = 0.215 kg were applied to the reference node of the analytical indenter surface. The pendulum action was modeled as spring-damper system, with the specified k and c values, attached to the indenter on one end and a fixed point at the other end, as shown in Figure 2.7.

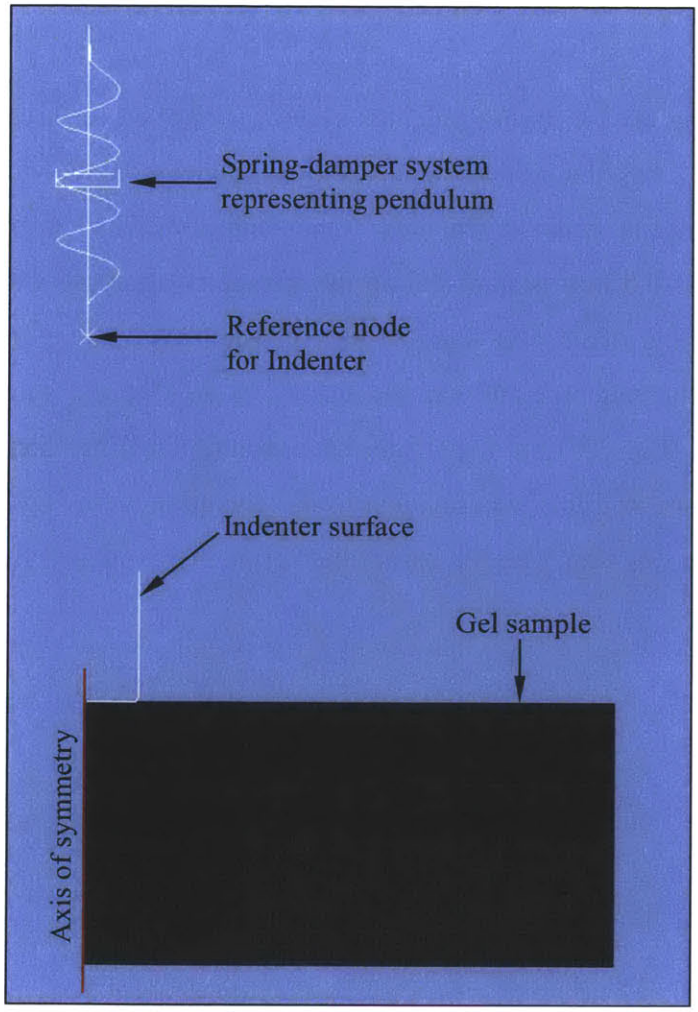

Figure 2.7: *Computational FEM model*

The contact interaction is modeled between the indenter surface and the top surface of the sample, using a node-to-surface contact discretization and small-sliding tracking approach. The node-to-surface discretization ensures that the indenter surface does not penetrate through the surface of the material and it is also less computationally intensive than the surface-to-surface discretization. The small-sliding approach also saves computational cost and it assumes that there will be little relative sliding between the two contact surfaces [40]. The friction in the contact formulation is set to zero, as it is assumed that friction is negligible in the interaction between the indenter and the material.

2.2.2 Loading

The impact loading on the spring-indenter system is applied in three steps. Initially, at Step Zero (Figure 2.9a), the indenter is at rest, just making contact with the surface of the gel and the spring is relaxed. In Step One (Figure 2.9b), an initial compressive displacement x_{eq} of 0.5 mm is imposed on the spring by applying a suitable force at the top end of the spring. This was done to be consistent with the experiment, where the contact between the indenter and sample occurs in a plane 0.5 mm from the vertical equilibrium plane (Figure 2.8). Therefore the pendulum still has some potential energy when contact occurs, and this is equivalent to the potential energy added to the spring by the compression in this step. The top end of the spring is maintained fixed after this step.

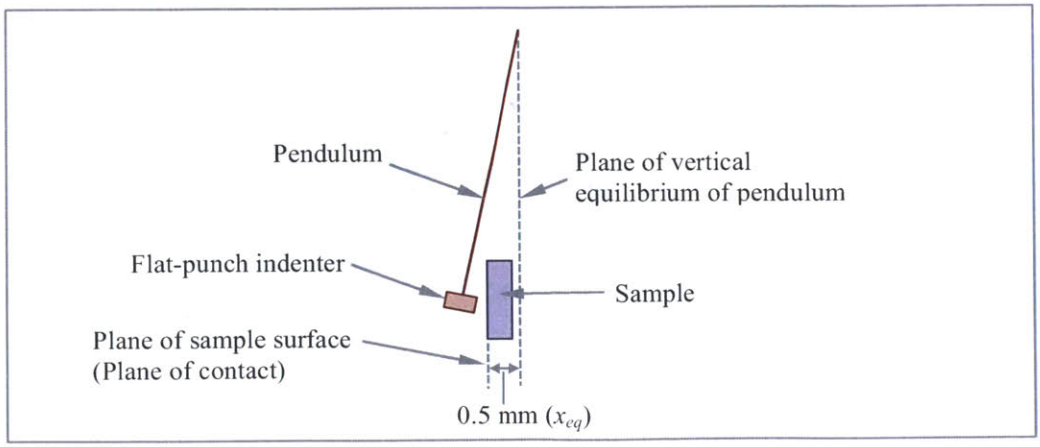

Figure 2.8: *Schematic showing plane of contact in the experimental setup*

In Step Two (Figure 2.9c), the indenter is moved away from its initial position of contact with the material. This is equivalent to the experimental action where the pendulum is moved away from the sample before impact. Before running the final simulation, the distance by which the indenter is moved away is adjusted, by iteratively changing the upward force f_{up} applied on the indenter in this step, until the velocity v_{in} with which the indenter impacts the material in Step Three matches the impact velocity reported in the experiment. This calibrated force f_{up} is used in the final simulation used for analysis.

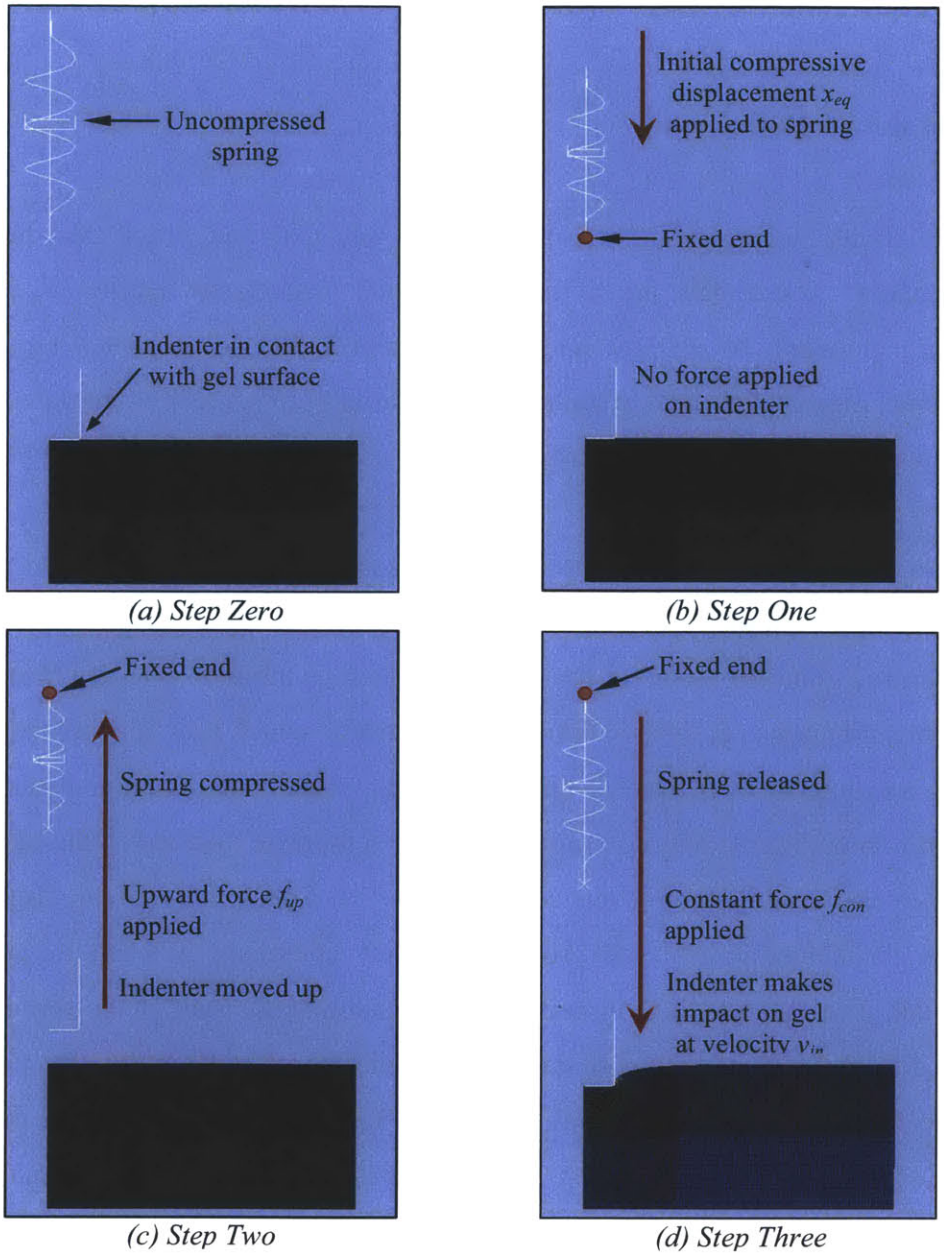

***Figure 2.9**: Steps of loading on the spring-indenter system*

Step Three (Figure 2.9d) is a Dynamic step where the spring-indenter system is released from its compressed state. A constant force f_{con} is also applied on the indenter, which is equal to the constant force applied to the pendulum in the experiment. In this way, the impact force and impact velocity values are made consistent between the experiment and the simulation. The displacement and the velocity in the axial direction at the indenter reference node are obtained from this step and these are compared to the displacement and velocity profiles from the experiment.

2.2.3 Material Definition

The simulations were run for various PDMS gels that had previously been tested experimentally. These gels are composed of two viscoelastic phases, a chemically crosslinked network of PDMS and a non-reactive PDMS solvent. The effective macroscopic response of this two-phase viscoelastic composite was captured with the help of the commercially available multiscale material modeling software, Digimat.

The Digimat software has the option of using several modules. Sequential multiscale modeling can be implemented through Digimat-MF, a mean field homogenization module, and Digimat-FE, a direct finite element analysis module. The one most suited to the current study however, is the Digimat-CAE module, which uses concurrent multiscale modeling and interfaces between Digimat-MF/FE and the macroscale analysis software. Instead of computing the overall properties of the composite material in the beginning of the analysis and keeping them constant throughout the Abaqus simulation, Digimat-CAE calculates the changing material properties of the composite at each iteration. Thus Abaqus and Digimat are in constant communication with each other throughout the simulation, with Digimat supplying the material definition at each integration point and at each time step, and Abaqus supplying the current load and stress state of the material for Digimat to update its computation [20]. Digimat-MF offers Mori-Tanaka, Double-Inclusion and Multi-inclusion homogenization schemes. The Mori-Tanaka model was found to be well suited for our PDMS gels.

The properties of the two viscoelastic phases of the microstructure are represented by a Prony series. The Prony series is based on the Generalized Maxwell model of viscoelasticity, which uses several spring and dashpot elements to represent the elastic and viscous behaviors of the material respectively. As opposed to the Maxwell model, which only uses one spring and one dashpot element, this model takes into account that viscoelastic materials consist of molecular segments of varying lengths contributing to varying relaxation times.

The Prony series for the shear stress relaxation modulus is:

$$G(t) = G_0 - \sum_{i=1}^{N} G_i \left[1 - e^{-t/\tau_i}\right] \qquad \text{---------- } \textit{Equation 2.1}$$

where $G_0 = G(t=0)$ is the elastic shear modulus.

Normalizing Eq. 2.1 by G_0, we obtain the dimensionless shear stress relaxation modulus as:

$$g(t) = \frac{G(t)}{G_0} = 1 - \sum_{i=1}^{N} g_i \left[1 - e^{-t/\tau_i}\right] \qquad \text{---------- } \textit{Equation 2.2}$$

where N, $g_i = \frac{G_i}{G_0}$ and τ_i are material constants which can be obtained by curve-fitting Eq. 2.2 to experimental data obtained from a stress relaxation test on the material.

The Prony series used to represent the material phases in the present study were calculated from the shear storage modulus *(G')* and shear loss modulus *(G'')* obtained from rheological tests. The rheological experiments on the solvent phases were conducted by the ARL and those on the solvent-extracted matrix phases by Dr. Roza Mahmoodian of the Van Vliet Group. The extraction of the solvent from the gels to obtain the matrix phases for testing was performed by Wen Shen of the Van Vliet Group. Appendix A1 describes this solvent extraction procedure in detail.

The shear storage and shear loss moduli are represented in terms of Prony series parameters as follows [41]:

$$G'(\omega) = G_0\left[1 - \sum_{i=1}^{N} g_i\right] + G_0 \sum_{i=1}^{N} \frac{g_i \tau_i^2 \omega^2}{1 + \tau_i^2 \omega^2} \qquad \text{---------- } \textit{Equation 2.3}$$

$$G''(\omega) = G_0 \sum_{i=1}^{N} \frac{g_i \tau_i \omega}{1 + \tau_i^2 \omega^2} \qquad \text{---------- } \textit{Equation 2.4}$$

The number of terms in the series N is assumed and initial estimates for parameters G_0, g_i and τ_i are used to calculate $G'(\omega)$ and $G''(\omega)$ using Equation 2.3 and Equation 2.4. The least square errors between these calculated values and the experimental values are then minimized by a MATLAB optimization algorithm to get the values of the Prony series parameters. The number of Prony series terms N was assumed as 10, which was an optimal number to capture the viscoelastic nature of the range of gel phases used in the study. Appendix A2 contains the MATLAB code written by Dr. R. Mahmoodian (Van Vliet Group) to calculate the Prony series from the rheology data.

Chapter 3: Validation of Model

The computational model was validated by running simulations of impact indentation on four PDMS gel samples fabricated by the ARL, and comparing their energy dissipation characteristics with those obtained from the experiments run by Dr. I. Kalcioglu (Van Vliet Group). The viscoelastic properties of the solvent and network phases of the gels as well as the volume fraction of the phases were used as the material input for Digimat. The Prony series used to represent the viscoelastic nature of the phases were obtained by Dr. R. Mahmoodian (Van Vliet Group) by the method described in Section 2.2.3.

Table 3.1 describes the parametric features of the four composite polymer gels used for validation. These gels were chosen because they were the least sticky of all the fabricated samples, reducing the effects of adhesion in the experiment. This was an important criterion since adhesion was not modeled in the simulation.

Designation used in present work	Solvent Molecular Weight (kg/mol)	Solvent designation used in [7], [11]	Solvent Volume Fraction (%)	Network Volume Fraction (%)	Stoichiometric ratio of network phase (silane:vinyl)
Gel 1	308	T308	50	50	4:1
Gel 2	308	T308	60	40	4:1
Gel 3	139	T139	60	40	4:1
Gel 4	139	T139	60	40	3:1

Table 3.1: *PDMS gel designation and composite parameters*

Tables 3.2 - 3.5 detail the Prony series parameters (G_0, g_i, τ_i) of the network and solvent phases of the four composite PDMS gels. The dynamic modulus of the network and solvent phases of these gels calculated from the Prony series using Equations 2.3 and 2.4 are shown in Figures 3.1 - 3.4.

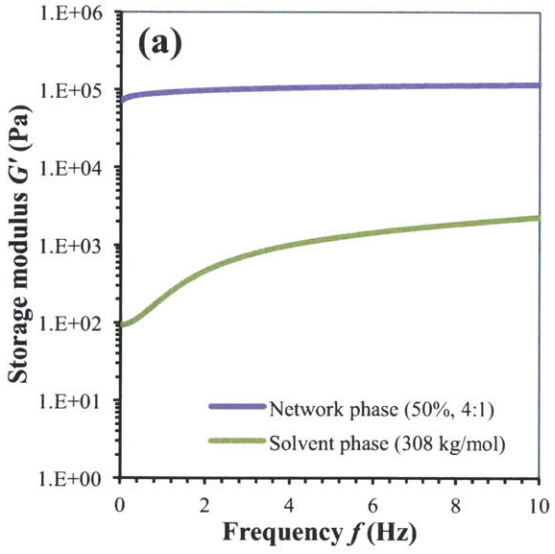

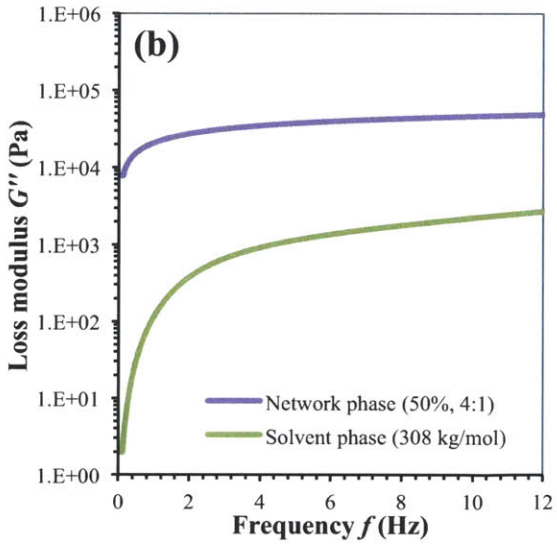

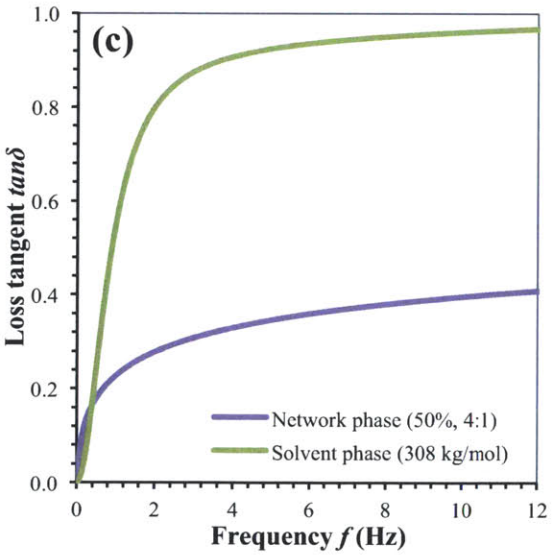

Figure 3.1: ***(a)*** *Storage modulus,* ***(b)*** *Loss modulus and* ***(c)*** *Loss tangent of network and solvent phases of Gel 2 (Experimental data on solvent phase acquired by ARL collaborators, J. Lenhart and R. Mrozek. Experimental data on network phase acquired by Dr. R. Mahmoodian, Van Vliet Group)*

Network phase (50%, 4:1)		**Solvent phase (308 kg/mol)**	
G_0 = 92.962 kPa		G_0 = 189.64 kPa	
τ_i (s)	g_i	τ_i (s)	g_i
0.0100	0.0554	0.0100	0.6761
0.0278	0.1368	0.0373	0.0747
0.0774	0.0646	0.1390	0.2325
0.2154	0.0942	0.5180	0.0030
0.5995	0.0709	1.9307	0.0127
1.6681	0.0620		
4.6416	0.0507		
12.915	0.0341		
35.938	0.0221		
100.00	0.0381		

Table 3.2: *Prony series parameters for network and solvent phases of Gel 1 (Data acquired by Dr. R. Mahmoodian, Van Vliet Group)*

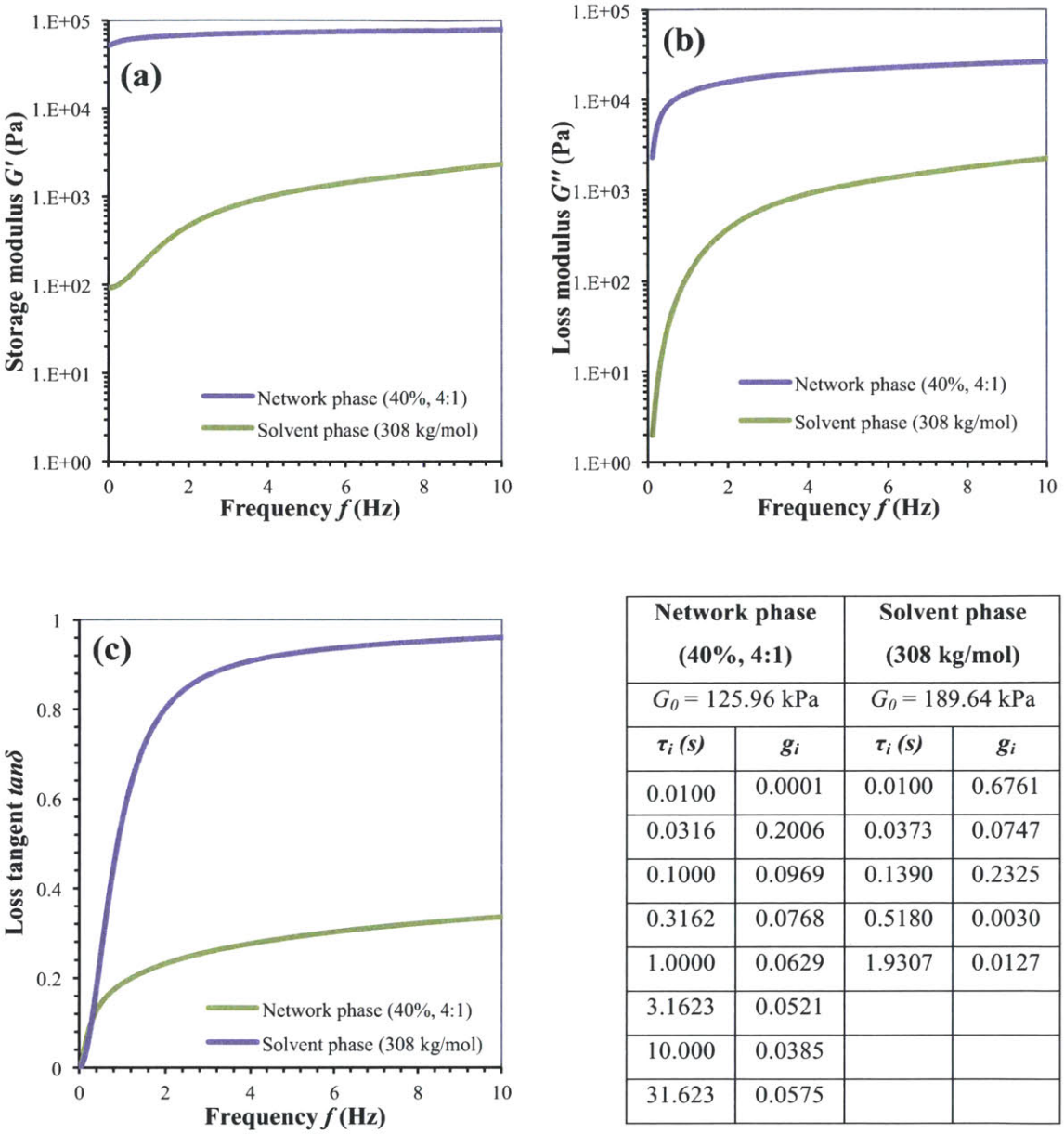

Figure 3.2: *(a) Storage modulus, (b) Loss modulus and (c) Loss tangent of network and solvent phases of Gel 2 (Experimental data on solvent phase acquired by ARL collaborators, J. Lenhart and R. Mrozek. Experimental data on network phase acquired by Dr. R. Mahmoodian, Van Vliet Group)*

Network phase (40%, 4:1)		**Solvent phase (308 kg/mol)**	
G_0 = 125.96 kPa		G_0 = 189.64 kPa	
τ_i (s)	g_i	τ_i (s)	g_i
0.0100	0.0001	0.0100	0.6761
0.0316	0.2006	0.0373	0.0747
0.1000	0.0969	0.1390	0.2325
0.3162	0.0768	0.5180	0.0030
1.0000	0.0629	1.9307	0.0127
3.1623	0.0521		
10.000	0.0385		
31.623	0.0575		

Table 3.3: *Prony series parameters for network and solvent phases of Gel 2 (Data acquired by Dr. R. Mahmoodian, Van Vliet Group)*

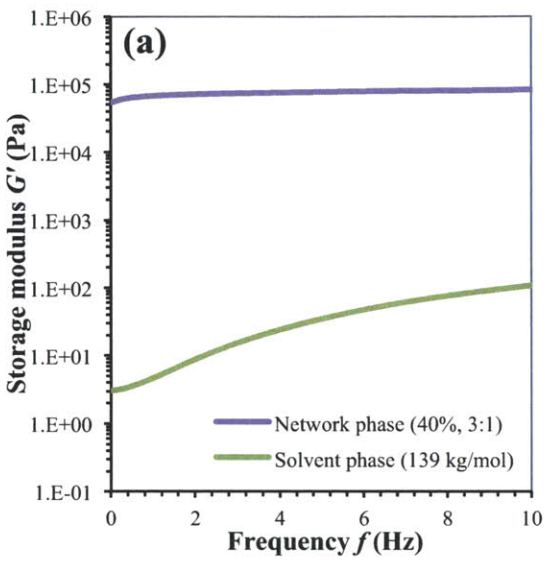

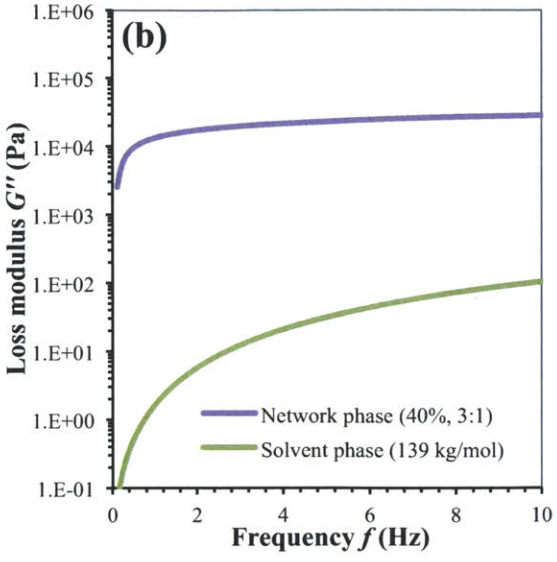

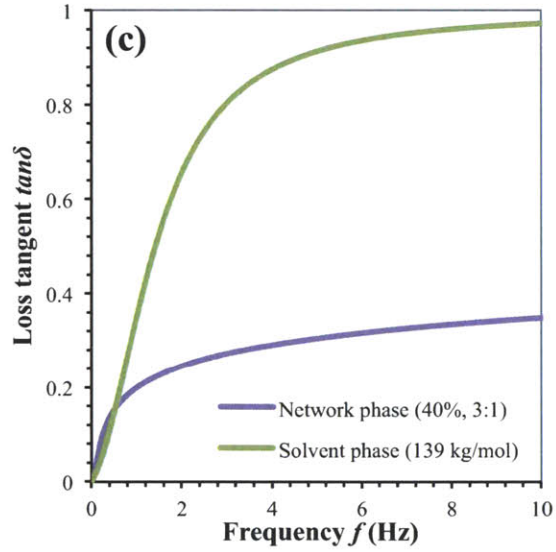

Figure 3.3: ***(a)*** *Storage modulus,* ***(b)*** *Loss modulus and* ***(c)*** *Loss tangent of network and solvent phases of Gel 3 (Experimental data on solvent phase acquired by ARL collaborators, J. Lenhart and R. Mrozek. Experimental data on network phase acquired by Dr. R. Mahmoodian, Van Vliet Group)*

Network phase (40%, 3:1)		**Solvent phase (139 kg/mol)**	
G_0 = 125.96 kPa		G_0 = 189.64 kPa	
τ_i (s)	g_i	τ_i (s)	g_i
0.0100	0.0190	0.0100	0.9327
0.0316	0.2314	0.0631	0.0615
0.1000	0.0677	0.3981	0.0057
0.3162	0.0804		
1.0000	0.0591		
3.1623	0.0521		
10.000	0.0399		
31.623	0.0588		
100.00	0.0001		

Table 3.4: *Prony series parameters for network and solvent phases of Gel 3 (Data acquired by Dr. R. Mahmoodian, Van Vliet Group)*

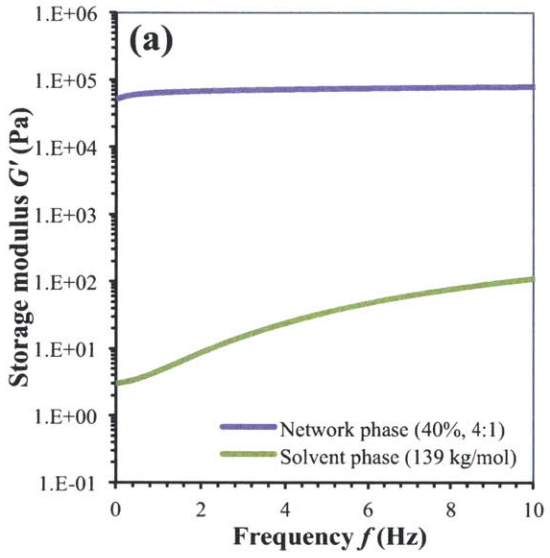

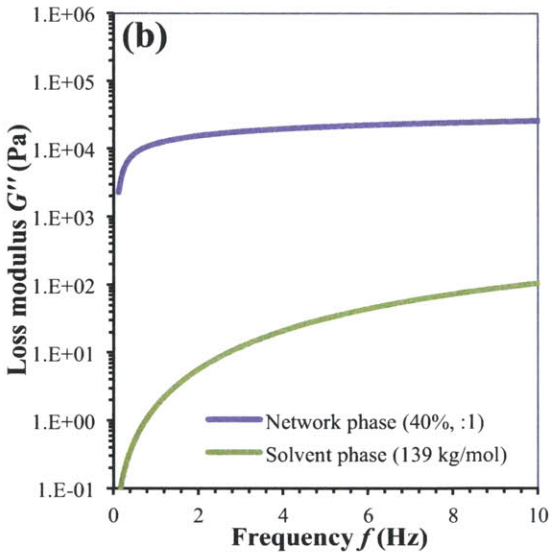

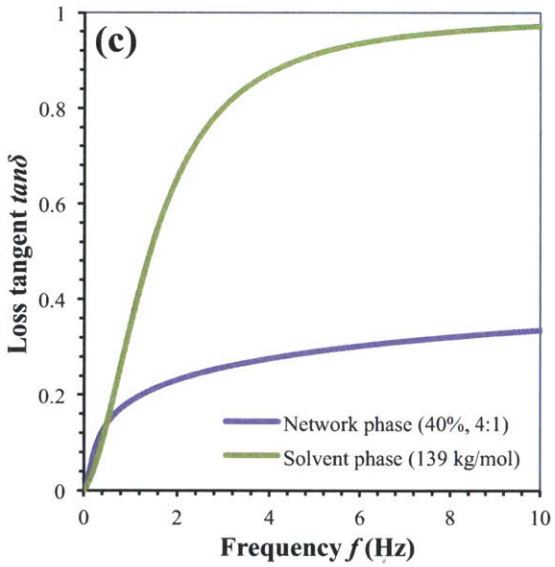

Figure 3.4: ***(a)*** *Storage modulus,* ***(b)*** *Loss modulus and* ***(c)*** *Loss tangent of network and solvent phases of Gel 4 (Experimental data on solvent phase acquired by ARL collaborators, J. Lenhart and R. Mrozek. Experimental data on network phase acquired by Dr. R. Mahmoodian, Van Vliet Group)*

Network phase (40%, 4:1)		**Solvent phase (139 kg/mol)**	
G_0 = 125.96 kPa		G_0 = 189.64 kPa	
τ_i (s)	g_i	τ_i (s)	g_i
0.0100	0.0001	0.0100	0.9327
0.0316	0.2006	0.0631	0.0615
0.1000	0.0969	0.3981	0.0057
0.3162	0.0768		
1.0000	0.0629		
3.1623	0.0521		
10.000	0.0385		
31.623	0.0575		

Table 3.5: *Prony series parameters for network and solvent phases of Gel 4 (Data acquired by Dr. R. Mahmoodian, Van Vliet Group)*

3.1 Parameters of Comparison: K, Q, x_{max}

Three parameters were used to quantify the energy dissipation characteristics of the material (tissue or polymer gel). They were used for comparison between experimental and simulated data.

1. Energy dissipation capacity, K

   This is a measure of the energy dissipated during the initial impact of the indenter (Figure 3.5). It is defined as

$$K = \frac{Energy\ dissipated\ by\ the\ material\ during\ the\ first\ impact\ cycle}{Energy\ input\ into\ the\ material\ during\ the\ first\ impact\ cycle}$$

$$K = \frac{E_{in} - E_{out} - E_{dp}}{E_{in} - E_{dp}} \quad [J/J]$$

$$E_{in} = \frac{1}{2}mv_{in}^2 + \frac{1}{2}kx_{in}^2\ ,\ E_{out} = \frac{1}{2}mv_{out}^2 + \frac{1}{2}kx_{out}^2$$

$$x_{in} = x_{eq} - d_{in}\ ,\ x_{out} = x_{eq} - d_{out}$$

   where m is the mass (in kg) and k is the spring constant (in N/m) of the pendulum or spring. v_{in} and v_{out} are the velocities (in m/s) of the indenter at the beginning and end of the first impact cycle, respectively. Hence the terms $\frac{1}{2}mv_{in}^2$ and $\frac{1}{2}mv_{out}^2$ are the kinetic energies (in J) of the indenter at the beginning and end of the cycle. In the experiment; x_{in} and x_{out} are the distances (in m) between the equilibrium plane of the pendulum and the positions of the pendulum at the beginning and end of the first impact cycle. In the simulation, x_{in} and x_{out} correspond to the compressive displacement (in m) on the spring from its equilibrium state, at the beginning and end of the first impact cycle. Hence the terms $\frac{1}{2}kx_{in}^2$ and $\frac{1}{2}kx_{out}^2$ are the potential energies (in J) of the indenter at the beginning and end of the cycle. In the experiment, x_{eq} is the distance between the equilibrium plane of the pendulum and the free surface of the sample. In the simulation, x_{eq} is the initial compressive displacement applied on the spring in Step One of loading (Section 2.2.2). d_{in} and d_{out}

are the displacements (in m) of the indenter from the free surface of the sample at the beginning and end of the cycle, respectively. E_{in} and E_{out} are the total energies (in J) of the indenter at the beginning and end of the cycle. E_{dp} is the energy dissipated (in J) by the pendulum or spring during the cycle through damping. Appendix A3 contains the MATLAB code used to calculate K.

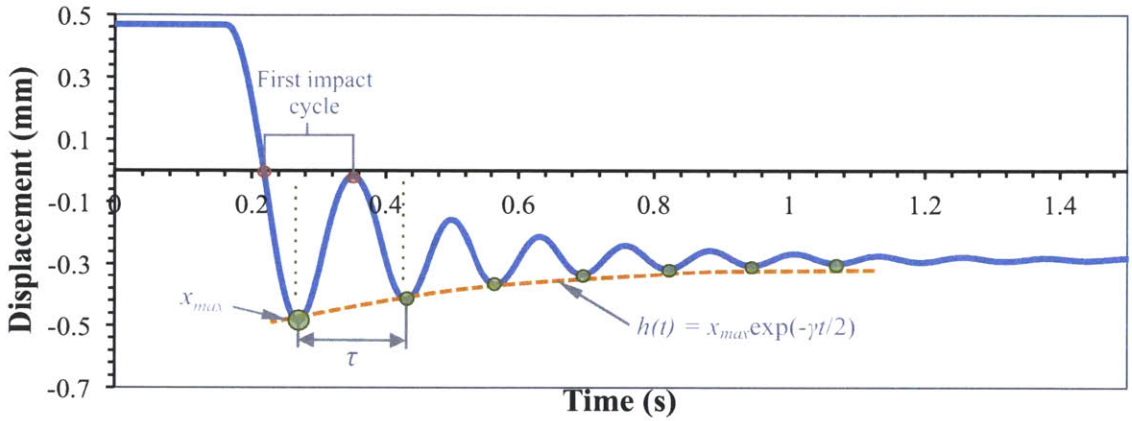

Figure 3.5: *Sample displacement profile of a PDMS gel to describe Q and* x_{max}

2. Quality factor, Q

   This is a measure of energy dissipation rate, proportional to

$$Q \sim \frac{2\pi}{\tau\gamma} \text{ [unitless]}$$

   The peaks of the displacement profile are fitted to an exponentially time-dependent curve

$$h(t) = x_{max}e^{-\gamma t/2}$$

   where τ is the time period between the first two peaks in seconds (Figure 3.5) and γ is the exponential coefficient in 1/second. Appendix A4 contains the MATLAB code used to calculate Q.

3. Maximum penetration depth, x_{max}

   This is the maximum depth (in mm) that the indenter penetrates during the initial impact, measured from the unindented free surface of the sample. It is a measure of impact resistance of the material. It is calculated by finding the minimum of the displacement profile (Figure 3.5).

3.2 Validation of Multiscale Approach

The simulated responses of Gel 1 obtained when using the concurrent multiscale Abaqus-Digimat model described in Section 2.2 were compared with those obtained when using a macroscale Abaqus model and a sequential multiscale Abaqus-Digimat model. The macroscale simulation with Abaqus defines the polymer on the continuum level only as a homogenous viscoelastic material. The Prony series parameters of this material, which were calculated from rheological experiments on the composite gel conducted by Dr. R. Mahmoodian (Van Vliet Group), are listed in Table 3.6 and its dynamic modulus is shown against those of the composite phases in Figure 3.6. In the sequential multiscale Abaqus-Digimat model, the Prony series of the two microscale phases are first input into Digimat, which computes the properties an equivalent single-phase macroscale material using a homogenization method. The Prony series of this equivalent Digimat material is then used in the Abaqus simulation to obtain the energy dissipation response. The Prony series of the equivalent Digimat material is listed in Table 3.7 and its dynamic modulus is also shown in Figure 3.6. As expected, the storage and loss moduli of the composite gel and the equivalent Digimat material lie in between those of the solvent and network phases.

Composite material (Gel 1)			
$G_0 = 111.36$ kPa			
τ_i (s)	g_i	τ_i (s)	g_i
0.0100	0.0468	0.7627	0.0130
0.0172	0.0086	1.3111	0.0805
0.0296	0.0397	3.8747	0.0420
0.0508	0.0326	6.6608	0.0033
0.0873	0.1024	11.450	0.0121
0.1501	0.0970	19.684	0.0166
0.2581	0.1572	100.00	0.0243
0.4437	0.0546		

Table 3.6: *Prony series parameters for composite Gel 1 (Data acquired by Dr. R. Mahmoodian, Van Vliet Group)*

Equivalent Digimat material			
$G_0 = 151.28$ kPa			
τ_i (s)	g_i	τ_i (s)	g_i
0.0100	0.0233	1.0000	0.1156
0.0215	0.0458	2.1544	0.0887
0.0462	0.0088	4.6414	0.0641
0.1000	0.0487	10.000	0.0100
0.2154	0.0093	21.544	0.0348
0.4642	0.3183	100.00	0.0394

Table 3.7: *Prony series parameters for equivalent Digimat material for Gel 1*

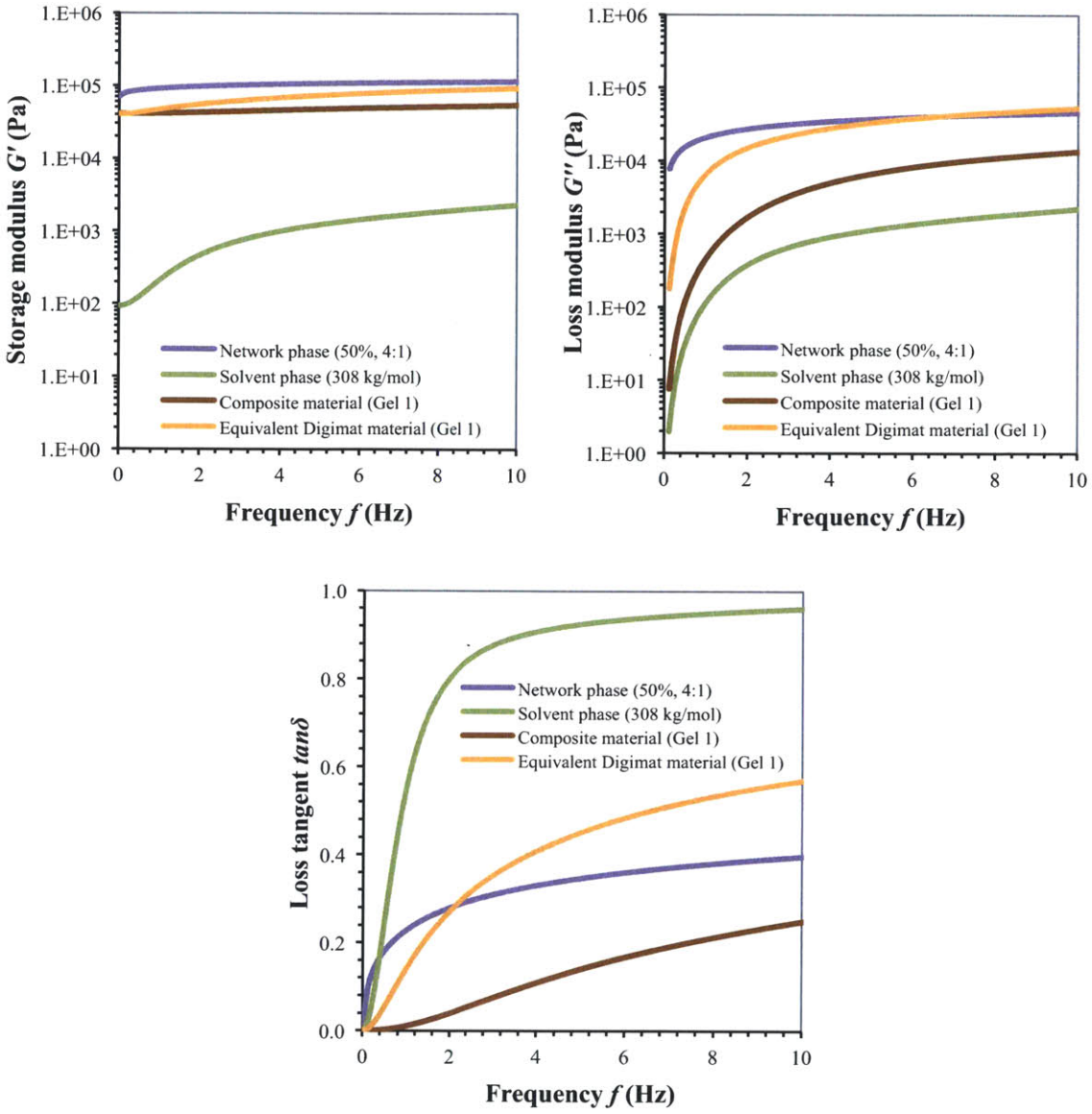

Figure 3.6: ***(a)*** *Storage modulus,* ***(b)*** *Loss modulus and* ***(c)*** *Loss tangent of network phase, solvent phase, composite material and equivalent Digimat material of Gel 1 (Experimental data on solvent phase acquired by ARL collaborators, J. Lenhart and R. Mrozek. Experimental data on network phase and composite gel acquired by Dr. R. Mahmoodian, Van Vliet Group)*

All loading and boundary conditions were kept the same in all three cases, the only difference being the way in which the material was defined. In the case of the macroscale model, Gel 1 is considered as homogenous and the Prony series of this overall composite material is used to define the material in Abaqus. In the sequential and concurrent multiscale models, Gel 1 is considered as a two-phase material that is heterogeneous at

the microscale and the Prony series of the two phases are used to define the material in Digimat, which uses the Mori-Tanka homogenization technique in both cases. In the sequential approach, the Digimat homogenization is executed only once to compute the equivalent material properties that are then used in Abaqus to simulate the macroscale response. Whereas in the concurrent approach, Digimat computes the macroscale response due to the two-phase microstructure at each node and time step of the Abaqus simulation using the current macroscopic stress/strain field as the boundary condition for each RVE.

Figures 3.7 and 3.8 show the displacement and velocity profiles respectively for the experimental response of Gel 1 at impact velocity 16.5 mm/s, compared with the simulated responses obtained from the macroscale model, the sequential multiscale model and the concurrent multiscale Abaqus-Digimat model. We can see that the concurrent multiscale approach captures the energy dissipation behavior of the material much better under the impact loading conditions, than the other two methods. This is because the concurrent multiscale model takes into account the effect of the interactions between the network (solid inclusion) and solvent (fluid matrix) phases in the microstructure on the macroscale response at each node and time step of the simulation. Using only the Prony series of the overall composite material, whether derived from experiments, as in the macroscale model, or from Digimat homogenization, as in the sequential multiscale model, does not capture the dissipation of impact energy due to the solid-fluid interactions in the microstructure. This is clearly seen in the comparison of parameters K (Figure 3.9) and Q (Figure 3.10), which show that the energy dissipated in the first cycle as well as the energy dissipation rate in these simulations are much lower than expected from the experiments. The impact resistance measured by parameter x_{max} (Figure 3.11) is also not captured as accurately by these methods as by the concurrent multiscale model.

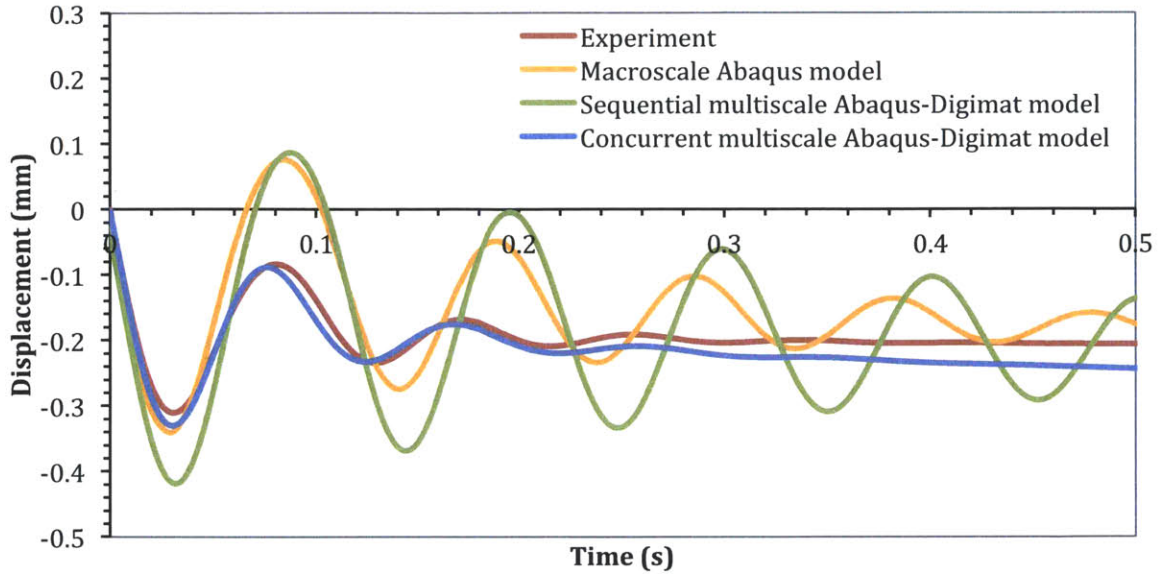

Figure 3.7: *Comparison of displacement profiles of Gel 1 from experiment, and simulations using macroscale Abaqus model, sequential Abaqus-Digimat multiscale model and concurrent Abaqus-Digimat multiscale model (impact velocity v_{in} = 16.5 mm/s)*

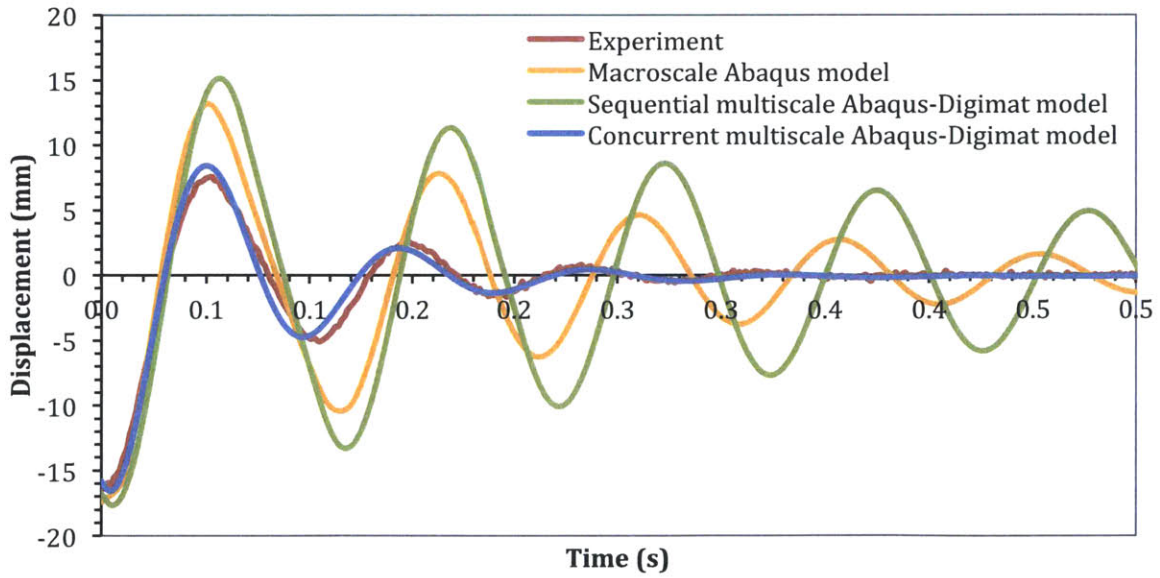

Figure 3.8: *Comparison of velocity profiles of Gel 1 from experiment, and simulations using macroscale Abaqus model, sequential Abaqus-Digimat multiscale model and concurrent Abaqus-Digimat multiscale model (impact velocity v_{in} = 16.5 mm/s)*

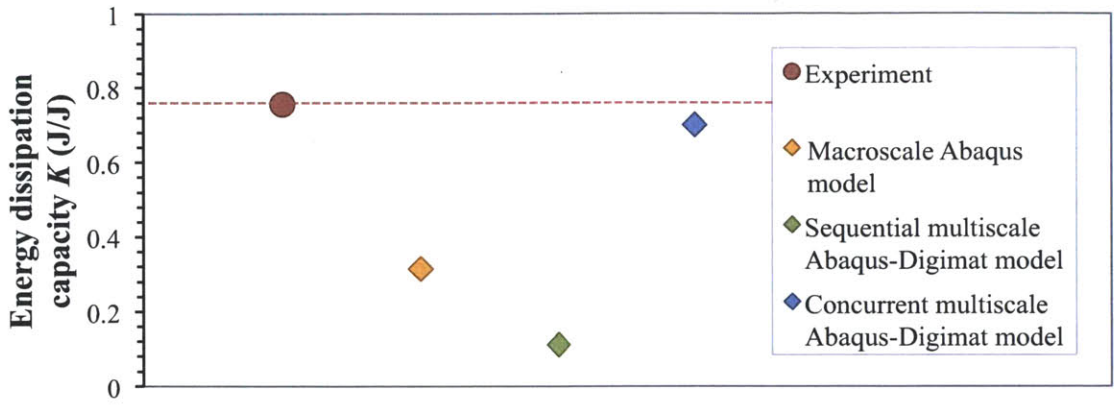

Figure 3.9: *Comparison of energy dissipation capacity K of Gel 1 from experiment, and simulations using macroscale Abaqus model, sequential Abaqus-Digimat multiscale model and concurrent Abaqus-Digimat multiscale model (impact velocity v_{in} = 16.5 mm/s)*

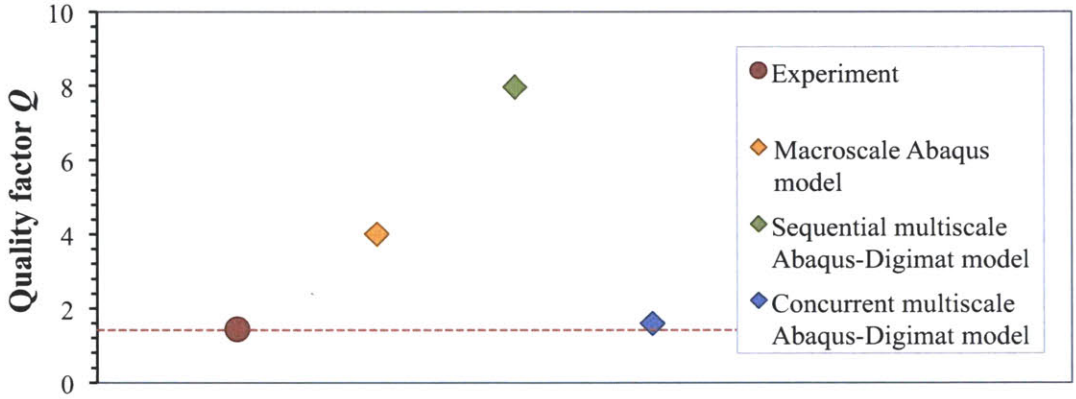

Figure 3.10: *Comparison of quality factor Q of Gel 1 from experiment, and simulations using macroscale Abaqus model, sequential Abaqus-Digimat multiscale model and concurrent Abaqus-Digimat multiscale model (impact velocity v_{in} = 16.5 mm/s)*

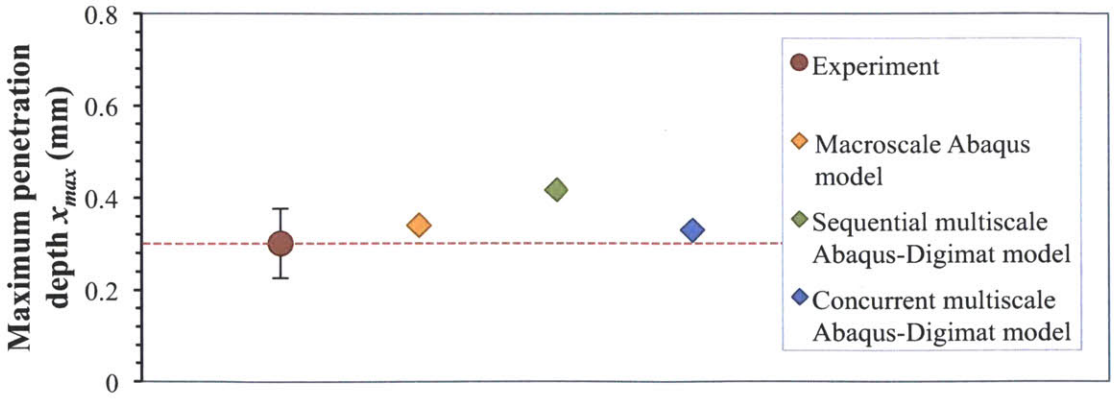

Figure 3.11: *Comparison of maximum penetration depth x_{max} of Gel 1 from experiment, and simulations using macroscale Abaqus model, sequential Abaqus-Digimat multiscale model and concurrent Abaqus-Digimat multiscale model (impact velocity v_{in} = 16.5 mm/s)*

3.3 Validation of Simulations against Experiments

The impact indentation experiments on Gels 1 to 4 were carried out by Dr. I. Kalcioglu (Van Vliet Group) over a range of impact velocities up to 20 mm/s. The different experimental impact velocities were achieved by varying the constant force applied to the pendulum through the electromagnetic voice coil. In the computational model, the same impact velocities and loading conditions were simulated by adjusting the force f_{up} applied in Step Two to move the indenter away from the sample surface and by applying the same constant experimental force f_{con} on the indenter during loading Step Three (Section 2.2.2). The K, Q and x_{max} parameters were calculated for each case and they are compared with the experimental values in this section.

The error bars for experimental and simulated Q values were calculating by considering the uncertainty in Q as explained in Section 3.5, and the error bars for the experimental K and x_{max} values were obtained by taking into account the uncertainty in the instant of contact as described in Section 3.6.

Gel 1:

Figures 3.12, 3.13 and 3.14 show the experimental and simulated K, Q and x_{max} values respectively for Gel 1 at different impact velocities. The corresponding range of impact kinetic energies was 4.5 μJ to 29.2 μJ. Simulated K for Gel 1 show good matching with experimental values with a slight deviation at higher impact velocities. The simulated Q and x_{max} values approximate the experimental values fairly well throughout the range of impact velocities.

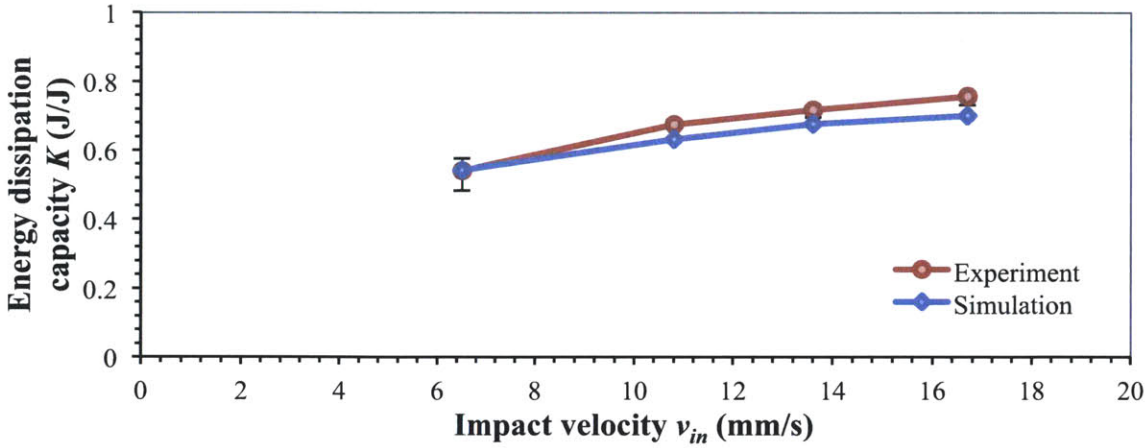

Figure 3.12: *Comparison of energy dissipation capacity K from experiment and simulation for Gel 1*

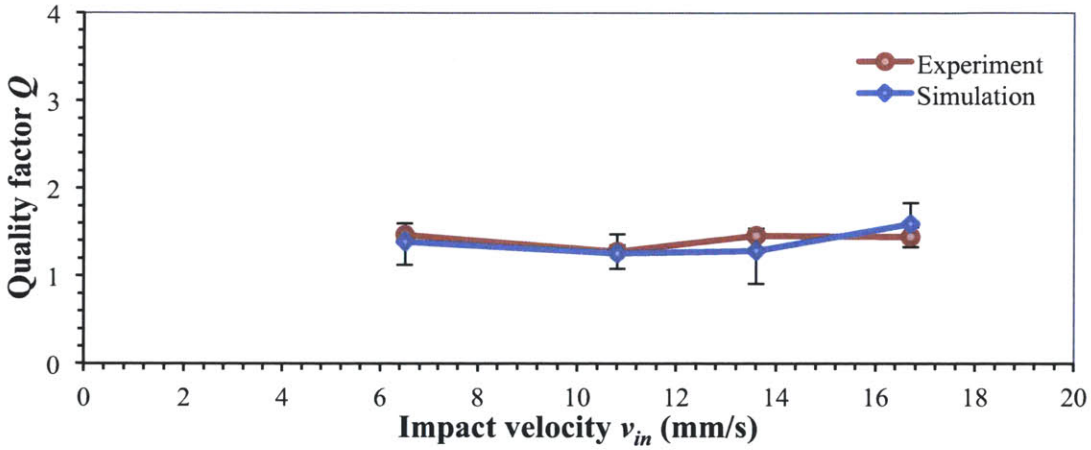

Figure 3.13*: Comparison of quality factor Q from experiment and simulation for Gel 1*

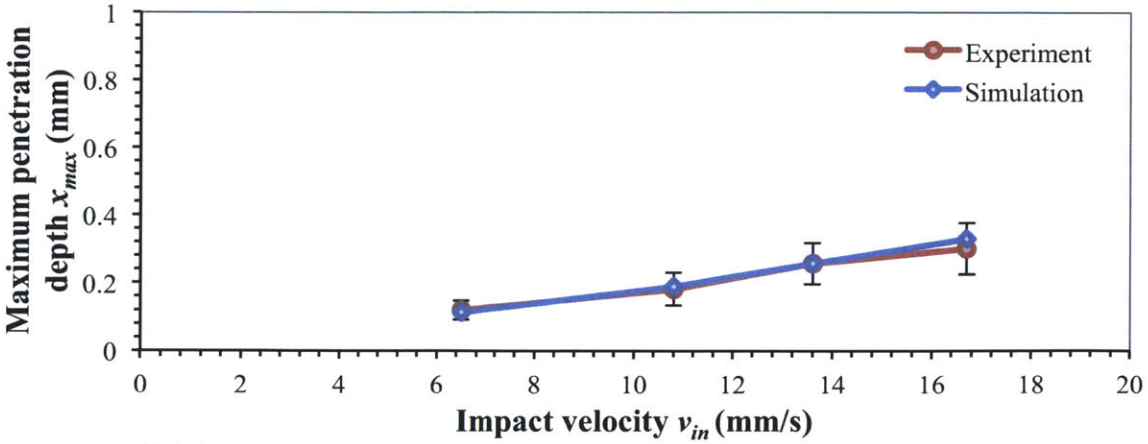

Figure 3.14: *Comparison of maximum penetration depth x_{max} from experiment and simulation for Gel 1*

Gel 2:

Gel 2 showed the best matching, among the four gels tested, between simulations and experiments for both K (Figure 3.15) and x_{max} (Figure 3.16) values at all impact velocities. The impact kinetic energies for Gel 2 ranged from 0.8 μJ to 17.6 μJ. The parameter Q could not be calculated with sufficient accuracy for comparison in Gels 2, 3 and 4. This is explained in Section 3.5.

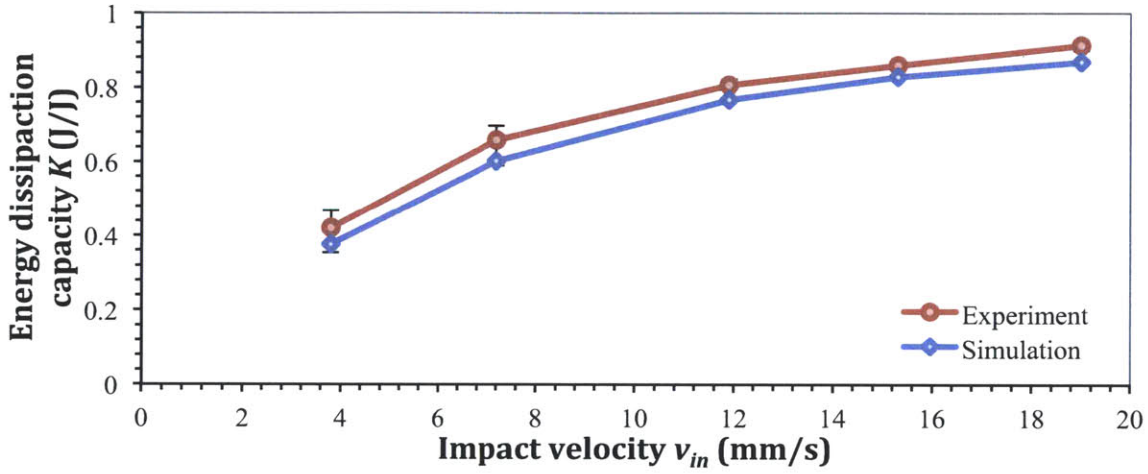

Figure 3.15: *Comparison of energy dissipation capacity K from experiment and simulation for Gel 2*

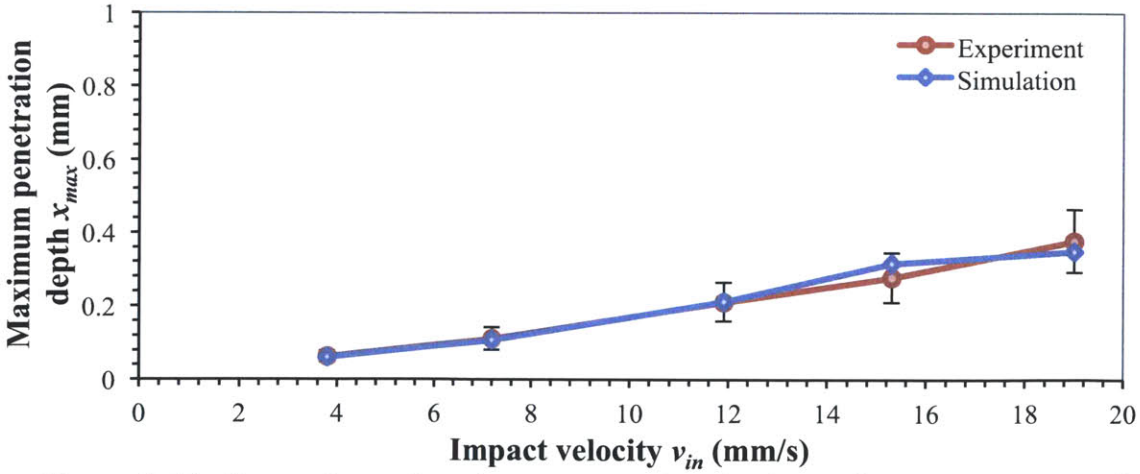

Figure 3.16: *Comparison of maximum penetration depth x_{max} from experiment and simulation for Gel 2*

Gel 3:

Figure 3.17 compares the experimental and simulated K values for Gel 3, showing that the simulated values deviating lower than the experimental ones at higher impact velocities. Figure 3.18 compares the x_{max} values, and we see that the simulated values are slightly higher than the experimental ones at higher velocities. The range of impact kinetic energies for Gel 3 was 1.6 μJ to 38.4 μJ.

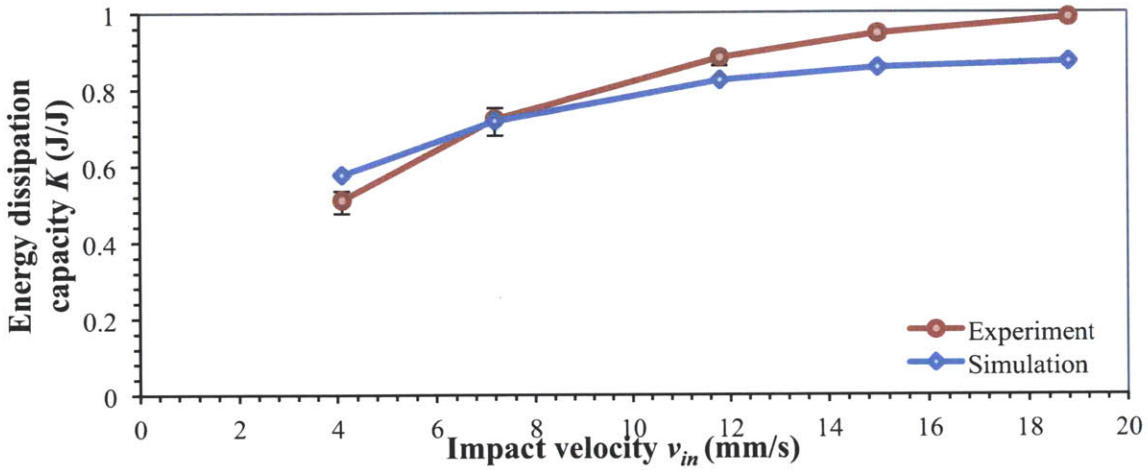

Figure 3.17: *Comparison of energy dissipation capacity K from experiment and simulation for Gel 3*

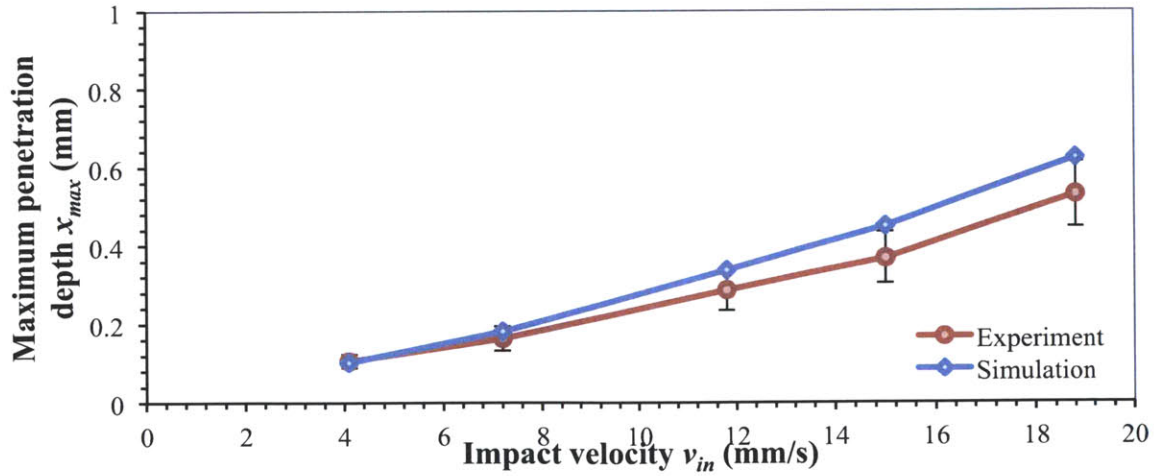

Figure 3.18: *Comparison of maximum penetration depth x_{max} from experiment and simulation for Gel 3*

Gel 4:

Figures 3.19 and 3.20 compare the K and x_{max} parameters respectively from experiments and simulations on Gel 4. The range of impact kinetic energies was 1.8 μJ to 40.5 μJ. The K and x_{max} values show good matching at lower impact velocities but there is a divergence at higher velocities.

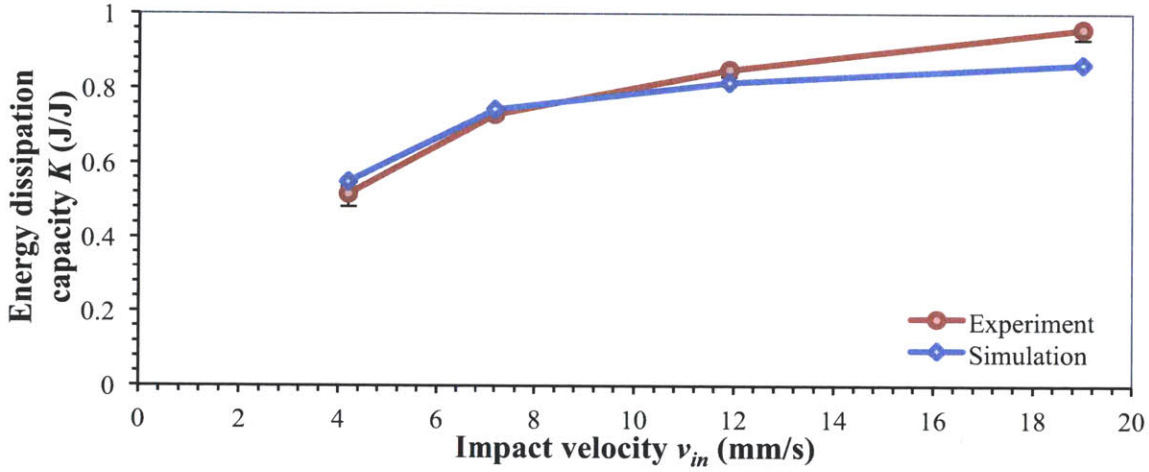

Figure 3.19: *Comparison of energy dissipation capacity K from experiment and simulation for Gel 4*

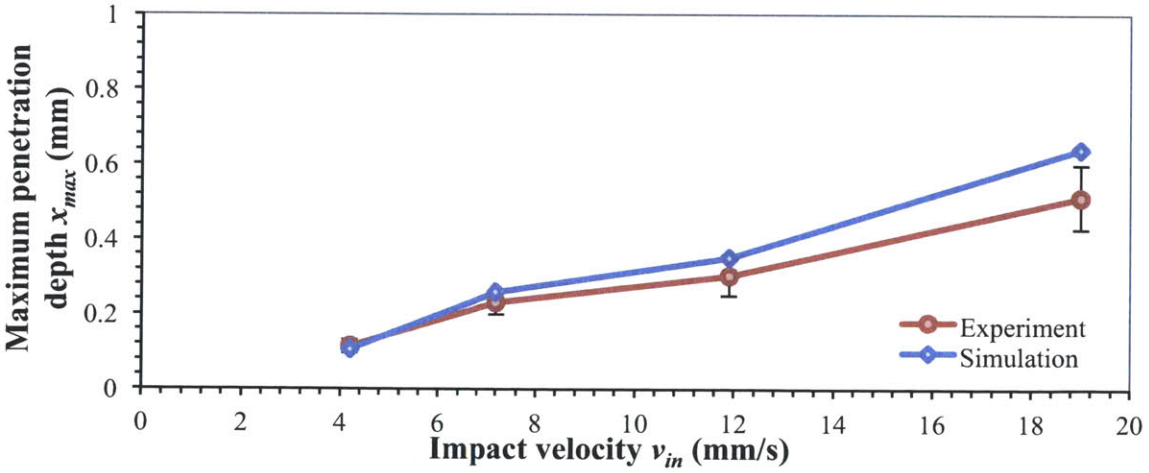

Figure 3.20: *Comparison of maximum penetration depth x_{max} from experiment and simulation for Gel 4*

3.4 Effect of Adhesion

Although the gels chosen for comparison with simulations were the least sticky of the fabricated samples, adhesion does play a role in the experiment. Several of the fabricated gel samples had to be disregarded for the validation purposes of this work, since the adhesive forces active in the experiment could not be accounted for accurately in this simulation model.

Figures 3.21 and 3.22 show the displacement and velocity profiles for experimental and simulated response for a gel that was not used for validation because it was too sticky. The gel had a solvent molecular weight of 1.1 kg/mol, 60% solvent loading and a 2.25:1 stoichiometric ratio. We can see from the experimental velocity profile that the energy is dissipated very quickly without many cycles. K and x_{max} were much lower in the simulation than in the experiment, and Q could not be calculated accurately from the experimental profile. It was concluded that this additional dissipation was due to the adhesive forces between the sample surface and the pendulum.

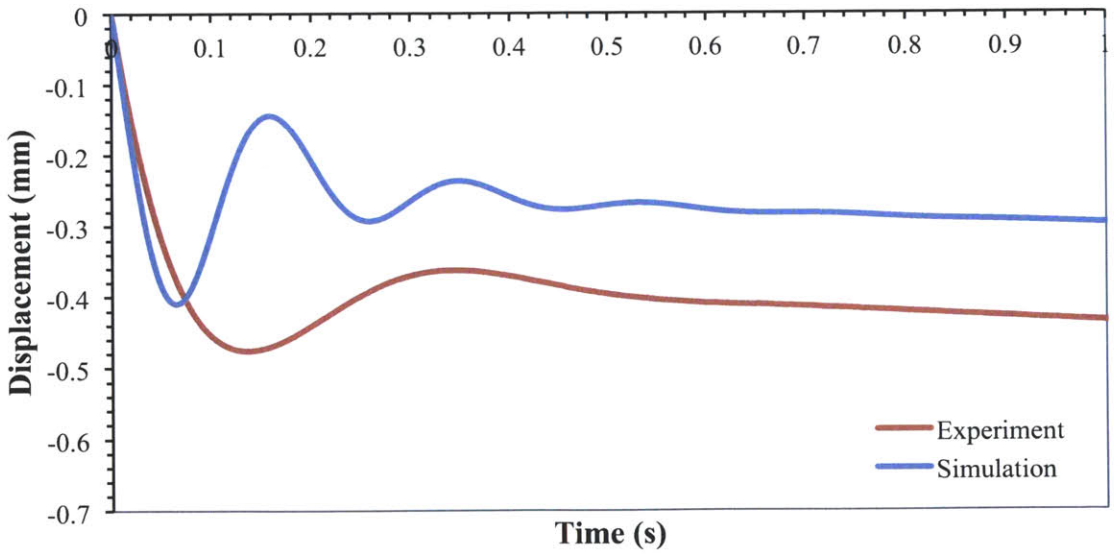

Figure 3.21: *Comparison of displacement profiles from experiment and simulation for a sticky gel (solvent molecular weight 1.1 kg/mol, solvent volume fraction 60%, stoichiometric ratio 2.25:1) at impact velocity v_{in} = 9.6 mm/s (impact kinetic energy = 9.9 μJ)*

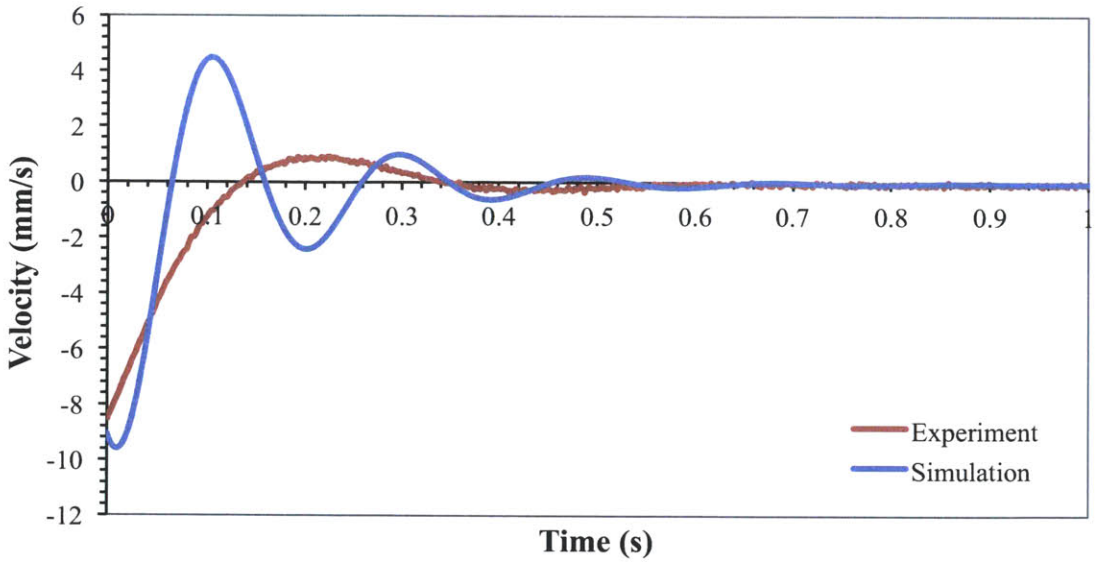

Figure 3.22: *Comparison of velocity profiles from experiment and simulation for a sticky gel (solvent molecular weight 1.1 kg/mol, solvent volume fraction 60%, stoichiometric ratio 2.25:1) at impact velocity v_{in} = 9.6 mm/s (impact kinetic energy = 9.9 μJ)*

Adhesion is due to intermolecular forces, usually van der Waals forces, between two surfaces, when they are in close proximity. During the indentation experiment on a sticky gel sample, adhesive interaction between the polymer gel surface and the pendulum surface plays a significant role in the energy dissipation response of the gel, through both normal and lateral adhesive forces.

Incorporating adhesion in finite element models usually involves using the Lennard-Jones function (Figure 3.23(a)), which most realistically represents the van der Waals interaction between surfaces [42]. Alternatively, a simpler approximation of the Lennard-Jones model, namely the triangular model (Figure 3.23(b)), can be used [43]. This is the model used by Abaqus in its cohesive element formulation.

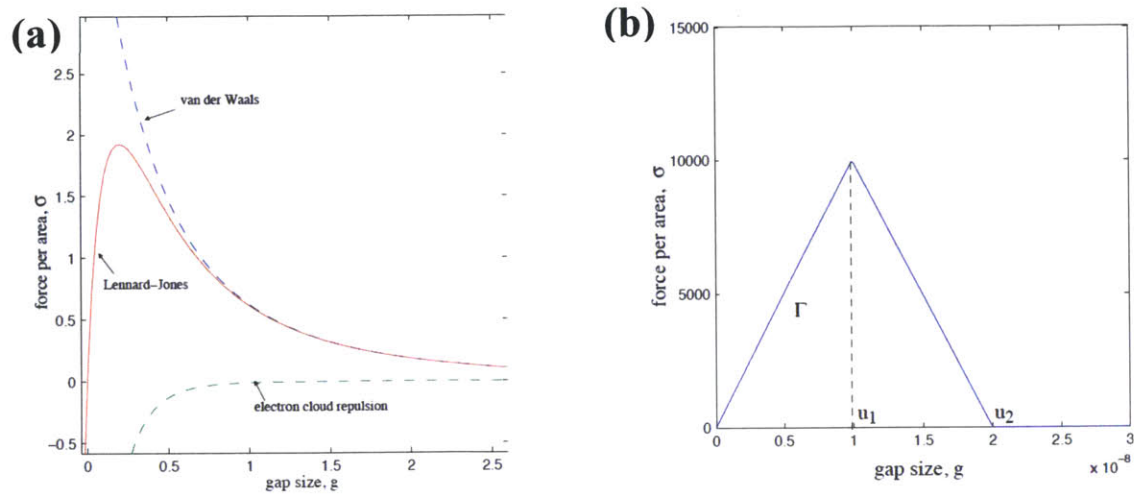

Figure 3.23: (a) *Lennard-Jones model and* ***(b)*** *Triangular model for adhesion between surfaces (Images from [43])*

The models in Figure 3.23 assume that the attractive forces of adhesion act within a certain gap size between the two surfaces, and that they are zero when the gap is zero. However, in our indentation experiment, once the initial contact of the pendulum with the gel surface is established, they remain in contact for the remainder of the response. Therefore, a model that uses zero force at zero gap between surfaces would be inadequate to represent the adhesive interaction in the experiment. This is why the cohesive elements in Abaqus could not be used to account for adhesion in the finite element model.

Instead of using Abaqus' triangular model for adhesion, a body force on the pendulum proportional to its penetration depth into the surface of the gel was considered. This was based on the assumption that the adhesive force must be proportional to the surface area of the pendulum (including the flat surface and the cylindrical sides) in contact with the gel surface, which in turn must be proportional to the penetration depth for an axisymmetric flat-tipped pendulum. Since there was no way of knowing the proportionality constant for such a linear relationship, different constants were tried out, so that we could get a qualitative idea of how this model of adhesion would affect the simulated response.

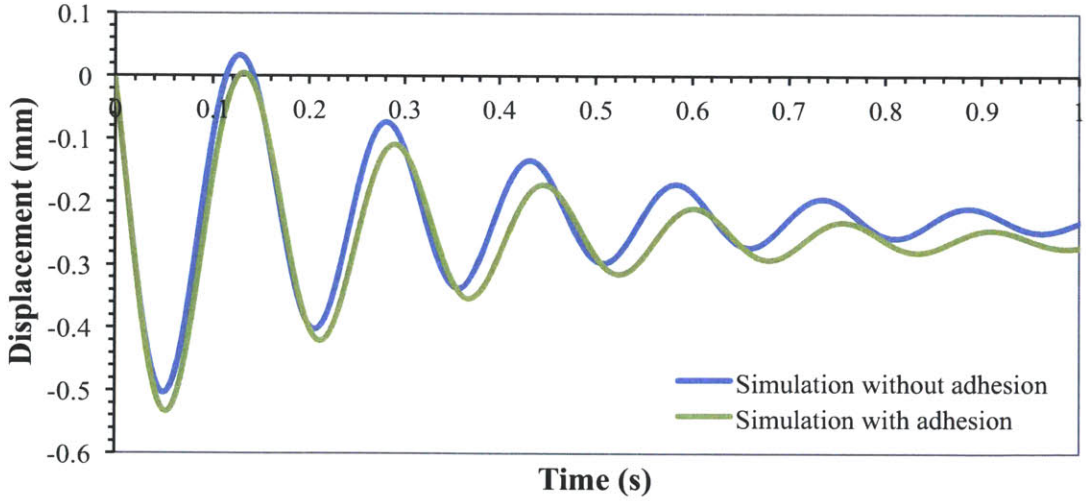

Figure 3.24: *Comparison of simulated displacement profiles without and with adhesion model for a PDMS gel (solvent molecular weight 1.1 kg/mol, solvent volume fraction 50%, stoichiometric ratio 4:1) at impact velocity v_{in} = 13.8 mm/s (impact kinetic energy = 20.5 μJ)*

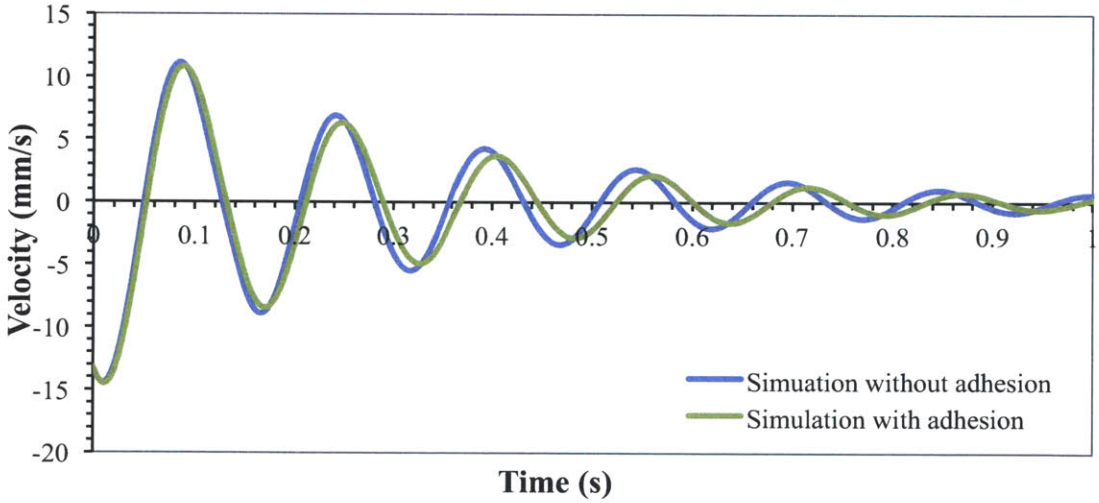

Figure 3.25: *Comparison of simulated velocity profiles without and with adhesion model for a PDMS gel (solvent molecular weight 1.1 kg/mol, solvent volume fraction 50%, stoichiometric ratio 4:1) at impact velocity v_{in} = 13.8 mm/s (impact kinetic energy = 20.5 μJ)*

Figures 3.24 and 3.25 compare the displacement and velocity profiles of the simulated responses of a PDMS gel of solvent molecular weight 1.1 kg/mol, solvent volume fraction 50% and stoichiometric ratio 4:1, without any adhesion and with the above assumed adhesion model. With adhesion, K and x_{max} were found to increase, and Q was

found to decrease. The increase in K and x_{max} as an effect of adhesion was as expected, but did not adequately account for the increased dissipation of energy in the sticky gels such as the one showed in Figure 3.22.

It is probable that the adhesive forces in the indentation experiment are also a function of the velocity of the indenter. This was not successfully modeled in the present study.

3.5 Uncertainty in Q

The parameter Q could not be calculated accurately for some gels used in the study. As explained in Section 3.1, Q is calculated by fitting an exponential curve to the peaks of the displacement profile. However, the displacement profiles for gels like Gel 2 (Figure 3.26) do not have a discernible third peak, making it problematic to fit an exponential curve. The Q values also differed depending on how many peaks were considered in fitting the exponential curve. The error bars for the experimental and simulated Q values in Section 3.3 were calculated by fitting exponential curves to different number of peaks and taking the lowest and highest values of Q obtained.

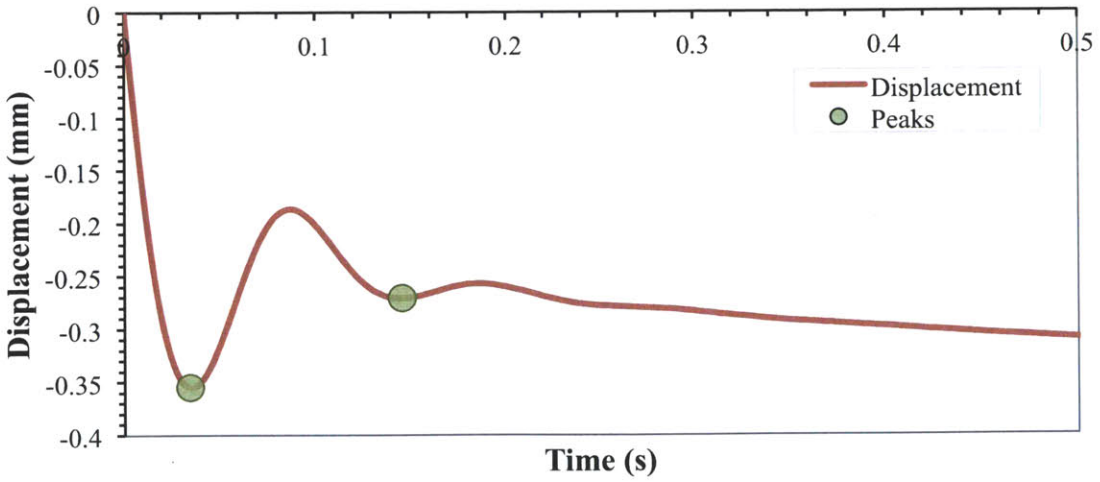

Figure 3.26: *Displacement profile from experiment on Gel 2 at impact velocity v_{in} = 12.8 mm/s (impact kinetic energy = 17.6 μJ) showing the peaks*

3.6 Uncertainty in Experimental Point of Contact

In the impact indentation experiments, the surface of the sample is not in the plane of vertical equilibrium of the pendulum (length L = 45 mm) but rather forward of it by 0.5 mm. This means that the flat punch indenter first makes contact with the sample with its edge at angle of 0.64° and not its entire flat surface (Figure 3.27). This makes it hard to detect the actual instant of contact of the indenter with the sample in the experiment.

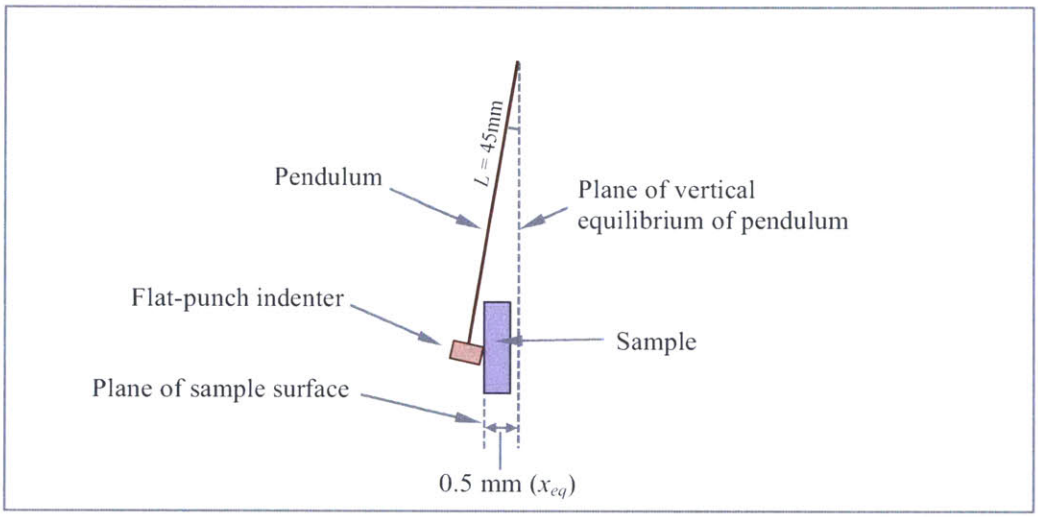

Figure 3.27: *Schematic showing how the flat-punch indenter contacts the sample surface edge-first*

Figures 3.28 and 3.29 show the experimental velocity and displacement profiles respectively for a sample gel with only the initial contact calibration with the Berkovich tip, and compare them to the simulated profiles. It can be seen that the experimental velocity profile appears to be shifted forward in comparison to the simulated one. This can be explained if we correct the experimental instant of contact to be the time when the velocity drops sharply (Figure 3.28).

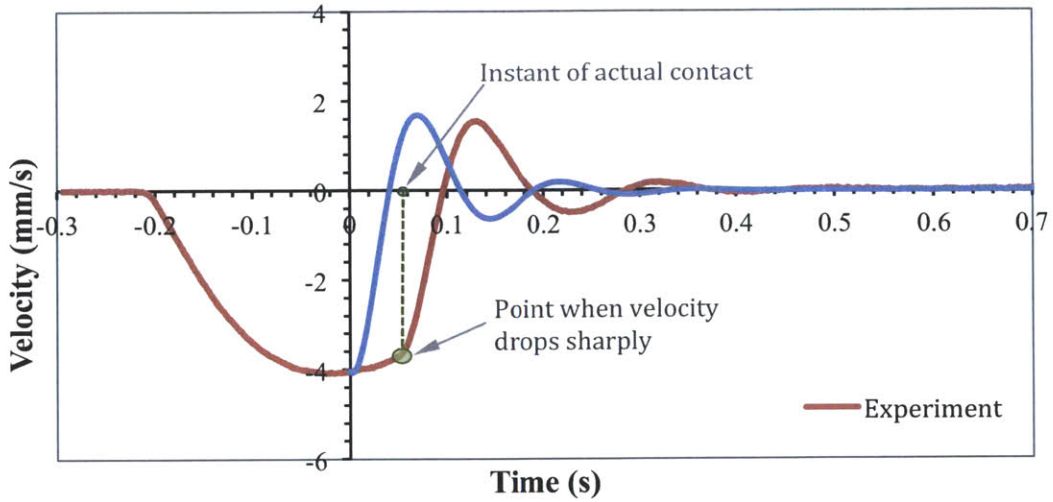

Figure 3.28: *Comparison of velocity profiles from experiment (without corrected point of contact) and simulation for Gel 4 at impact velocity v_{in} = 4.1 mm/s (impact kinetic energy = 1.8 μJ)*

This correction in the instant of contact requires us to also adjust the displacement profile, setting the displacement at this instant as the actual zero displacement (Figure 3.29).

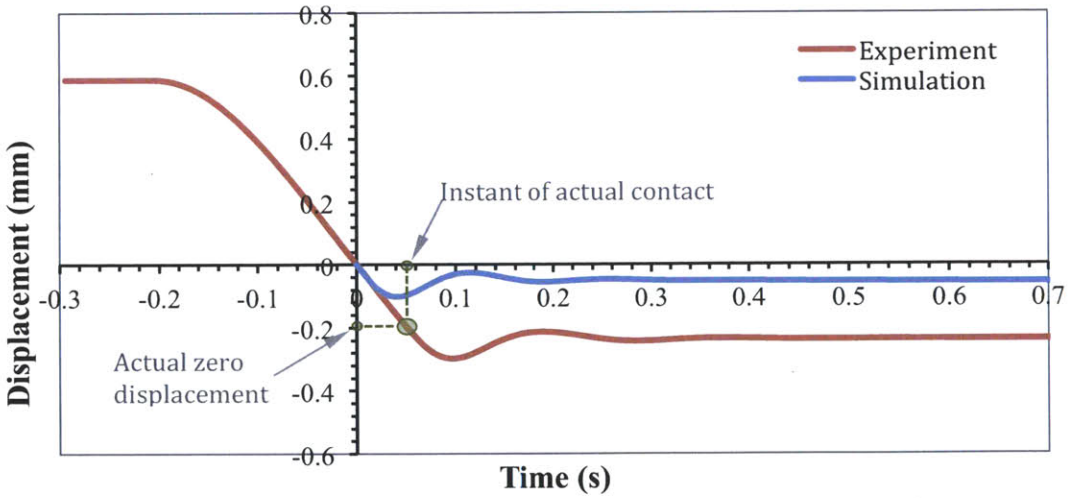

Figure 3.29: *Comparison of displacement profiles from experiment (without corrected point of contact) and simulation for Gel 4 at impact velocity v_{in} = 4.1 mm/s (impact kinetic energy = 1.8 μJ)*

Figures 3.30 and 3.31 show the experimental velocity and displacement profiles respectively for the same gel with corrected point of contact, and compare them to the simulated profiles. It can be seen that they match much better with this correction of the contact point identification, especially the first cycle and the final resting displacement of

the indenter. This correction, however, has to be done manually by detecting the point where the velocity drops sharply, and it is not always easy to identify the exact point, leaving an uncertainty in the actual instant of contact and actual zero displacement. The error bars in the experimental K and x_{max} values in Section 3.3 were obtained by considering an error of ±0.0045 seconds in the instant of contact and calculated the maximum and minimum K and x_{max} values in this range.

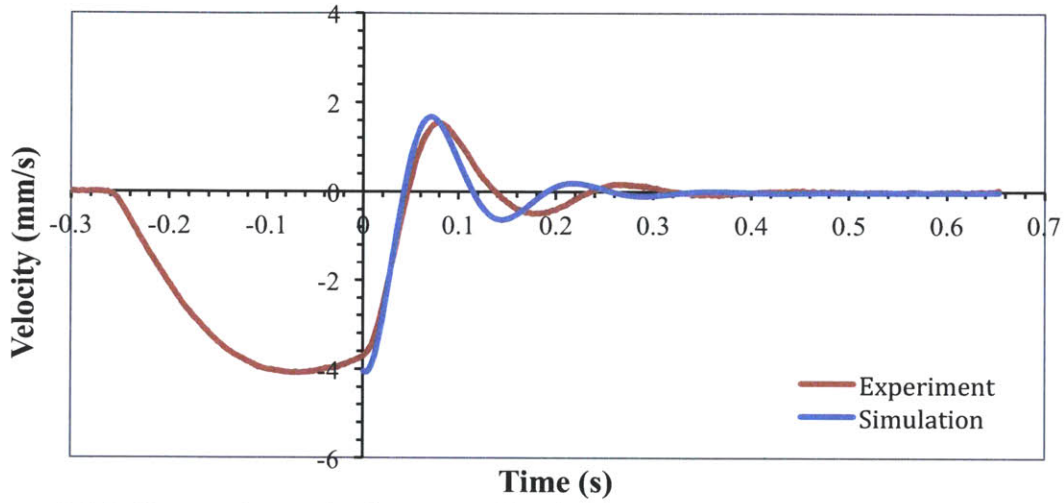

Figure 3.30: *Comparison of velocity profiles from experiment (with corrected point of contact) and simulation for Gel 4 at impact velocity v_{in} = 4.1 mm/s (impact kinetic energy = 1.8 μJ)*

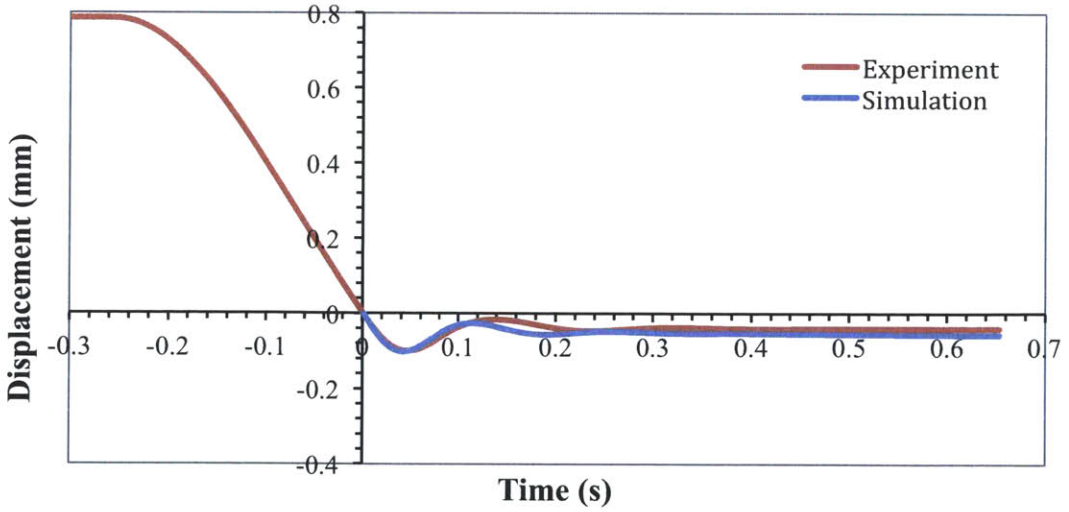

Figure 3.31: *Comparison of displacement profiles from experiment (with corrected point of contact) and simulation for Gel 4 at impact velocity v_{in} = 4.1 mm/s (impact kinetic energy = 1.8 μJ)*

Chapter 4:
Using the Model to Optimize Tissue Simulant Gels

4.1 Optimization Method

The Abaqus-Digimat model was used to optimize the material properties of a candidate tissue simulant gel. A MATLAB code was used to do this optimization (Appendix A5). The tissue simulant gel is assumed to be a composite PDMS gel with a PDMS solvent phase and a crosslinked PDMS solid network phase, just as before. In order the decrease the number of variables being optimized, the solvent properties and volume fraction were assumed, and the Prony series of the network phase is optimized. The optimization of the network phase is then performed for several volume fractions of different solvents, the viscoelastic properties (Prony series) of which were obtained by Dr. R. Mahmoodian (Van Vliet Group). The experimental displacement data, against which these two-phase PDMS tissue simulants were optimized against, had been obtained by Dr. I. Kalcioglu (Van Vliet Group). Dr. R. Mahmoodian also contributed to implementing the execution of the optimization code on the group computer cluster for a faster parallel optimization.

Equation 2.2, showing the Prony series for the normalized shear stress relaxation modulus, is stated here again for reference:

$$g(t) = \frac{G(t)}{G_0} = 1 - \sum_{i=1}^{N} g_i \left[1 - e^{-t/\tau_i}\right] \qquad \text{---------- Equation 2.2}$$

In the present study, the number of terms in the series N and the relaxation times τ_i are appropriately assumed, and the variables G_0 and g_i are optimized. The τ_i were taken to be similar to the network phases of the fabricated gels, in the range 0.01 to 100 seconds. The number of Prony series terms was assumed as 10 (N=10), which had been found to be optimal to capture the viscoelastic nature of the range network phases of the fabricated gels used in the study, and hence 11 variables (G_0, g_1, g_2, ..., g_{10}) were optimized.

The optimization in MATLAB is performed by the constrained optimization function *fmincon*. This function finds the minimum of a nonlinear function with multiple variables within specified upper and lower bounds, and constrained by up to two linear conditions [44]. In our case, the normalized mean squared error (*NMSE*) between the displacement profiles of the experimental data on the tissue and the simulated data on the tissue simulant, as defined by Equation 4.1, is minimized.

$$NMSE = \frac{\Sigma_i[d_{sim}(t_i) - d_{exp}(t_i)]^2}{\Sigma_i[d_{exp}(t_i)]^2} \qquad \text{---------- } \textit{Equation 4.1}$$

where d_{sim} and d_{exp} are the experimental displacement of the tissue and the simulated displacement of the tissue simulant, respectively, at time step t_i.

Appropriate lower and upper bounds, as well as the constraint condition on the sum of g_i, are specified according to Equations 4.2 and 4.3.

$$0 < g_i < 1 \qquad \text{---------- } \textit{Equation 4.2}$$

$$\sum_{i=1}^{N} g_i < 1 \qquad \text{---------- } \textit{Equation 4.3}$$

During each iteration of *fmincon,* the user-written function *rundigi* (Appendix A5) is called. *rundigi* writes a new Digimat material file for the gel according to the current properties of the network phase, and then runs the Abaqus-Digimat indentation simulation on this new composite gel. The displacement data is extracted by the Abaqus user-subroutine *postd* (Appendix A6) from the output files of the simulation. The normalized mean squared error between this data and the experimental displacement response of the tissue is computed and returned by *rundigi* to *fmincon*. Over several iterations, *fmincon* varies the material properties of the network phase to minimize this error function for constant (Prony series) properties of the solvent.

The MATLAB optimization was carried out separately for two solvents at different volume fractions. Their designation and molecular weights are noted in Table 4.1 and their Prony series parameters are listed in Table 4.2. The dynamic modulus of the PDMS solvents A and B is plotted in Figure 4.1. The tissue simulant gel was first optimized

against rat heart tissue and then against rat liver tissue, varying the solid network (Prony series) properties for either Solvent A or B in both test cases. The indentation experiments on the rat tissues had been performed by Dr. I. Kalcioglu (Van Vliet Group) as part of her research work.

Designation used in present work	Solvent Material	Solvent Molecular Weight (kg/mol)	Solvent designation used in [7], [11]
Solvent A	PDMS	1.1	T1
Solvent B	PDMS	308	T308

Table 4.1: *Solvent designation and molecular weights*

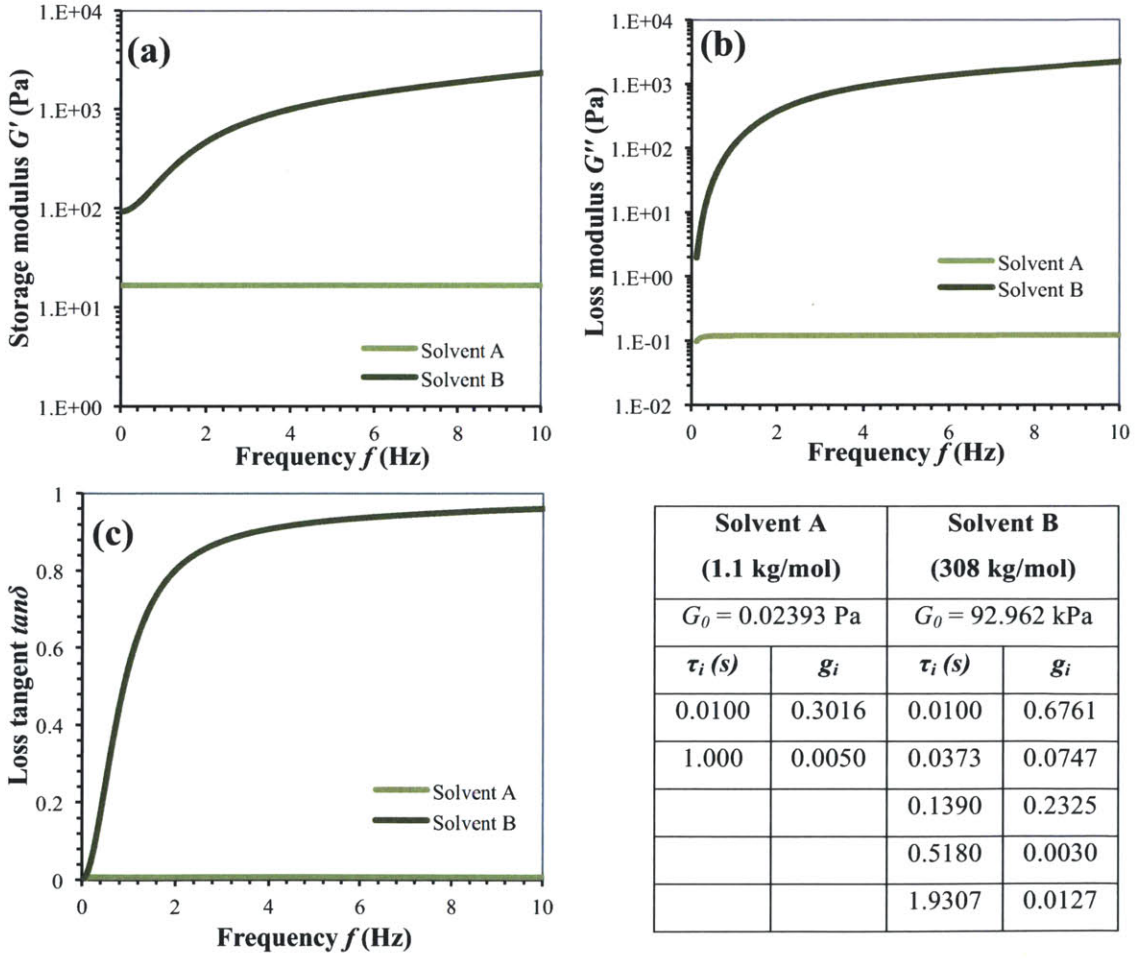

Figure 4.1: ***(a)*** *Storage modulus,* ***(b)*** *Loss modulus and* ***(c)*** *Loss tangent of Solvent A and Solvent B (Experimental data acquired by ARL collaborators, J. Lenhart and R. Mrozek)*

Solvent A (1.1 kg/mol)		**Solvent B (308 kg/mol)**	
G_0 = 0.02393 Pa		G_0 = 92.962 kPa	
τ_i **(s)**	g_i	τ_i **(s)**	g_i
0.0100	0.3016	0.0100	0.6761
1.000	0.0050	0.0373	0.0747
		0.1390	0.2325
		0.5180	0.0030
		1.9307	0.0127

Table 4.2: *Prony series parameters for Solvents A and B (Data acquired by Dr. R. Mahmoodian, Van Vliet Group)*

4.2 Optimization to Rat Heart Tissue

The optimization of the simulated gels was first carried out against experimental displacement data on rat heart tissue for different volume fractions of Solvent A (Figures 4.2 - 4.4) and Solvent B (Figures 4.5 - 4.8). The Prony series of the viscoelastic solid network was considered optimized for a certain volume fraction of the solvent when the normalized mean squared error, defined by Equation 4.1, was at its minimum. The maximum impact velocity used in the experiments on rat heart tissue was 8.4 mm/s and so this velocity was used for the simulations in the optimization.

I. 60% Solvent A

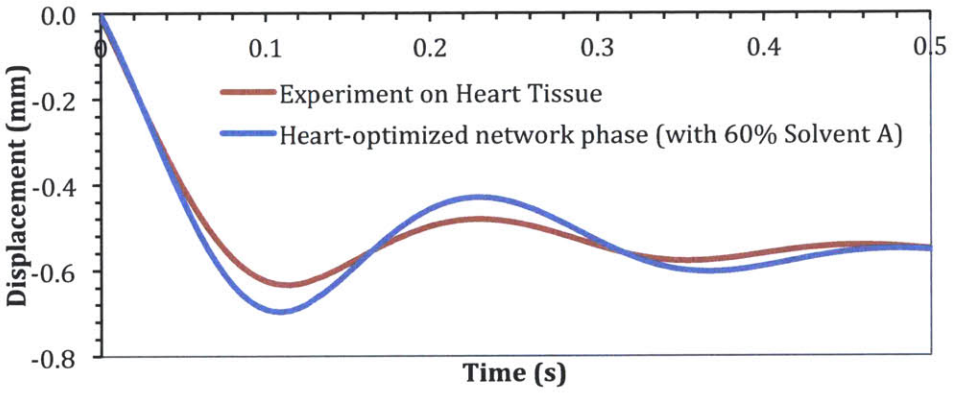

Figure 4.2: *Optimization of network phase against rat heart tissue with 60% Solvent A (Experimental data acquired by Dr. I. Kalcioglu, Van Vliet Group)*

II. 70% Solvent A

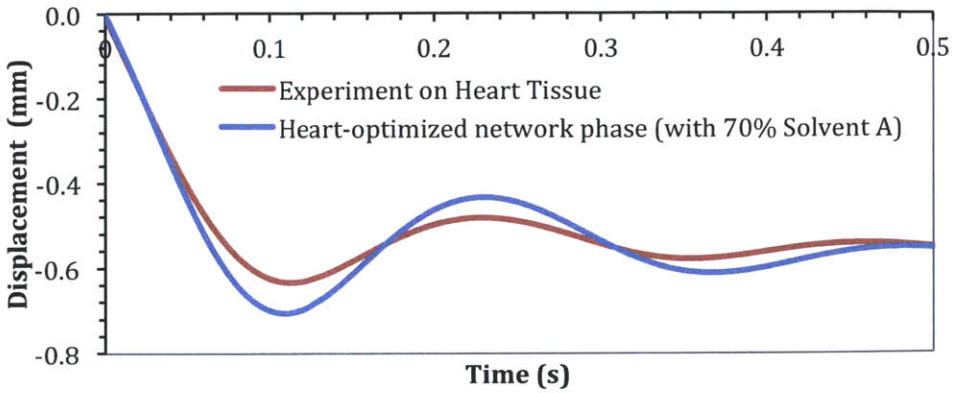

Figure 4.3: *Optimization of network phase against rat heart tissue with 70% Solvent A (Experimental data acquired by Dr. I. Kalcioglu, Van Vliet Group)*

III. 80% Solvent A

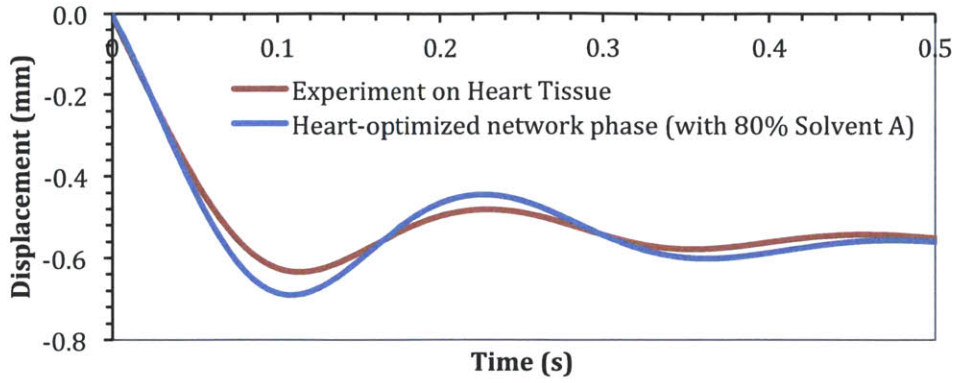

Figure 4.4: *Optimization of network phase against rat heart tissue with 80% Solvent A (Experimental data acquired by Dr. I. Kalcioglu of Van Vliet Group)*

IV. 50% Solvent B

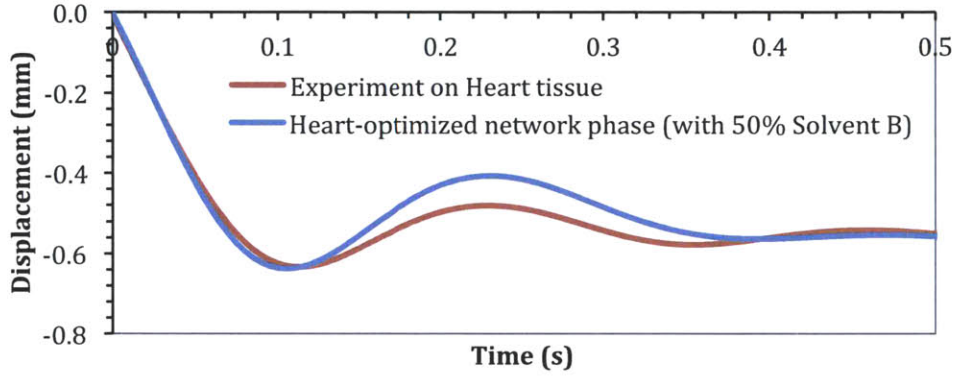

Figure 4.5: *Optimization of network phase against rat heart tissue with 50% Solvent B (Experimental data acquired by Dr. I. Kalcioglu of Van Vliet Group)*

V. 60% Solvent B

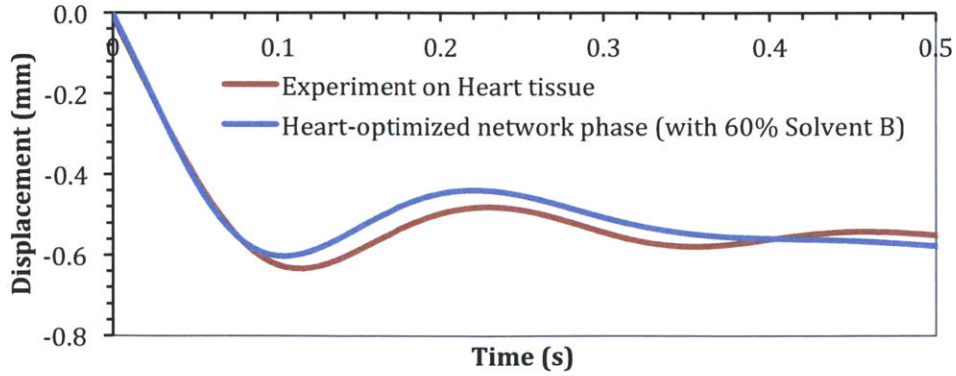

Figure 4.6: *Optimization of network phase against rat heart tissue with 60% Solvent B (Experimental data acquired by Dr. I. Kalcioglu, Van Vliet Group)*

VI. 70% Solvent B

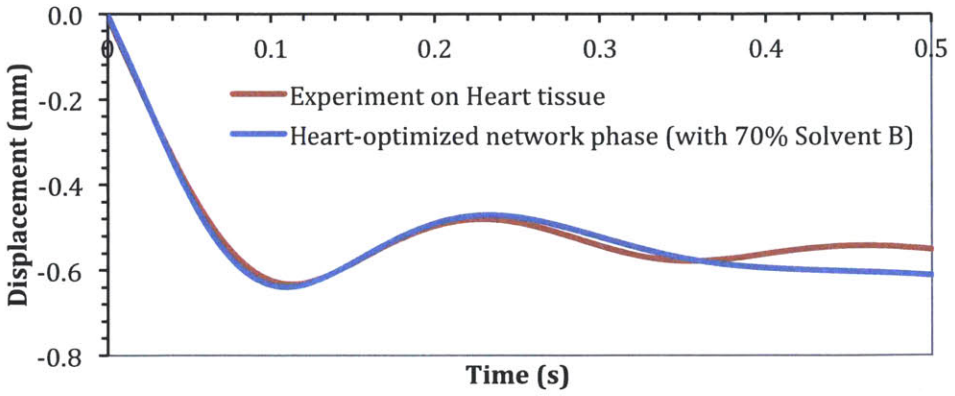

Figure 4.7: *Optimization of network phase against rat heart tissue with 70% Solvent B (Experimental data acquired by Dr. I. Kalcioglu, Van Vliet Group)*

VII. 80% Solvent B

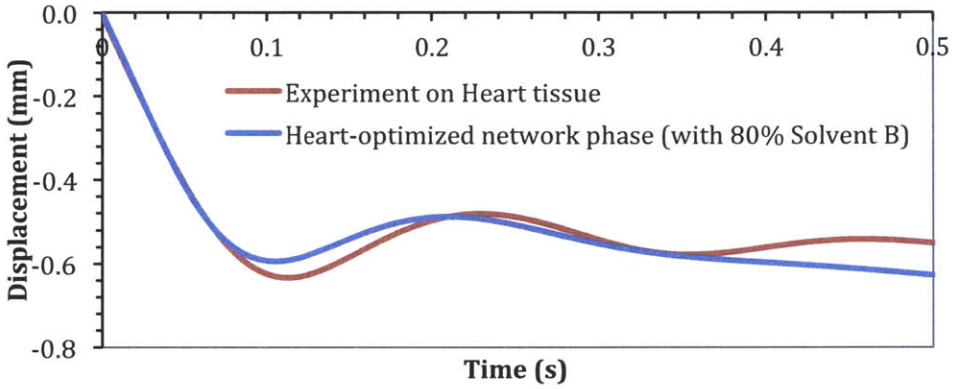

Figure 4.8: *Optimization of network phase against rat heart tissue with 80% Solvent B (Experimental data acquired by Dr. I. Kalcioglu, Van Vliet Group)*

4.2.1 Shear relaxation modulus and Prony series parameters of heart-optimized network phases

Figure 4.9 shows the dynamic modulus of the network phases of the heart-optimized gels with the different volume fractions of Solvent A and Solvent B. The corresponding optimized Prony series parameters (G_0, g_i) of the network phases are listed in Tables 4.3 and 4.4.

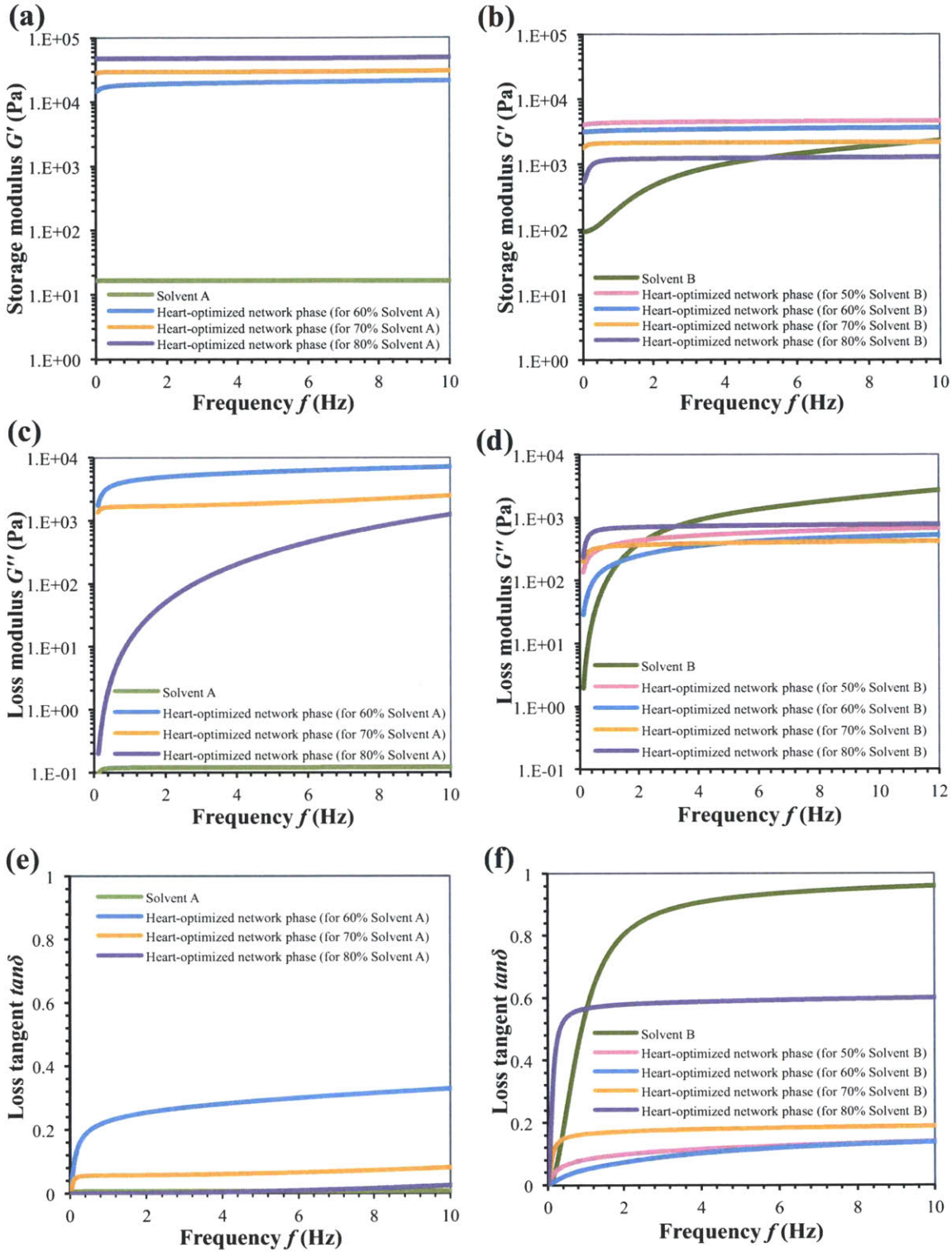

Figure 4.9: (a,b) *Storage modulus,* ***(c,d)*** *Loss modulus and* ***(e,f)*** *Loss tangent of heart-optimized network phases for different volume fractions of Solvents A and B (Experimental data on solvents acquired by ARL collaborators, J. Lenhart and R. Mrozek)*

As Solvent A has a very low initial shear modulus (G_0 = 0.0239 kPa), we can see from Figure 4.9(a) that, as the solvent volume fraction increases, the storage modulus of the optimized network phase has to be higher to compensate. On the other hand, Solvent B has a high initial shear modulus (G_0 = 92.962 kPa) and so for higher solvent volume fractions, storage modulus of the optimized network phase decreases as seen in Figure 4.9(b).

Heart-optimized network phase (for 60% Solvent A)		**Heart-optimized network phase (for 70% Solvent A)**		**Heart-optimized network phase (for 80% Solvent A)**	
G_0 = 62.240 kPa		G_0 = 83.860 kPa		G_0 = 147.510 kPa	
τ_i (s)	g_i	τ_i (s)	g_i	τ_i (s)	g_i
0.0100	0.0151	0.0100	~ 0	0.0100	~ 0
0.0278	0.0577	0.0278	~ 0	0.0278	0.1215
0.0774	0.5591	0.0774	0.6451	0.0774	0.5527
0.2154	0.0164	0.2154	~ 0	0.2154	~ 0
0.5995	0.0223	0.5995	~ 0	0.5995	~ 0
1.6681	0.0151	1.6681	~ 0	1.6681	~ 0
4.6416	0.0150	4.6416	~ 0	4.6416	~ 0
12.915	0.0151	12.915	~ 0	12.915	~ 0
35.938	0.0291	35.938	~ 0	35.938	~ 0
100.00	0.0216	100.00	0.0202	100.00	~ 0

Table 4.3: *Prony series parameters for heart-optimized network phases (for different volume fractions of Solvent A)*

Heart-optimized network phase (for 50% Solvent B)		**Heart-optimized network phase (for 60% Solvent B)**		**Heart-optimized network phase (for 70% Solvent B)**		**Heart-optimized network phase (for 80% Solvent B)**	
G_0 = 10.596 kPa		G_0 = 7.143 kPa		G_0 = 7.023 kPa		G_0 = 5.774 kPa	
τ_i (s)	g_i	τ_i (s)	g_i	τ_i (s)	g_i	τ_i (s)	g_i
0.0100	0.4765	0.0100	0.3502	0.0100	0.6089	0.0100	0.6108
0.0278	0.0541	0.0278	0.1217	0.0278	0.0655	0.0278	0.0477
0.0774	0.0106	0.0774	0.0028	0.0774	0.0078	0.0774	0.1107
0.2154	0.0106	0.2154	0.0026	0.2154	0.0038	0.2154	0.0058
0.5995	0.0181	0.5995	0.0189	0.5995	0.0038	0.5995	0.0058
1.6681	0.0106	1.6681	0.0356	1.6681	0.0038	1.6681	0.0058
4.6416	0.0106	4.6416	0.0088	4.6416	0.0037	4.6416	0.0058
12.915	0.0106	12.915	0.0158	12.915	0.0038	12.915	0.0058
35.938	0.0106	35.938	0.0025	35.938	0.0179	35.938	0.1067
100.00	0.0106	100.00	0.0026	100.00	0.0279	100.00	0.0058

Table 4.4: *Prony series parameters for heart-optimized network phases (for different volume fractions of Solvent B)*

4.2.2 Comparing fitting error, K, Q and x_{max} for the heart-optimized gels

Figure 4.10 compares the normalized mean squared fitting error (NMSE) for the optimized gels. We can see that the 80% Solvent A and 70% Solvent B optimizations are the closest to the heart tissue in this aspect. In terms of parameter K (Figure 4.11), the Solvent B optimizations, especially at 60% and 70%, show lower deviation from the tissue than the Solvent A ones. Q could not be calculated for Solvent B optimizations since the second bounce could not be identified in their displacement profiles. Q values of the Solvent A optimizations were comparable with that of the heart tissue, the 80% gel showing the closest match (Figure 4.12). Solvent B optimized gels also better approximated the x_{max} value of the tissue, especially at the higher volume fractions 70% and 80% (Figure 4.13).

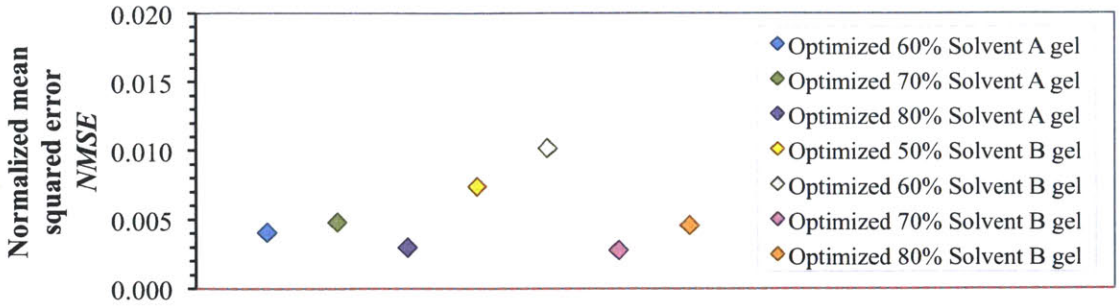

Figure 4.10: *Comparison of normalized mean squared error NMSE for gels with Solvent A and Solvent B optimized against rat heart tissue (Impact velocity v_{in} = 8.4 mm/s)*

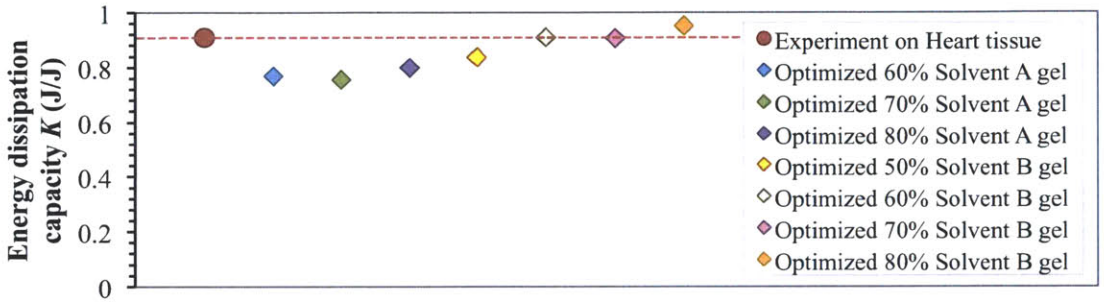

Figure 4.11: *Comparison energy dissipation capacity K for gels with Solvent A and Solvent B optimized against rat heart tissue (Impact velocity v_{in} = 8.4 mm/s)*

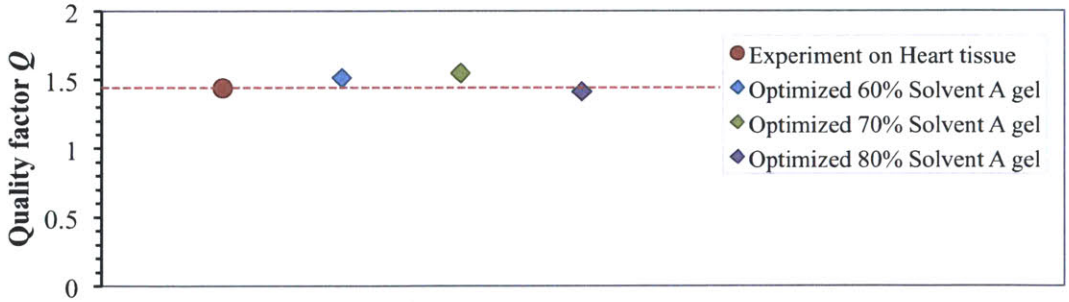

Figure 4.12: *Comparison of quality factor Q for gels with Solvent A optimized against rat heart tissue (Impact velocity v_{in} = 8.4 mm/s)*

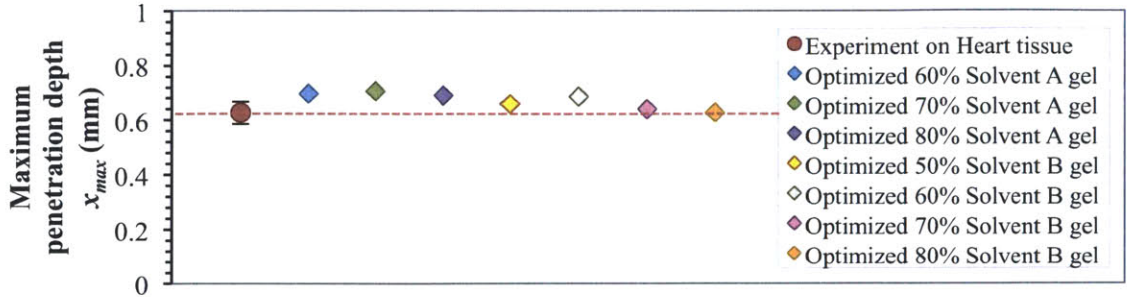

Figure 4.13: *Comparison of maximum penetration depth x_{max} for gels with Solvent A and Solvent B optimized against rat heart tissue (Impact velocity v_{in} = 8.4 mm/s)*

4.2.3 Best optimizations to Rat Heart Tissue

The closest optimizations to the rat heart tissue with Solvent A and Solvent B, both having similar *NMSE* values, are shown in Figure 4.14. The 70% Solvent B optimization follows the first bounce of the rat heart tissue almost exactly, correlating to a better matching of K value (with 0.5%) and x_{max} value (within 2%), but diverges after that without a discernible second bounce. The 80% Solvent A optimization shows a slightly greater x_{max} (by 10%) and lower K (by 12%) than the heart tissue in the first cycle but matches better in the second cycle and approximates the Q value within 2%.

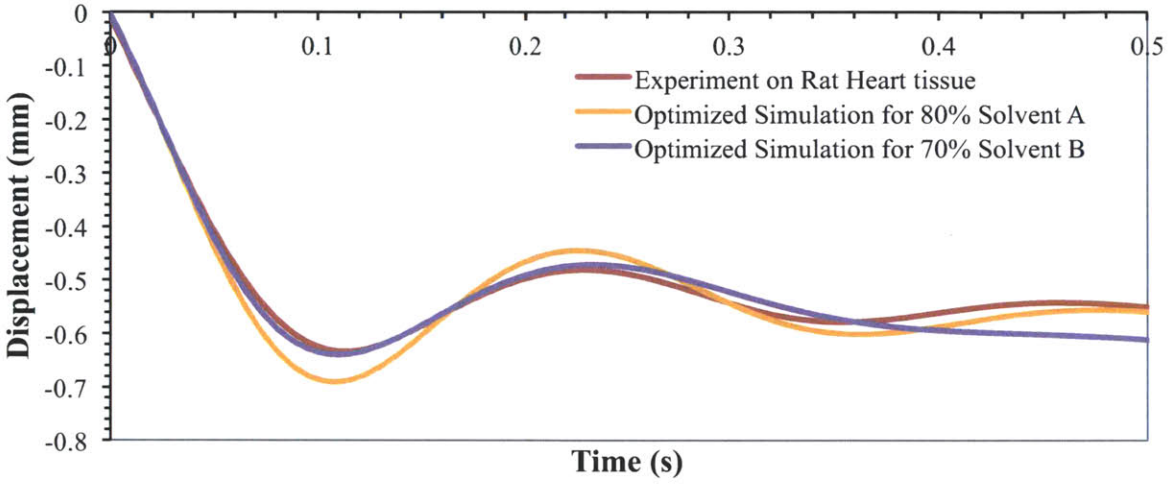

Figure 4.14: *Comparison of displacement profiles for impact velocity v_{in} = 8.4 mm/s of the best heart-optimized gels and the rat heart tissue (Experimental data acquired by Dr. I. Kalcioglu, Van Vliet Group)*

Thus, if one's goal is to optimize all three impact energy dissipation characteristics with 12%, the optimized gel design comprises 80% Solvent A and the PDMS network phase defined by the third column of Table 4.3. If the goal is to match only K and x_{max} with 2%, the optimized gel design is 70% Solvent B with the PDMS network phase defined by the third column of Table 4.4. For a more refined optimization, the code in Appendix A5 can be modified to add the solvent fraction as an additional variable to be optimized, with bounds around 80% for Solvent A and 70% for Solvent B.

4.3 Optimization to Rat Liver Tissue

The optimization of the simulated gels was also carried out against the rat liver tissue with different volume fractions of PDMS Solvent A (Figures 4.15 - 4.16) and PDMS Solvent B (Figures 4.17 - 4.19). As in the case of heart optimizations, the Prony series of the viscoelastic solid network was optimized for a each volume fraction of the solvents by minimizing the normalized mean squared error, defined by Equation 4.1. The maximum impact velocity used in the experiments on rat liver tissues was 8.2 mm/s, and so this velocity was used for the simulations in the optimization.

I. 60% Solvent A

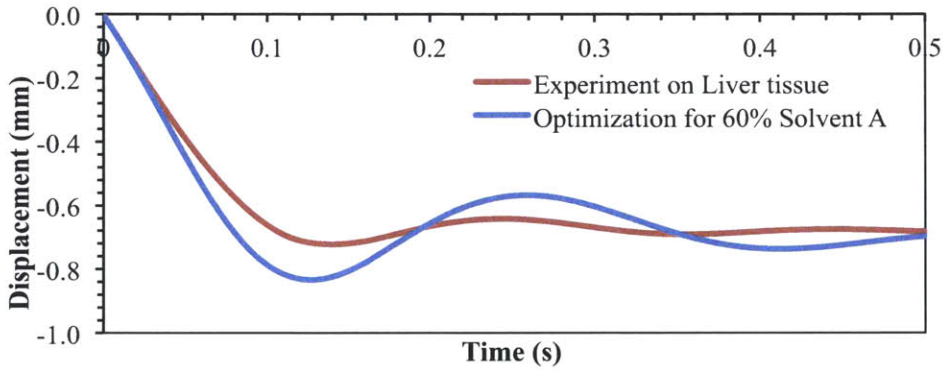

Figure 4.15: *Optimization against rat liver tissue for 60% Solvent A (Experimental data acquired by Dr. I. Kalcioglu, Van Vliet Group)*

II. 70% Solvent A

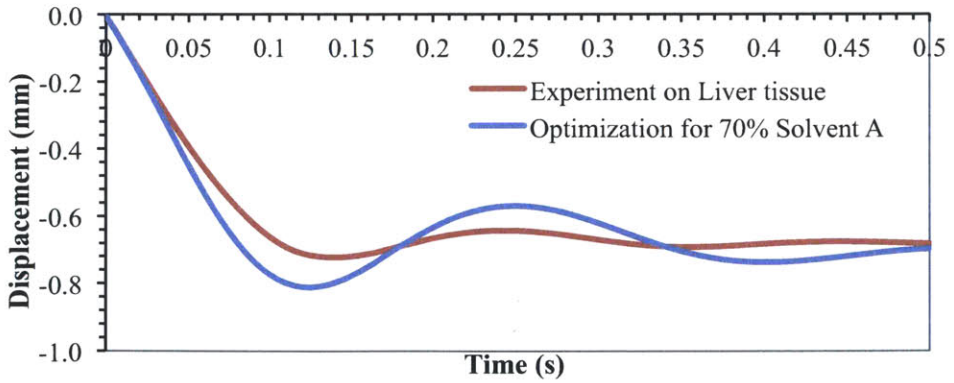

Figure 4.16: *Optimization against rat liver tissue for 70% Solvent A (Experimental data acquired by Dr. I. Kalcioglu, Van Vliet Group)*

III. 60% Solvent B

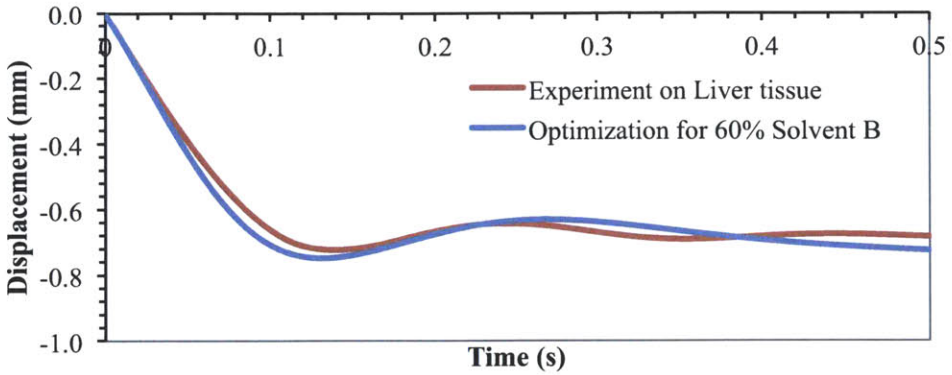

Figure 4.17: *Optimization against rat liver tissue for 60% Solvent B (Experimental data acquired by Dr. I. Kalcioglu, Van Vliet Group)*

IV. 70% Solvent B

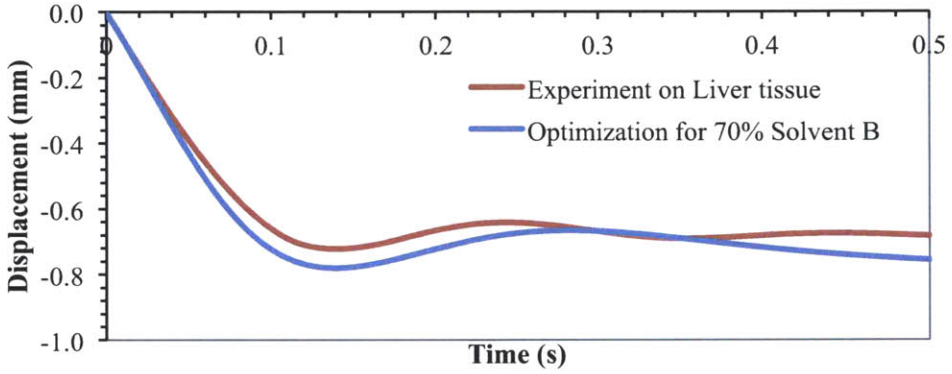

Figure 4.18: *Optimization against rat liver tissue for 70% Solvent B (Experimental data acquired by Dr. I. Kalcioglu, Van Vliet Group)*

V. 90% Solvent B

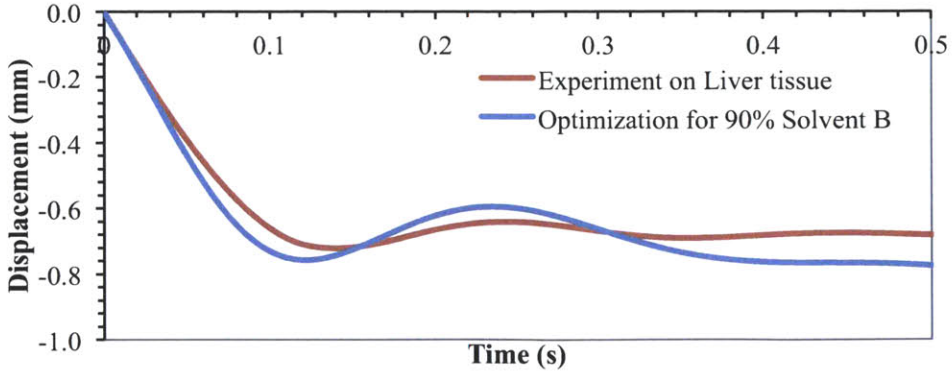

Figure 4.19: *Optimization against rat liver tissue for 90% Solvent B (Experimental data acquired by Dr. I. Kalcioglu, Van Vliet Group)*

4.3.1 Shear relaxation modulus and Prony series parameters of liver-optimized network phases

The dynamic modulus of the network phases of the liver-optimized gels with the different volume fractions of Solvent A and Solvent B are shown in Figure 4.20.

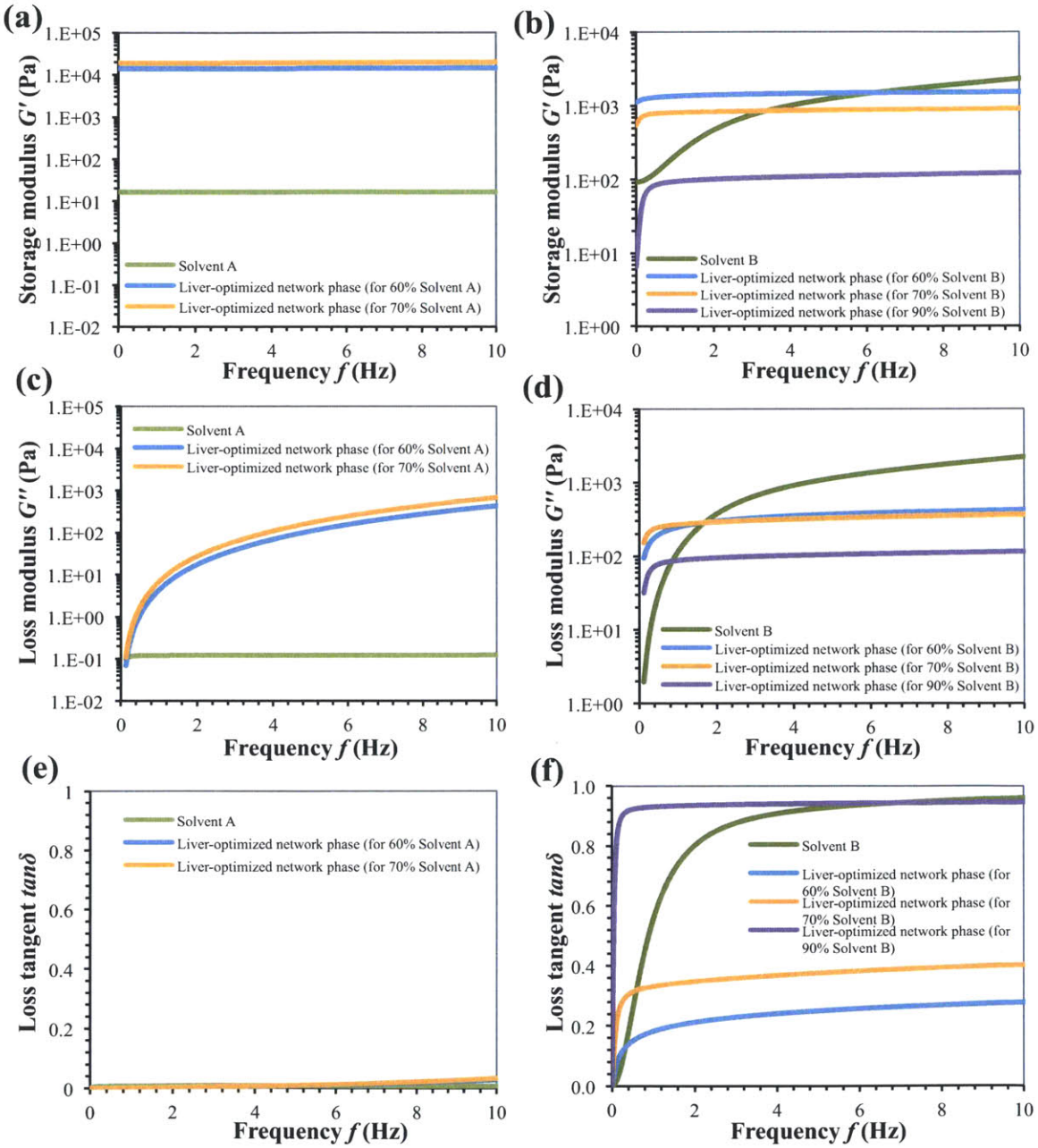

Figure 4.20: (a,b) *Storage modulus,* ***(c,d)*** *Loss modulus and* ***(e,f)*** *Loss tangent of and liver-optimized network phases for different volume fractions of Solvents A and B (Experimental data on solvents acquired by ARL collaborators, J. Lenhart and R. Mrozek)*

Liver-optimized network phase (with 60% Solvent A)		Liver-optimized network phase (with 70% Solvent A)	
G_0 = 42.474 kPa		G_0 = 64.764 kPa	
τ_i (s)	g_i	τ_i (s)	g_i
0.0100	~ 0	0.0100	~ 0
0.0278	0.6681	0.0278	~ 0
0.0774	~ 0	0.0774	0.7010
0.2154	~ 0	0.2154	~ 0
0.5995	~ 0	0.5995	~ 0
1.6681	~ 0	1.6681	~ 0
4.6416	~ 0	4.6416	~ 0
12.915	~ 0	12.915	~ 0
35.938	~ 0	35.938	~ 0
100.00	~ 0	100.00	~ 0

Table 4.5: *Prony series parameters for liver-optimized network phases (for different volume fractions of Solvent A)*

Liver-optimized network phase (with 60% Solvent B)		Liver-optimized network phase (with 70% Solvent B)		Liver-optimized network phase (with 90% Solvent B)	
G_0 = 8.810 kPa		G_0 = 5.889 kPa		G_0 = 0.408 kPa	
τ_i (s)	g_i	τ_i (s)	g_i	τ_i (s)	g_i
0.0100	0.6899	0.0100	0.7715	0.0100	0.1108
0.0278	0.1084	0.0278	0.0521	0.0278	0.0292
0.0774	0.0144	0.0774	0.0050	0.0774	0.4307
0.2154	0.0088	0.2154	0.00109	0.2154	0.1445
0.5995	0.0088	0.5995	0.00119	0.5995	0.0074
1.6681	0.0088	1.6681	0.0073	1.6681	0.0267
4.6416	0.0088	4.6416	0.0034	4.6416	0.0225
12.915	0.0088	12.915	0.0026	12.915	0.0060
35.938	0.0087	35.938	0.0186	35.938	0.1915
100.00	0.0087	100.00	0.0241	100.00	0.0146

Table 4.6: *Prony series parameters for liver-optimized network phases (for different volume fractions of Solvent B)*

Tables 4.5 and 4.6 list the liver-optimized Prony series parameters (G_0, g_i) of the network phases.

As for the optimizations against heart tissue's energy dissipation, the storage modulus of the liver-optimized network phase increased for higher volume fractions of Solvent A (G_0 = 0.0239 kPa) and decreased for higher volume fractions of Solvent B (G_0 = 92.962 kPa).

4.3.2 Comparing fitting error, *K*, *Q* and x_{max} for the liver-optimized gels

The normalized mean squared fitting error (NMSE) for the liver-optimized gels are compared in Figure 4.21, which shows that the 60% Solvent B optimization was the closest to the liver tissue. The Solvent B optimizations show much better matching in *K* (Figure 4.22) and x_{max} (Figure 4.24) values with the tissue than the Solvent A ones. Q values could not be calculated for the Solvent B gels due to their lack of a second peak. The 60% Solvent A optimization had a comparable *Q* value with the tissue (Figure 4.23) but its *NMSE* was very high.

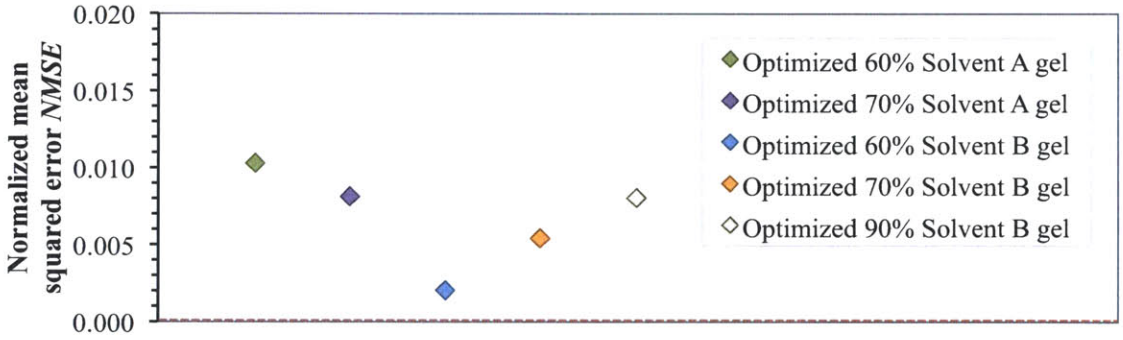

Figure 4.21: *Comparison of normalized mean squared error NMSE for the optimized gels with Solvent A and Solvent B against rat liver tissue (Impact velocity v_{in} = 8.2 mm/s)*

Figure 4.22: *Comparison of energy dissipation capacity K for the optimized gels with Solvent A and Solvent B against rat liver tissue (Impact velocity v_{in} = 8.2 mm/s)*

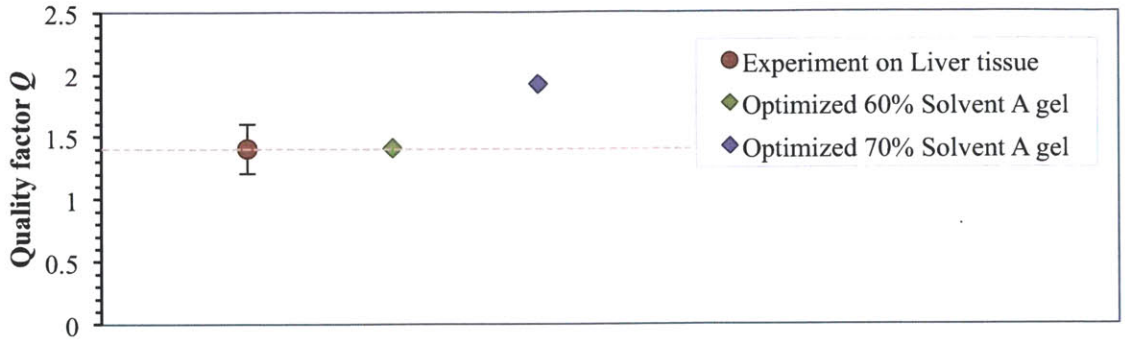

Figure 4.23: *Comparison of quality factor Q for the optimized gels with Solvent A against rat liver tissue (Impact velocity v_{in} = 8.2 mm/s)*

Figure 4.24: *Comparison of maximum penetration depth x_{max} for the optimized gels with Solvent A and Solvent B against rat liver tissue (Impact velocity v_{in} = 8.2 mm/s)*

4.3.3 Best optimizations to Rat Liver Tissue

Figure 4.25 compares the displacement profiles of the liver tissue and the best optimizations with Solvent A and Solvent B. The 60% Solvent B optimized gel was the best match to the liver tissue in terms of K (within 1%), x_{max} (within 2%) and minimum NMSE. Although it fairly approximates the tissue in the first cycle, it deviates after that without a second bounce. The 70% Solvent A gel was the best optimization obtained with Solvent A, but it is still quite dissimilar to the tissue profile with a lower K (by 14%), a much higher Q (by 37%) and a higher x_{max} (by 11%). On average, for Solvent A, the deviation of the comparison parameters from tissue values were found to be much higher for liver optimizations than for heart optimizations, suggesting that the Solvent A PDMS gels do not capture the behavior of liver tissues satisfactorily, especially the impact resistence and quick dissipation in the first impact cycle.

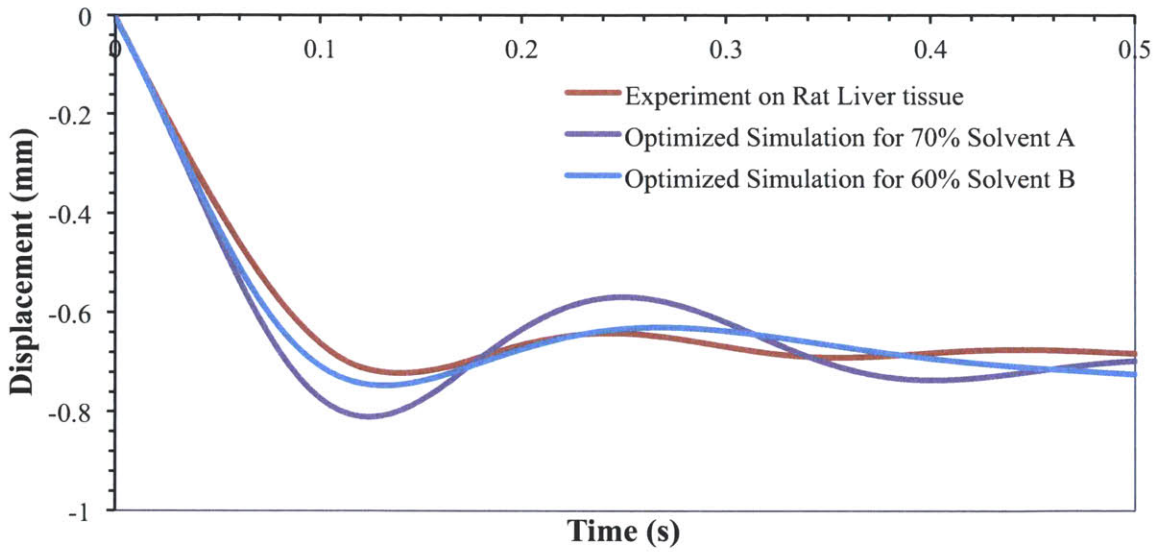

Figure 4.25: *Comparison of displacement profiles for impact velocity v_{in} = 8.2 mm/s of the best liver-optimized gels and the rat liver tissue (Experimental data acquired by Dr. I. Kalcioglu, Van Vliet Group)*

In the case of liver tissue, the impact energy is dissipated quickly in the first cycle, with no discernible third peak in the displacement profile. This causes a large error of almost 20% in the experimental Q value (Figure 4.23) making it more challenging to match this energy dissipation characteristic in a tissue simulant. To match only K and x_{max} with 2%, the optimized gel design comprises of 60% Solvent B and the PDMS network phase defined by the first column of Table 4.6. For a more refined optimization of solvent volume fraction, the code in Appendix A5 can be modified to add the volume fraction as an additional variable to be optimized, setting the bounds around 60%.

4.4 Comparing Tissue-optimized Gels and ARL-fabricated Gels

The dynamic modulus of the heart and liver tissues are compared against those of the network phases of the ARL-fabricated gels and the network phases of the tissue-optimized gels containing 60% Solvent A, in Figures 4.26 - 4.28, and 60% Solvent B, in Figures 4.30 - 4.32. The dynamic modulus of the rat heart and liver tissues were obtained experimentally by Dr. I. Kalcioglu (Van Vliet Group) [12]. The ARL-fabricated gels

considered in Figures 4.26 - 4.28 all had 60% of Solvent and those considered in Figures 4.30 - 4.32 all had 60% of Solvent B. The solvent was extracted from these gels by Wen Shen (Van Vliet Group) to obtain the dry network phases, on which rheological experiments were performed by Dr. R. Mahmoodian (Van Vliet Group) to obtain the dynamic moduli of the network phases, which are shown in Figures 4.26 - 4.32. The network phases of the heart- and liver-optimized gels were obtained by implementing the optimization method (Section 4.1) for two-phase PDMS gels containing 60% Solvent A (Figures 4.26 - 4.28) and 60% Solvent B (Figures 4.30 - 4.32) and optimizing the composite gels to match the impact energy dissipation characteristics of heart and liver tissues, respectively.

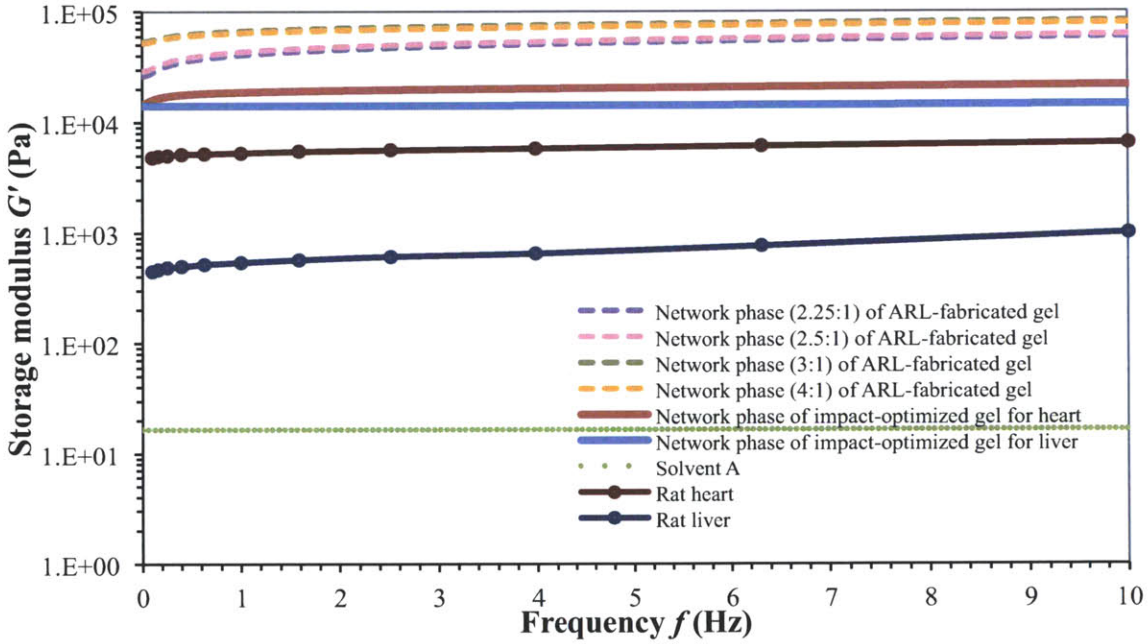

Figure 4.26: *Storage modulus of liver and heart tissues compared with that of Solvent A, network phases of impact-optimized tissue simulant gels and network phases of ARL-fabricated gels of different stoichiometric ratios. The optimization of the network phases was done so that the composite tissue simulant gel, which contained 60% Solvent A, matched the impact characteristics of corresponding tissue. The ARL-fabricated gels also had 60% Solvent A before the solvent was extracted to obtain the dry network phase. (Experimental data on network phases of ARL-fabricated gels acquired by Dr. R. Mahmoodian, Van Vliet Group. Experimental data on solvent acquired by ARL collaborators, J. Lenhart and R. Mrozek. Experimental data on rat heart and liver tissues acquired by Dr. I. Kalcioglu [12])*

Although the 60% Solvent A heart-optimization, 60% Solvent B heart-optimization and 60% Solvent A liver-optimization were not among the best optimizations for heart and liver tissues (Sections 4.2.3 and 4.3.3), they are used in this comparison nonetheless, since we had the material properties for several ARL-fabricated gels of different network stoichiometric ratios containing 60% Solvents A and B. In this way, by keeping the solvent-phase the same across the gels, we can study the trends in the shear rheology of tissue-optimized network phases and ARL-fabricated network phases.

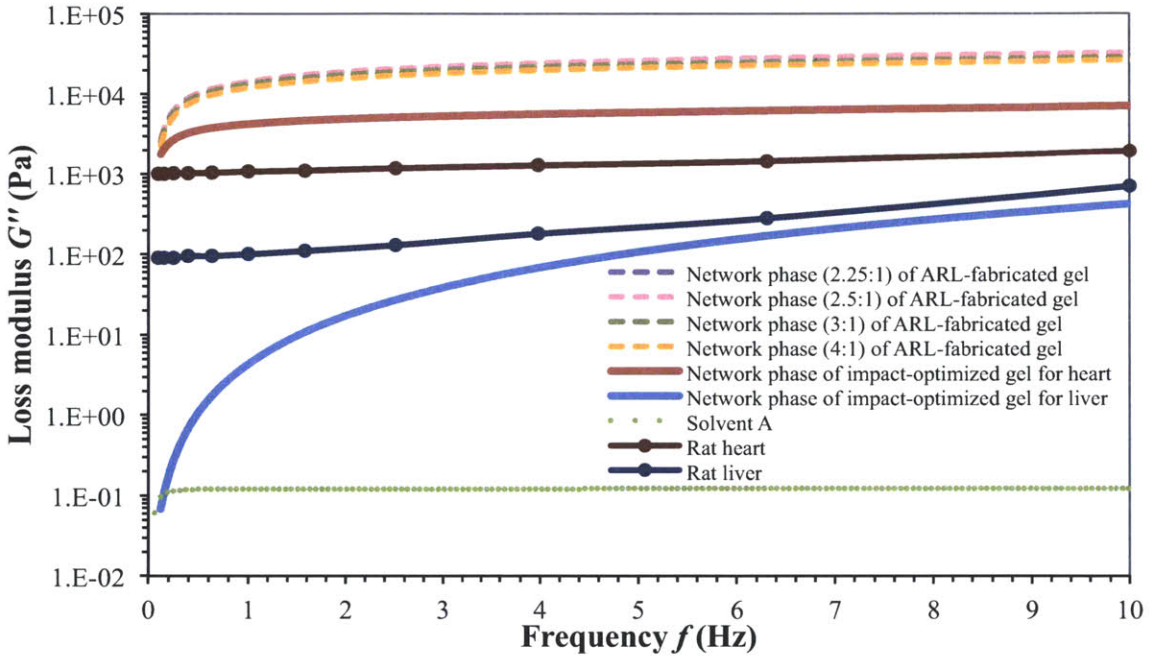

Figure 4.27: *Loss modulus of liver and heart tissues compared with that of Solvent A, network phases of impact-optimized tissue simulant gels and network phases of ARL-fabricated gels of different stoichiometric ratios. The optimization of the network phases was done so that the composite tissue simulant gel, which contained 60% Solvent A, matched the impact characteristics of corresponding tissue. The ARL-fabricated gels also had 60% Solvent A before the solvent was extracted to obtain the dry network phase. (Experimental data on network phases of ARL-fabricated gels acquired by Dr. R. Mahmoodian, Van Vliet Group. Experimental data on solvent acquired by ARL collaborators, J. Lenhart and R. Mrozek. Experimental data on rat heart and liver tissues acquired by Dr. I. Kalcioglu [12])*

From Figures 4.26, 4.27, 4.30 and 4.31, we can observe that, for a better-optimized tissue simulant gel which matches the impact energy characteristics, the storage and loss moduli of the network phase have to be much lower than those of the ARL-fabricated network phases. From the trend of decreasing storage modulus with decreasing silane group to vinyl group stoichiometric ratio (Figures 4.26 and 4.29), we can predict that lower stoichiometric ratios of the network phase should be used to design tissue simulant gels to better match the energy dissipation of the tissues. This was also observed previously by Dr. I. Kalcioglu (Van Vliet Group) [12]. Unfortunately, the gels of lower stoichiometric ratio also tend to be stickier, as was observed from the previous batch of ARL-fabricated gels.

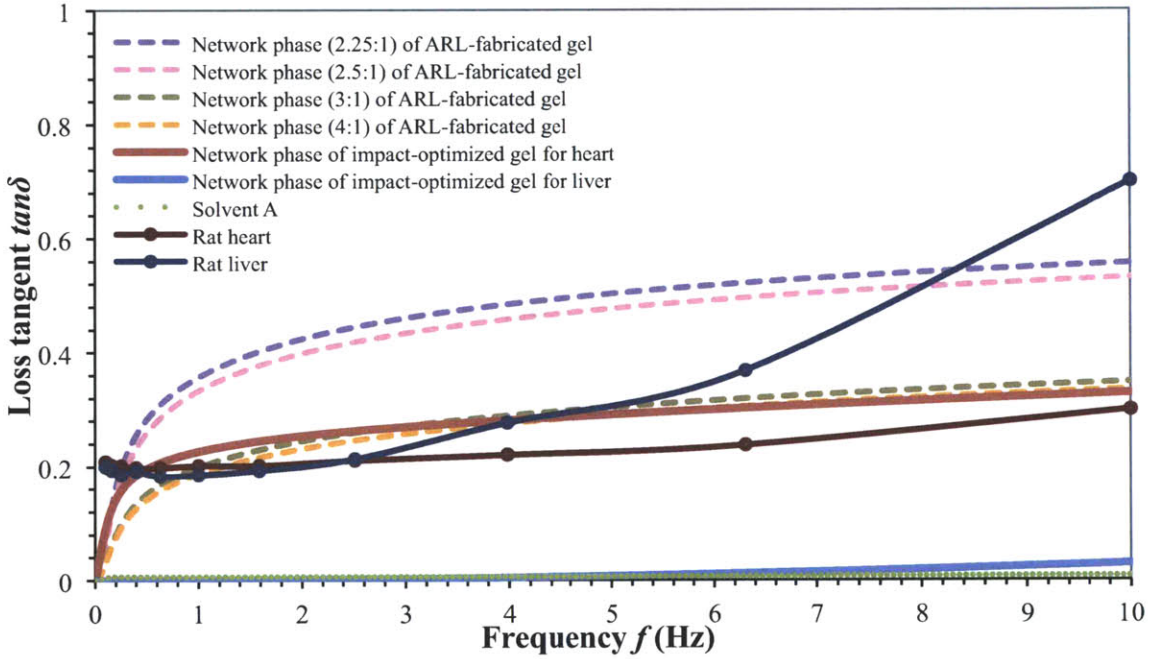

Figure 4.28: *Loss tangent of liver and heart tissues compared with that of Solvent A, network phases of impact-optimized tissue simulant gels and network phases of ARL-fabricated gels of different stoichiometric ratios. The optimization of the network phases was done so that the composite tissue simulant gel, which contained 60% Solvent A, matched the impact characteristics of corresponding tissue. The ARL-fabricated gels also had 60% Solvent A before the solvent was extracted to obtain the dry network phase. (Experimental data on network phases of ARL-fabricated gels acquired by Dr. R. Mahmoodian, Van Vliet Group. Experimental data on solvent acquired by ARL collaborators, J. Lenhart and R. Mrozek. Experimental data on rat heart and liver tissues acquired by Dr. I. Kalcioglu [12])*

In Figures 4.26 - 4.32, the dynamic moduli of the network and solvent phases of the impact-optimized tissue simulant gels as well as the dynamic moduli of the tissues are shown. However, the overall dynamic moduli of the composite impact-optimized tissue simulant gels are not shown, since in the concurrent multiscale simulation, Digimat does not compute the material properties of an equivalent composite gel. Hence, we cannot know from the current data whether the shear rheology of the composite tissue simulant gels, optimized to match the impact energy dissipation characteristics of tissues, would be similar to the shear rheology of the tissues themselves.

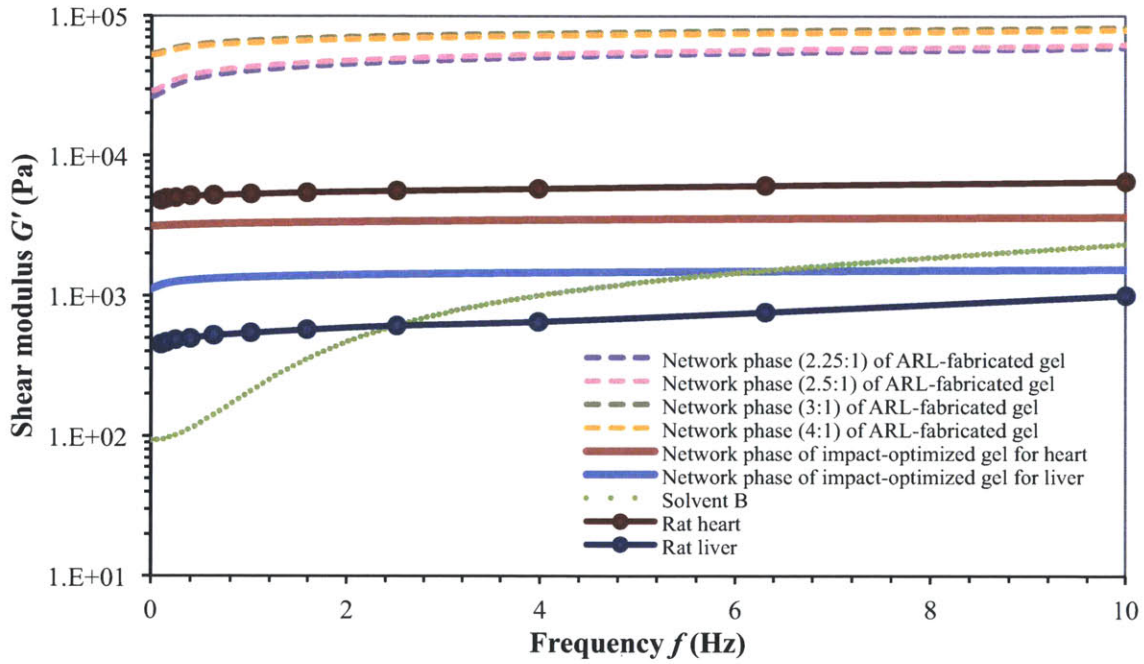

Figure 4.29: *Storage modulus of liver and heart tissues compared with that of Solvent B, network phases of impact-optimized tissue simulant gels and network phases ARL-fabricated gels of different stoichiometric ratios. The optimization of the network phases was done so that the composite tissue simulant gel, which contained 60% Solvent B, matched the impact characteristics of corresponding tissue. The ARL-fabricated gels also had 60% Solvent B before the solvent was extracted to obtain the dry network phase. (Experimental data on network phases of ARL-fabricated gels acquired by Dr. R. Mahmoodian, Van Vliet Group. Experimental data on solvent acquired by ARL collaborators, J. Lenhart and R. Mrozek. Experimental data on rat heart and liver tissues acquired by Dr. I. Kalcioglu [12])*

It is possible to modify the concurrent multiscale simulation with an Abaqus model that simulates the conditions of a rheological experiment, in order to computationally obtain the shear rheology of the composite optimized-tissue simulant gel, defined by the impact-optimized network phase and assumed solvent phase in Digimat. In such a case, if this computationally-obtained dynamic modulus of the impact-optimized tissue simulant was found to be similar to the dynamic modulus of the corresponding tissue, it would make the design of tissue simulant gels simpler, since it is easier to match shear rheology of gels and tissues than to match impact energy characteristics.

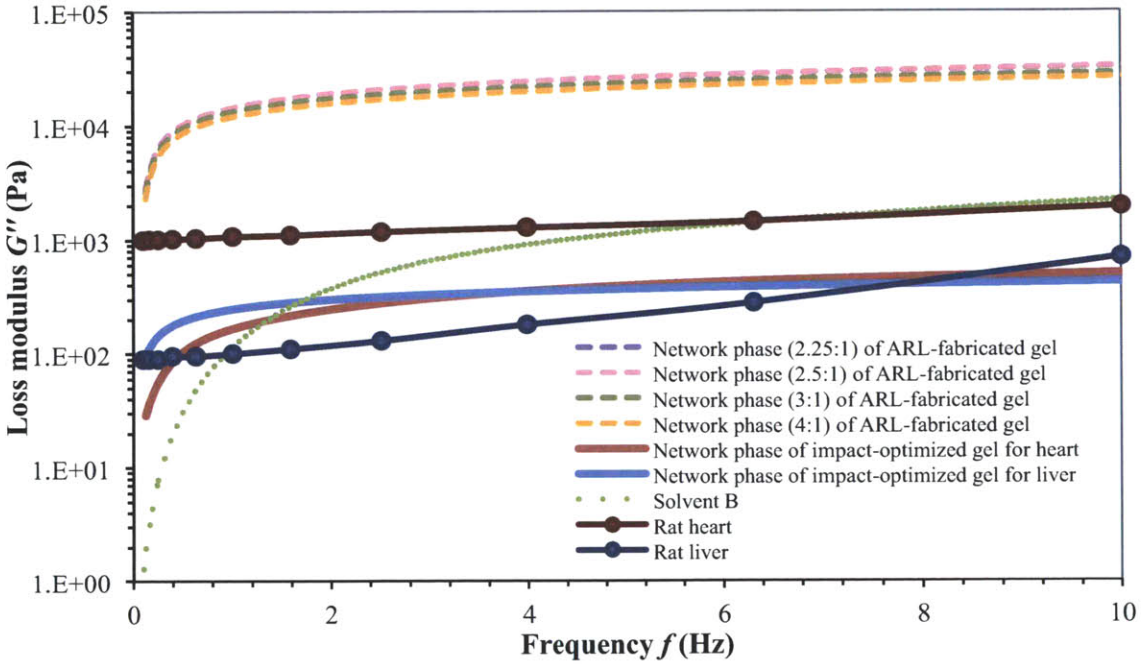

Figure 4.30: *Loss modulus of liver and heart tissues compared with that of Solvent B, network phases of impact-optimized tissue simulant gels and network phases ARL-fabricated gels of different stoichiometric ratios. The optimization of the network phases was done so that the composite tissue simulant gel, which contained 60% Solvent B, matched the impact characteristics of corresponding tissue. The ARL-fabricated gels also had 60% Solvent B before the solvent was extracted to obtain the dry network phase. (Experimental data on network phases of ARL-fabricated gels acquired by Dr. R. Mahmoodian, Van Vliet Group. Experimental data on solvent acquired by ARL collaborators, J. Lenhart and R. Mrozek. Experimental data on rat heart and liver tissues acquired by Dr. I. Kalcioglu [12])*

However, from her experimental analysis on tissues and ARL-fabricated PDMS gels, Dr. I. Kalcioglu (Van Vliet Group) found no such correlation between the matching of shear rheology of tissues and tissue simulant gels, and the matching of their impact energy dissipation characteristics [12]. It is unlikely that a computational analysis of the shear rheology of composite impact-optimized tissue simulant gels would show otherwise.

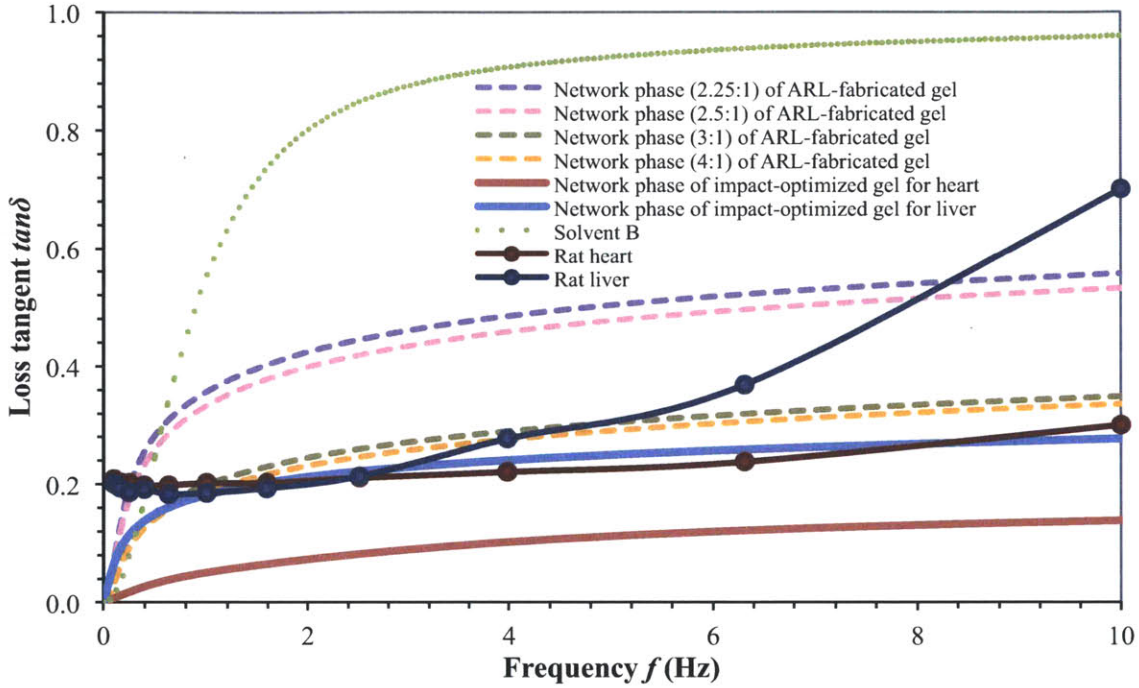

Figure 4.31: *Loss tangent of liver and heart tissues compared with that of Solvent B, network phases of impact-optimized tissue simulant gels and network phases ARL-fabricated gels of different stoichiometric ratios. The optimization of the network phases was done so that the composite tissue simulant gel, which contained 60% Solvent B, matched the impact characteristics of corresponding tissue. The ARL-fabricated gels also had 60% Solvent B before the solvent was extracted to obtain the dry network phase. (Experimental data on network phases of ARL-fabricated gels acquired by Dr. R. Mahmoodian, Van Vliet Group. Experimental data on solvent acquired by ARL collaborators, J. Lenhart and R. Mrozek. Experimental data on rat heart and liver tissues acquired by Dr. I. Kalcioglu [12])*

4.5 Limitations of Optimization

The function *fmincon* is sensitive to the initial assumption of the optimized variables (G_0, g_1, g_2, ..., g_{10}) and may be trapped within a local minimum of the error function. The known Prony parameters of fabricated gels with similar solvent and volume fraction were used as initial values to reduce this possibility. However, a satisfactory optimization was not achieved in some cases. For example, 80% Solvent A and 80% Solvent B against liver tissue could not be optimized, due to termination at local minima near the initial solution.

Since the solvent properties were assumed, the best optimizations may also depend on the solvent chosen. For some solvents, even the best optimization might still not be a good approximation of the tissue behavior, indicating that the particular solvent is not a good choice for fabricating a simulant of the tissue. For example, in the previous section, it was inferred that Solvent A is not a good fit for designing liver tissue simulants. One advantage of the present simulation approach is the ability to identify this limitation rapidly.

In the present study, the relaxation times τ_i were assumed to have similar values as the Prony series of the network phase of the ARL-fabricated gels. For a better optimization, the τ_i could also be optimized, although this would lead to almost double the number of variables needed to be optimized, and thus require much longer computation times.

Chapter 5: Conclusion

5.1 Summary of Chapters

The first chapter presented the need for computational optimization of impact energy dissipation in gels, including but not limited to design of soft-tissue simulant. Some of the materials considered for making tissue simulant polymer gels, and the method previously used for testing them against tissues were reported. A computational model using finite element analysis and multiscale material modeling was proposed so as to better predict the material properties of optimal gels. The different methods of multiscale modeling were also introduced.

The second chapter described the impact indentation experiment used previously to test and compare the mechanical behaviors of candidate tissue simulant gels and tissues. The coupled finite-element, multiscale material model developed to simulate this experiment was then detailed and the Prony series representation used to define the viscoelastic behaviors of the composite gel constituents was explained.

In the third chapter, the coupled model developed in the previous chapter was validated against experiments on composite PDMS gels. The parameters used to quantify the mechanical responses of the gels and tissues to the impact indentation were introduced, and used for comparison of the simulated and experimental behaviors of the gels. The parameters showed good correlation between simulation and experiment, demonstrating that the computational model was an adequate representation of the experiment. The limitations of the model due to adhesive effects in experiment, which could not be sufficiently implemented, and the ambivalence of the experimental instant of impact were also illustrated.

In the fourth chapter, the validated computational model was employed in an iterative optimization program that aims to predict the material properties of a good tissue simulant gel. This optimization was carried out against rat heart and liver tissues and the properties of the best candidate PDMS gels with two solvents were estimated in each case. For both rat heart and rat liver tissues, the network phase viscoelastic properties (Prony series) and solvent volume fraction were predicted for tissue simulants that matched K and x_{max} within 2%. The solvent in both cases had a molecular weight of 308 kg/mol (Solvent B). This solvent, however, was found to be less appropriate for designing tissue simulants that matched the energy dissipation rate parameter Q. The other solvent considered for optimization had a much lower molecular weight of 1.1 kg/mol (Solvent A). Optimized tissue simulants with this solvent approximated the Q value of the tissues better but there was a trade-off in the matching of K and x_{max}. For an optimal matching of all three impact energy dissipation characteristics, a solvent of molecular weight in between those of Solvents A (308 kg/mol) and B (1.1 kg/mol) may be considered and the network phase and volume fraction optimized.

5.2 Perspectives

The fabrication and experimental testing of candidate tissue simulant gels is a time-consuming procedure. The computational model developed in the present study is an effort to make this process simpler by providing material scientists a tool to predict the optimum material parameters needed in the synthesis of gels designed to target energy dissipation characteristics. The multiscale material model provides automated optimization of macroscopic behavior of gels by tweaking the properties of the material microstructure, such as the mechanical behavior and volume fractions of the phases in a composite gel.

Although the current study was limited to the low impact velocities used in the experiment, the computational model could also be used to investigate the behavior of the

tissue simulants at much higher impact velocities, which are more realistic for ballistic testing but cannot be achieved in the indentation experiment.

The adhesive forces observed in the experiment were only qualitatively accounted for in this work, and hence the model could not be validated against the stickier PDMS gel samples. Also, during the iterative optimization of the simulant gels, the effects of adhesion on the experimental behavior of the tissues could not be excluded. This made it challenging to accurately match the gel response to the actual behavior of the tissue. A more robust method of quantifying the adhesion, taking into consideration that these forces possibly depend on contact area, depth of penetration as well as relative velocity between surfaces, may merit further research. However, it should be noted that it would be difficult to predict the adhesiveness of the computationally-optimized simulant gels before they are fabricated.

In the present work, only PDMS gels were considered since the experiments conducted by Dr. I. Kalcioglu (Van Vliet Group) were primarily on these gels and this experimental data was required for validation purposes. The computational model and optimization can certainly be modified to test out other types of gels against tissues or other energy dissipating materials. Different material models can also be used for the constituent phases of the composites, and the composite need not be limited to two phases. Digimat allows the definition of multiple phases and several material constitutive models such as elasto-plastic and elasto-viscoelastic deformation. These options could be explored to identify other possible candidates for tissue simulant materials.

The finite element model can also be changed to incorporate a layered tissue simulant material, with different layers having different microstructures and different thicknesses. This would require defining each of the material layers in Digimat. The coupled analysis would be more computationally expensive, but it is also a feasible direction to look into consider to optimize impact energy dissipation of engineered materials via computational predictions.

BIBLIOGRAPHY

[1] Fackler, M. L., Surinchak, J. S., Malinowski, J. A., & Bowen, R. E. (1984). Bullet Fragmentation: A Major Cause of Tissue Disruption. *The Journal of Trauma , 24* (1), 35-39.

[2] Nicholas, N. C., & Welsch, J. R. (2004). *Institute for Non-Lethal Defense Technologies Report: Ballistic Gelatin.* Institute for Non-Lethal Defense Technologies, Applied Research Laboratory The Pennsylvania State University, University Park.

[3] Kalcioglu, Z. I., Qu, M., Strawhecker, K. E., Shazly, T., Edelman, E., VanLandingham, M. R., et al. (2011). Dynamic impact indentation of hydrated biological tissues and tissue surrogate gels. *Philosophical Magazine , 91* (7-9), 1339-1355.

[4] Moy, P., Weerasooriya, T., Juliano, T. F., VanLandingham, M. R., & Chen, W. (2006). Dynamic Response of an Alternative Tissue Simulant, Physically Associating Gels (PAG). *Proceedings of the Society for Experimental Mechanics Conference.*

[5] Lenhart, J. L., Cole, P. J., Unal, B., & Hedden, R. (2007). Development of nonaqueous polymer gels that exhibit broad temperature performance. *Applied Physics Letters , 91* (6).

[6] Kalcioglu, Z. I., Qu, M., Strawhecker, K. E., VanLandingham, M. R., & Van Vliet, K. J. (2010). Multiscale characterization of relaxation times of surrogate gels and soft tissues. *27th Army Science Conference Proceedings.*

[7] Lenhart, J. L., Mrozek, R. A., Andzelm, J. W., VanLandingham, M. R., Shull, K., & Otim, K. (2011). Multi-functional soft polymer composites: broadly enabling materials for the defense community. *34th Annual Meeting of the Adhesion Society 2011.* Savannah: The Adhesion Society.

[8] Hong, W., Zhao, X., Zhou, J., & Suo, Z. (2008). A theory of coupled diffusion and large deformation in polymeric gels. *Journal of the Mechanics and Physics of Solids , 56* (5), 1779-1793.

[9] Mrozek, R. A., Cole, P. J., Cole, S. M., Schroeder, J. L., Schneider, D. A., Hedden, R. C., et al. (2010). Design of nonaqueous polymer gels with broad temperature performance: Impact of solvent quality and processing conditions. *Journal of Materials Research , 25* (6), 1105-1117.

[10] Kuo, A. C. (1999). Poly(dimethylsiloxane). In J. E. Mark (Ed.), *Polymer Data Handbook* (pp. 411-435). Oxford University Press, Inc.

[11] Mrozek, R. A., Cole, P. J., Otim, K. J., Shull, K. R., & Lenhart, J. L. (2011). Influence of Solvent Size on the Mechanical Properties and Rheology of Polydimethylsiloxane-Based Polymeric Gels. *Polymer , 52* (15), 3422-3430.

[12] Kalcioglu, Z. I. (2013, February). Mechanical Behavior of Tissue Simulants and Soft Tissues Under Extreme Loading Conditions (Doctoral Dissertation). Massachusetts Institute of Technology, Cambridge, MA.

[13] Juliano, T. F., Forster, A. M., Drzal, P. L., Weerasooriya, T., Moy, P., & VanLandingham, M. R. (2006). Multiscale Mechanical Characterization of Biomimetic Physically Associating Gels. *Journal of Materials Research , 21* (8), 2084-2092.

[14] Kalcioglu, Z. I., Mahmoodian, R., Hu, Y., Suo, Z., & Van Vliet, K. J. (2012). From macro- to microscale poroelastic characterization of polymeric hydrogels via indentation. *Soft Matter , 8*, 3393-3398.

[15] Kalanovic, D., Ottensmeyer, M. P., Gross, J., Buess, G., & Dawson, S. L. (2003, January). Independent testing of soft tissue visco-elasticity using indentation and rotary shear deformations. *Studies in Health Technology and Informatics , 94*, pp. 137-143.

[16] Juliano, T. F., Moy, P., Forster, A. M., Weerasooriya, T., VanLandingham, M. R., & Drzal, P. L. (2006). *Multiscale mechanical characterization of biomimetic gels for army applications.* U. S. Army Resear (e-Xstream engineering, 2010)ch Laboratory, Weapons & Materials Research Directorate, Aberdeen Proving Ground.

[17] Kalcioglu, Z. I. (2013, February). Mechanical Behavior of Tissue Simulants and Soft Tissues Under Extreme Loading Conditions.

[18] Constantinides, G., Tweedie, C. A., Savva, N., Smith, J. F., & Van Vliet, K. J. (2009). Quantitative Impact Testing of Energy Dissipation at Surfaces. *Experimental Mechanics , 49* (4), 511-522.

[19] Constantinides, G., Tweedie, C. A., Holbrook, D. M., Barragan, P., Smith, J. F., & Van Vliet, K. J. (2008). Quantifying deformation and energy dissipation of polymeric surfaces under localized impact. *Materials Science and Engineering: A , 489* (1-2), 403-412.

[20] e-Xstream engineering. (2012, January). Digimat Documentation.

[21] Jeulin, D., Kanit, T., & Forest, S. (2004). Representative Volume Element: A Statistical Point of View. In D. J. Bergman, & E. Inan (Eds.), *Continuum Models and Discrete Systems* (Vol. 158, pp. 21-27). Springer Netherlands.

[22]Aboudi, J. (1989). Micromechanical Analysis of Composites by the Method of Cells. *Applied Mechanics Reviews , 42* (7), 193-221.

[23] Kalamkarov, A. L., Andrianov, I. V., & Danishevs'kyy, V. V. (2009). Asymptotic Homogenization of Comoposite Materials and Structures. *Applied Mechanics Reviews , 62* (3).

[24] Friebel, C., Doghri, I., & Legat, V. (2006). General mean-field homogenization schemes for viscoelastic composites containing multiple phases of coated inclusion. *International Journal of Solids and Structures , 43* (9), 2513-2541.

[25] e-Xstream engineering. (2010, February). Digimat for nano-composites.

[26] Perdahcıoğlu, E., & Geijselaers, H. J. (2011). Constitutive modeling of two phase materials using the mean field method for homogenization. *International Journal of Material Forming , 4* (2), 93-102.

[27] Eshelby, J. D. (1957). The determination of the elastic field of an ellipsoidal inclusion, and related problems. *Proceedings of the Royal Society of London. Series A, Mathematical and Physical Sciences , 241* (1226), 376-396.

[28] Klusemann, B., & Svendsen, B. (2010). Homogenization methods for multi-phase elastic composites: Comparisons and benchmarks. *Technische Mechanik , 30* (4), 374-386.

[29] Mori, T., & Tanaka, K. (1973). Average stress in matrix and elastic energy of materials with misfitting inclusions. *Acta Metallurgica , 21* (5), 571-574.

[30] Nemat-Nasser, S., & Hori, M. (1994). Double-Inclusion Model and Overall Moduli of Multi-Phase Composites. *Journal of Engineering Materials and Technology , 116* (3), 305-309.

[31] Pierard, O., Friebel, C., & Doghri, I. (2004). Mean-field homogenization of multi-phase thermo-elastic composites: a gemeral framework and its validation. *Composites Science and Technology , 64* (10-11), 1587-1603.

[32] Doghri, I., & Friebel, C. (2005). Effective elasto-plastic properties of inclusion-reinforced composites. Study of shape, orientation and cyclic response. *Mechanics of Materials , 37* (1), 45-68.

[33] Hill, R. (1965). A self-consistent mechanics of composite materials. *Journal of the Mechanics and Physics of Solids , 13* (4), 213-222.

[34] e-Xstream engineering. (2009, February). Multi-scale modeling of composite materials and stuctures with Digimat to Ansys.

[35] E, W., & Lu, J. (2011). *Multiscale modeling*, 6(10):11527. Retrieved from Scholarpedia: http://www.scholarpedia.org/article/Multiscale_modeling

[36] Constantinides, G., Kalcioglu, Z. I., McFarland, M., Smith, J. F., & Van Vliet, K. J. (2008). Probing mechanical properties of fully hydrated gels and biological tissues . *Journal of Biomechanics , 41* (15), 3285-3289.

[37] Durocher, L. L., Gasper, A., & Rhoades, G. (1978). A numerical comparison of Axisymmetric Finite Elements. *International Journal for Numerical Methods in Engineering , 12* (9), 1415-1427.

[38] Simulia. (2010). Axisymmetric Solid Element Library. In *Abaqus Analysis User's Manual* (Vol. IV, pp. 155-174).

[39] Simulia. (2010). Analytical Rigid Surface Definition. In *Abaqus Analysis User's Manual* (Vol. I, pp. 235-246).

[40] Simulia. (2010). Contact Formulations in Abaqus/Standard. In *Abaqus Analysis User's Manual* (Vol. V, pp. 689-713).

[41] Bergström , J. (2005). *Calculation of Prony Series Parameters From Dynamic Frequency Data.* Retrieved from PolymerFEM: http://polymerfem.com/polymer_files/Prony_Series_Conversion.pdf

[42] Cho, S.-S., & Park, S. (2004). Finite element modeling of adhesive contact using molecular potential. *Tribology Internaional , 37* (9), 763-769.

[43] Sylves, K. T. (2008). *Modeling and Design Optimization of Adhesion Between Surfaces at the Microscale.* Sandia National Laboratories.

[44] Mathworks. (n.d.). *MATLAB Documentation Center.* Retrieved from http://www.mathworks.com/help/optim/ug/fmincon.html

Appendix

A1. Solvent Extraction Procedure

In order to perform rheological experiments on the network phases of the PDMS gels, the solvent phase has to be extraction from the composite gel. The following procedure is used to extract the solvent:

- Immerse a 1cm x 1cm sample of the gel in 250mL of toluene.
- Replace the toluene every 4 days for 8 weeks using a pipette pump.
- Monitor the extraction once a week by measuring the weight of the recovered sol isolated from the toluene via rotovap. (The rotovap at the MIT Olsen Research group was used.)
- After extraction, replace the toluene with a 50/50 *v/v* toluene/isopropanol solution for 24 hours, followed by a 25/75 *v/v* toluene/isopropanol solution for 24 hours, and 100% isopropanol for 24 hours to deswell the gel sample.
- Air-dry the gel for 72 hours
- After complete drying, weigh the sample to determine the extent of extraction.

A2. MATLAB code to obtain Prony series from rheology data

```
clc
clear all
close all

global freq G_strg_exp G_loss_exp tau x0 G0

data = load('freqdata.txt'); % load experimental data
freq = data(:,1); % frequency in Hz
G_strg_exp = data(:,2); % storage modulus in Pa
G_loss_exp = data(:,3); % loss modulus in Pa

% Plot storage modulus
StorageM = figure('Name','Storage Modulus');
loglog(freq, G_strg_exp,'ro'); hold on;
ylabel('Storage Modulus(Pa)');
xlabel('Frequency (Hz)');
% Plot loss modulus
LossM = figure('Name','Loss Modulus');
loglog(freq, G_loss_exp,'ro'); hold on;
ylabel('Loss Modulus(Pa)');
xlabel('Frequency (Hz)');

n = length(freq); % number of fitting points
G_strg = zeros(1,n);
```

```
G_loss = zeros(1,n);

G0 = 0.3e6; % shear modulus, initial assumption
PronyLength = 15; % Max length of Prony series
Matrix = zeros(PronyLength,PronyLength+3);

for N = 1:PronyLength
    tau = logspace(-2,2,N); % generate relaxation times

    % Initial guess from lsqnonlin without constraint sum(gi)<1
    g = rand(1,N);
    g = g/sum(g); % Prony series parameters, initial assumption
    x0 = [G0, g]; % variables to be optimized
    lb = [0,zeros(1,N)]; % lower bounds for variables
    ub = [1e8,ones(1,N)]; % upper bounds for variables
    [x,resnorm] = lsqnonlin(@calc1,x0,lb,ub); %lsqnonlin minimizes
    squared sum of vectors from calc1

    % Constrained optimization with fmincon
    G0 = x(1); % use shear modulus from lsqnonlin
    x0 = x(2:end); % variables to be optimized
    lb = 1e-10*ones(1,N); % lower bounds for variables
    ub = 0.9999*ones(1,N); % upper bounds for variables
    A = ones(1,N);
    b = 0.999; % to set condition Ax0 < b since sum of Prony series
    parameters must be < 1
    options = optimset('Algorithm','active-set','ScaleProblem','obj-
    and-constr','TolFun',1e-10, 'TolX',1e-10, 'MaxIter',100); % change
    according to necessity
    [x,fval,exitflag,output,lambda,grad] =
    fmincon(@calc2,x0,A,b,[],[],lb,ub,[],options);
    % fmincon minimizes squared error from function calc2

    Matrix(N,1) = N; % store length of Priny series
    Matrix(N,2) = fval; % store minimized squared error
    Matrix(N,3) = sum(x); % store sum of Prony series parameters
    Matrix(N,4:4+N) = [G0 x];% store shera modulus and Prony series
    parameters
end

[minerror, i] = min(Matrix(:,2)); % find minimum squared error of all
cases
G0 = Matrix(i,4); % shear modulus
gi = Matrix(i,5:4+i); % Prony series parameters
taui = logspace(-2,2,i); % relaxation times
% Storage and loss modulus calculated from Prony series
for j=1:n
    G_strg(j) = G0*(1-sum(gi)+
    sum(gi.*taui.^2*freq(j)^2./(1+taui.^2*freq(j)^2)));
    G_loss(j) = G0*sum((gi.*taui*freq(j)./(1+taui.^2*freq(j)^2)));
end

% Plot to compare with experimental storage modulus
figure(StorageM)
loglog(freq, G_strg,'kd');hold on
% Plot to compare with experimental loss modulus
figure(LossM)
```

```
loglog(freq, G_loss,'kd');hold on

% Save final Prony series data
Pronydata(1,1) = G0;
Pronydata(2:i+1,1) = taui';
Pronydata(2:i+1,2) = gi';
csvwrite('PronySeries.dat', Pronydata);


function y = calc1(x0)

    global freq G_strg_exp G_loss_exp tau

    for j=1:length(freq)
        G_strg(j) = x0(1)*(1-sum(x0(2:end))) +
        x0(1)*sum((x0(2:end).*tau.^2*freq(j)^2)./(1+tau.^2*freq(j)^2));
        G_loss(j) =
        x0(1)*sum((x0(2:end).*tau*freq(j)./(1+tau.^2*freq(j)^2)));
    end
    y = [G_strg./G_strg_exp'-1, G_loss./G_loss_exp'-1];


function y = calc2(x)

    global freq G_strg_exp G_loss_exp tau G0

    for j=1:length(freq)
        G_strg(j) = G0*(1-sum(x)) +
        G0*sum(x.*tau.^2*freq(j)^2./(1+tau.^2*freq(j)^2));
        G_loss(j) = G0*sum(x.*tau*freq(j)./(1+tau.^2*freq(j)^2));
    end
    y = sum((G_strg./G_strg_exp'-1).^2 + (G_loss./G_loss_exp'-1).^2);
```

A3. MATLAB code to calculate parameter K

```
clear all
close all

u = load('m.txt'); % data file containing time, displacement & velocity

t = u(:,1); % time in s
d = -u(:,2); % displacement in m
v = -u(:,3); % velocity in m/s

m = 0.215; % mass of pendulum in kg
k = 10; % spring constant of pendulum in N/m
c = 0.96; % damping coefficient of pendulum in Ns/m

xeq = 0.5/10^3; % vertical equilibrium of pendulum from point of
contact with sample
```

```
[vin,M] = max(v); % velocity at beginning of first impact cycle

[vout,I] = min(v); % velocity at end of first impact cycle

e = 1;
for i = M:I-1;
    dampingforce(e) = mean([v(i) v(i+1)]) * c;
    energy(e) = abs(dampingforce(e)) * abs(d(i+1)-d(i));
    e=e+1;
end;
EdP = sum(energy); % energy dissipated by the pendulum in first impact
cycle

Ein = 0.5*m*vin^2 + 0.5*k*(xeq-d(M))^2; % pendulum energy at beginning
of first impact cycle

Eout = 0.5*m*vout^2 + 0.5*k*(xeq-d(I))^2; % pendulum energy at end of
first impact cycle

K = (Ein-Eout-EdP)/(Ein-EdP) % ratio of energy dissipated by sample to
energy input to sample, during first impact cycle
```

A4. MATLAB code to calculate parameter Q

```
clear all
close all

u = load('m.txt'); % data file containing time, displacement & velocity
t = u(:,1); % time in s
d = -u(:,2); % displacement in m
v = -u(:,3); % velocity in m/s

[maxs(1),imaxs(1)] = max(d); % maximum penetration: crest of first
impact cycle
[mins(1),j] = min(d(imaxs(1):end)); % trough of first impact cycle
imins(1) = imaxs(1) + j - 1;
peakthrsh = 0.00001*(maxs(1)-mins(1)); % threshold of crest-trough
difference for cycles considered

i = 1;
while (maxs(i)~=d(end)) && (mins(i)~=d(end))
    i = i + 1;
    [maxs(i),j] = max(d(imins(i-1):end)); % locate next crest
    imaxs(i) = imins(i-1) + j - 1;
    [mins(i),j] = min(d(imaxs(i):end)); % locate next trough
    imins(i) = imaxs(i) + j - 1;
    if((maxs(i)-mins(i)) < peakthrsh) % stop when crest-trough
    difference falls below threshold
        i = i - 1;
        break
    end
end

dres = mean([maxs(i-1) mins(i-1)]); % mean final displacement of
```

```
indenter

maxshft = maxs(1:i) - dres;
tmaxshft = t(imaxs(1:i))' - t(imaxs(1));

dshft = d(imaxs(1):end) - dres;
tshft = t(imaxs(1):end) - t(imaxs(1));

p = polyfit(tmaxshft,log(maxshft),1); % fit crests to exponential curve
maxfit = exp(p(1)*tshft+p(2));
plot(tshft,dshft,tshft,maxfit,tmaxshft,maxshft,'go')

tau = mean(diff(tmaxshft));

gt = 2*abs(p(1));

w = (2*pi)/tau; %frequency

Qwo = 93.3325/gt;
Q = Qwo*w/161.25
```

A5. MATLAB optimization codes

```
clc
clear all
close all
global texp dexp G0 scale

exp = load('exp.txt'); % load experimental data
texp = exp(:,1); % time in s
dexp = exp(:,2); % displacement in m

N=10; % assume N Prony series terms
G0 = 5e4; % shear modulus, initial assumption
scale = 1e6;
G0s = G0/scale; % scale shear modulus so its order of magnitude is
similar to that of the Prony series parameters

g = 5e-2*ones(1,N); % Prony series parameters, initial assumption
x0 = [G0s, g]; % variables to be optimized

lb = 1e-10*ones(1,N+1); % set lower bound for variables
ub = 0.9999*ones(1,N+1); % set upper bound for variables

A = [0,ones(1,N)];
b = 0.999; % to set condition Ax0 < b since sum of Prony series
parameters must be < 1

options = optimset('MaxIter',100,'DiffMinChange', 5e-3); % change
according to necessity
[x2,fval,exitflag,output,lambda,grad] =
fmincon(@rundigi,x0,A,b,[],[],lb,ub,[],options); % optimization
function minimizes squared error from function rundigi
```

```
G0 = x2(1)*scale % scale back shear modulus
g = x2(2:end) % optimized Prony series parameters
err = fval % returns squared error between experimental and optimized
simulation displacement data

% run Abaqus-Digimat with the optimized variables to obtain
displacement
% data of optimized simulation
writedigi(G0,g); % creates material file with optimized Prony series
% delete any previous versions of displacement file
! del disp.dat
% run abaqus job called spring
! abaqus job=spring interactive
% run abaqus subroutine to extract displacement data into disp.dat from
abaqus file spring.fil
! abaqus postd
exit;


function y = rundigi(x)
      global texp dexp scale

      G0 = x(1)*scale; % scale back shear modulus of current iteration
      g = x(2:end); % Prony series parameters of current iteration

      writedigi(G0,g); % creates material file with Prony series
      variables of current iteration
      % delete any previous versions of displacement file
      ! del disp.dat
      % run abaqus job called spring
      ! abaqus job=spring interactive
      % run abaqus subroutine to extract displacement data into
      disp.dat from abaqus output file spring.fil
      ! abaqus postd

      % get simulated time and displacement data of current iteration
      sim = load('disp.dat');
      tsim = sim(:,1); % time in s
      dsim = sim(:,2); % displacement in m
      n = length(dsim);

      % find location of first contact of indenter on sample
      for i = 1:n
          if(dsim(i) < 0)
              if(abs(dsim(i-1)) < abs(dsim(i)))
                  i = i - 1;
              end
              break
          end
      end

      l = length(texp);
      ds = dsim(i:i+l-1); % to compare same sections of experimental
      and simulated displacements
      y = sum((ds-dexp).^2)/sum(dexp.^2); % calculate normalized mean
      squared error which is used by fmincon function
```

```
function writedigi(G0,g)

      ! del material.txt

      f=fopen('material.txt','w'); % create temporary material file
      fprintf(f,'\n########################################');
      fprintf(f,'\nMATERIAL\nname = T308exgel_50_1_4\ntype =
      viscoelastic'); % change according to material
      fprintf(f,'\ndensity = 9.800000000000000e+002\nconsistent_tangent
      = on'); % change according to material
      fprintf(f,'\nviscoelastic_model = prony_series');
      fprintf(f,'\ninitial_shear = %1.15e',G0);

      K0 = 2*G0*(1+0.49)/(3*(1-2*0.49)); % calculate bulk modulus

      fprintf(f,'\ninitial_bulk = %1.15e',K0);
      fprintf(f,'\nshear_relaxation_time = 1.000000000000000e-
      002,2.782600000000000e-002,7.742600000000000e-
      002,2.154400000000000e-001,5.994800000000000e-
      001,1.668100000000000e+000,4.641600000000000e+000,1.291500000000000
      00e+001,3.593800000000000e+001,1.000000000000000e+002');
      fprintf(f,'\nshear_weight =
      %1.15e,%1.15e,%1.15e,%1.15e,%1.15e,%1.15e,%1.15e,%1.15e,%1.15e,%1
      .15e',g(1),g(2),g(3),g(4),g(5),g(6),g(7),g(8),g(9),g(10));
      fprintf(f,'\nbulk_relaxation_time = 1.000000000000000e-
      002,2.782600000000000e-002,7.742600000000000e-
      002,2.154400000000000e-001,5.994800000000000e-
      001,1.668100000000000e+000,4.641600000000000e+000,1.291500000000000
      00e+001,3.593800000000000e+001,1.000000000000000e+002');
      fprintf(f,'\nbulk_weight =
      %1.15e,%1.15e,%1.15e,%1.15e,%1.15e,%1.15e,%1.15e,%1.15e,%1.15e,%1
      .15e',g(1),g(2),g(3),g(4),g(5),g(6),g(7),g(8),g(9),g(10));
      fprintf(f,'\n\n########################################\nMATERI
      AL');
      fprintf(f,'\nname = T308solvent\ntype = viscoelastic\ndensity =
      9.800000000000000e+002'); % change according to solvent
      fprintf(f,'\nconsistent_tangent = on\nviscoelastic_model =
      prony_series');
      fprintf(f,'\ninitial_shear = 9.296200000000000e+004\ninitial_bulk
      = 4.617112700000000e+006'); % change according to solvent
      fprintf(f,'\nshear_relaxation_time = 1.000000000000000e-
      002,3.727600000000000e-002,1.389500000000000e-
      001,5.179500000000000e-
      001,1.930700000000000e+000,7.196900000000000e+000,2.682700000000000
      00e+001,1.000000000000000e+002');
      fprintf(f,'\nshear_weight = 6.761000000000000e-
      001,7.468800000000000e-002,2.324700000000000e-
      001,3.020400000000000e-003,1.272100000000000e-
      002,4.650000000000000e-008,3.110000000000000e-
      008,2.870000000000000e-008'); % change according to solvent
      fprintf(f,'\nbulk_relaxation_time = 1.000000000000000e-
      002,3.727600000000000e-002,1.389500000000000e-
      001,5.179500000000000e-
      001,1.930700000000000e+000,7.196900000000000e+000,2.682700000000000
      00e+001,1.000000000000000e+002');
      fprintf(f,'\nbulk_weight = 6.761000000000000e-
```

```
001,7.468800000000000e-002,2.324700000000000e-
001,3.020400000000000e-003,1.272100000000000e-
002,4.650000000000000e-008,3.110000000000000e-
008,2.870000000000000e-008'); % change according to solvent
fprintf(f,'\n\n########################################');
fprintf(f,'\nPHASE\nname = gel\ntype = matrix');
fprintf(f,'\nvolume_fraction = 2.000000000000000e-001\nmaterial =
T308exgel_50_1_4'); % change according to volume fraction
fprintf(f,'\n\n########################################');
fprintf(f,'\nPHASE\nname = sol\ntype = inclusion');
fprintf(f,'\nvolume_fraction = 8.000000000000000e-001\nbehavior =
deformable_solid'); % change according to volume fraction
fprintf(f,'\nmaterial = T308solvent\naspect_ratio =
1.000000000000000e+000'); % change according to solvent
fprintf(f,'\norientation = fixed\ntheta_angle =
9.000000000000000e+001');
fprintf(f,'\nphi_angle = 0.000000000000000e+000\ncoated = no');
fprintf(f,'\n\n########################################');
fprintf(f,'\nMICROSTRUCTURE\nname = Microstructure1\nphase =
gel\nphase = sol');
fprintf(f,'\n\n########################################');
fprintf(f,'\nRVE\ntype = classical\nmicrostructure =
Microstructure1');
fprintf(f,'\n\n########################################');
fprintf(f,'\nANALYSIS\nname = T308_50_1_4\ntype =
mechanical\nloading_name = Mechanical'); % change according to
material
fprintf(f,'\nfinal_time = 3.000000000000000e-002\nmax_time_inc =
3.000000000000000e-003');
fprintf(f,'\nmin_time_inc = 3.000000000000000e-004\nfinite_strain
= off');
fprintf(f,'\nfinite_rotation = off\noutput_name = output1\nload =
ABAQUS');
fprintf(f,'\nhomogenization = on\nhomogenization_model =
Mori_Tanaka');
fprintf(f,'\nintegration_parameter = 5.000000000000000e-
001\nnumber_angle_increments = 6');
fprintf(f,'\norientation_storage = memory\nstiffness =
off\ninitial_stresses = off');
fprintf(f,'\norientation_input = global\norientation_usage =
local');
fprintf(f,'\nplane_strain_element = on\norientation_skin =
do_not_use_moldflow_output');
fprintf(f,'\nOT_trace_tol = 1.000000000000000e-
001\nnumber_collocation_points = 16');
fprintf(f,'\n\n\n\n########################################');
fprintf(f,'\nOUTPUT\nname = output1\nRVE_data =
Default\nPhase_data = gel,Default');
fprintf(f,'\nPhase_data = sol,Default\nEngineering_data = None');
fprintf(f,'\nLog_data = Default\nDependent_data = Default\n');
fclose(f);

% save as .mat file for digimat material to be accessed by Abaqus
! copy material.txt material.mat
```

A6. Abaqus subroutine postd.f

```
      SUBROUTINE ABQMAIN
C=======================================================================
C This program must be compiled and linked with the command:
C     abaqus make job=jobname
C Run the program using the command:
C     abaqus jobname
C=======================================================================
C
C  Purpose:
C
C    This program extracts the time and displacement data stored in an ABAQUS
C    results file (.fil).
C
C  Input File names:  spring.fil
C

C  Output File name:  disp.dat
C
C=======================================================================
C
C  Variables used by this program:
C
C    ARRAY  -- Real array containing values read from results file
C              (.fil). Equivalenced to JRRAY.
C    JRRAY  -- Integer array containing values read from results file
C              (.fil). Equivalenced to ARRAY.
C    NRU    -- Number of results files (.fil) to be read.
C    LRUNIT -- Array containing unit number and format of results files:
C              LRUNIT(1,*) --> Unit number of input file.
C              LRUNIT(2,*) --> Format of input file.
C    LOUTF  -- Format of output file:
C              0 --> Standard ASCII format.
C              1 --> ABAQUS results file ASCII format.
C              2 --> ABAQUS results file binary format.
C    JUNIT  -- Unit number of file to be opened.
C    JRCD   -- Error check return code.
C              .EQ. 0 --> No errors.
C              .NE. 0 --> Errors detected.
C    KEY    -- Current record key identifier.
C
C=======================================================================
C
C  The use of ABA_PARAM.INC eliminates the need to have different
```

```
C  versions of the code for single and double precision.
C  ABA_PARAM.INC defines an appropriate IMPLICIT REAL statement
C  and sets the value of NPRECD to 1 or 2, depending on whether
C  the machine uses single or double precision.
C
C=======================================================================
      INCLUDE 'aba_param.inc'
      DIMENSION  ARRAY(513), JRRAY(NPRECD,513), LRUNIT(2,1)
      EQUIVALENCE (ARRAY(1), JRRAY(1,1))
C
C=======================================================================
C  Open the output file.
C
C=======================================================================
      OPEN(UNIT=9,FILE='disp.dat',STATUS='NEW')
C
      NRU = 1
      LOUTF = 0
      LRUNIT(1,1) = 8
      LRUNIT(2,1) = 2
C
      CALL INITPF('spring',NRU,LRUNIT,LOUTF)
C
      JUNIT = 8
C
      CALL DBRNU(JUNIT)
C
C=======================================================================
C  Read records from the results (.fil) file and process the data.
C  Cover a maximum of 10 million records in the file.
C
C=======================================================================
      DO 1000 K100 = 1, 100
      DO 1000 K1 = 1, 99999
        CALL DBFILE(0,ARRAY,JRCD)
        IF (JRCD .NE. 0) GO TO 1001
        KEY = JRRAY(1,2)
C
C=======================================================================
C  Get the heading (title) record.
C
C=======================================================================
        IF (KEY .EQ. 1922) THEN
          WRITE(9,1100) (ARRAY(IXX),IXX=3,12)
 1100     FORMAT(1X,10A8)
C
```

```
C=======================================================================
C  Get the time
C
C=======================================================================
      ELSE IF (KEY .EQ. 2000) THEN
        TIME = ARRAY(3)
C
C=======================================================================
C  Get the nodal displacement(KEY101)
C
C=======================================================================
      ELSE IF (KEY.EQ.101) THEN
        NODENUM = JRRAY(1,3)
         WRITE(9,3000) TIME, ARRAY(5)
 3000     FORMAT(E12.5, 6X, E12.5)
C=======================================================================
      END IF
C
 1000 CONTINUE
 1001 CONTINUE
C
    CLOSE (UNIT=9)
C
    RETURN
    END
```